Carderock Division
Naval Surface Warfare Center
Bethesda, Maryland 20817-5700

NSWCCD-50-TR--2004/030 April 2004

Hydromechanics Department
Research and Development Report

CHARACTERISTICS OF A CAMBERED CIRCULATION CONTROL AIRFOIL HAVING BOTH UPPER AND LOWER SURFACE TRAILING EDGE SLOTS

by

Jane Abramson

NSWCCD-50-TR--2004/030 Characteristics of a Cambered Circulation Control Airfoil Having Both Upper and Lower Surface Trailing Edge Slots

REPORT DOCUMENTATION PAGE

Form Approved OMB No. 0704-0188

1. REPORT DATE *(DD-MM-YYYY)*	2. REPORT TYPE	3. DATES COVERED *(From - To)*
30-Apr-2004	Final	-

4. TITLE AND SUBTITLE

Characteristics Of A Cambered Circulation Control Airfoil Having Both Upper And Lower Surface Trailing Edge Slots

5a. CONTRACT NUMBER

5b. GRANT NUMBER

5c. PROGRAM ELEMENT NUMBER

6. AUTHOR(S)

Jane Abramson

5d. PROJECT NUMBER

5e. TASK NUMBER

5f. WORK UNIT NUMBER
04-1-5600-205-30

7. PERFORMING ORGANIZATION NAME(S) AND ADDRESS(ES) AND ADDRESS(ES)

Naval Surface Warfare Center
Carderock Division
9500 Macarthur Boulevard
West Bethesda, MD 20817-5700

8. PERFORMING ORGANIZATION REPORT NUMBER

NSWCCD-50-TR-2004/030

9. SPONSORING / MONITORING AGENCY NAME(S) AND ADDRESS(ES)

Dr. R. Joslin
Office of Naval Research
800 North Quincy Street
Arlington, VA 22217-5660

10. SPONSOR/MONITOR'S ACRONYM(S)

11. SPONSOR/MONITOR'S REPORT NUMBER(S)

12. DISTRIBUTION / AVAILABILITY STATEMENT

Approved for public release: distribution unlimited.

13. SUPPLEMENTARY NOTES

14. ABSTRACT

A circulation control(CC) elliptic airfoil section with a thickness-to-chord ratio of 0.17 and 1-percent circular arc camber, was experimentally evaluated to determine its low speed aerodynamic characteristics. The model profile is that of a previously tested single upper surface trailing edge slot airfoil, modified to incorporate an additional blowing slot on the lower surface. The main objective of this initial test was to determine if the control range, that is the range of lift coefficient available at a given angle-of-attack and momentum coefficient, could be increased without compromising the performance previously obtained with the single slot version. Test results show that the control range is more than doubled and there is no impact on upper surface only blowing performance. The range of lift coefficient produced at an angle-of-attack of zero degrees, using a combination of upper and lower slot only blowing is CL from +3.6 to -4.0. Blowing efficiency when using the lower slot was found to be higher than that obtained when using the upper slot. This finding was somewhat unexpected, since lower surface blowing is equivalent to using CC on a negatively cambered airfoil. Data was aquired using either only the upper or lower surface slot or with dual blowing, that is simultaneous upper and lower slot blowing.

15. SUBJECT TERMS

Circulation Control Airfoil, Upper Surface Trailing Edge Blowing, Dual Blowing Boundary Layer Control, Lower Surface Trailing Edge Blowing

16. SECURITY CLASSIFICATION OF:			17. LIMITATION OF ABSTRACT	18. NUMBER OF PAGES	19a. NAME OF RESPONSIBLE PERSON
a. REPORT	b. ABSTRACT	c. THIS PAGE			19b. TELEPHONE NUMBER *(include area code)*
UNCLASSIFIED	UNCLASSIFIED	UNCLASSIFIED	UL	81	

THIS PAGE INTENTIONALLY LEFT BLANK

CONTENTS

NOTATION v
ABSTRACT 1
ADMINISTRATIVE INFORMATION 1
INTRODUCTION 1
MODEL AND TEST APPARATUS 2
RESULTS AND DISCUSSION 4
    LIFT 5
    DRAG 8
    PITCHING MOMENT 9
CONCLUSIONS 10
ACKNOWLEDGMENTS 11
REFERENCES 12

FIGURES

1. LSB17 and "parent airfoil" contours 13
2. Lift variation with Reynolds number 15
3. Variation of momentum coefficient with duct pressure and slot height 17
4. Comparison of lifting efficiency of the LSB17 and parent airfoil 19
5. Airfoil control range at a fixed angle-of-attack 20
6. Lift variation with momentum coefficient 21
7. Model NCCR1510-7067N, experimental pressure distribution from Reference 10 23
8. Lift variation with the square root of momentum coefficient 24
9. Lift variation as a function of momentum coefficient and slot height-to-chord ratio for USB 26
10. Lift variation with momentum coefficient 27
11. Lift variation with the square root of momentum coefficient 29
12. Lift variation as a function of momentum coefficient and slot height-to-chord ratio for LSB 31
13. Lift coefficient for dual and upper surface blowing 32
14. Ratio of upper to lower slot momentum coefficient when using dual blowing 33
15. Lift augmentation ratio 34
16. Minimum pressure coefficient as a function of lift 38
17. Drag coefficient variation with momentum coefficient 43
18. Equivalent lift-to-drag ratio for USB at $h/c = 0.0013$ 48
19. Variation in half-chord pitching moment as a function of momentum coefficient 49
B1. Line drawing of the LSB17 made from the coordinates of construction B8

TABLES

B1. Coordinates of construction for the LSB17 model B3

NOTATION

A_j	Jet exit area, ft^2
a_j	Sonic velocity in the jet, ft/sec
C_d	Sectional drag coefficient from momentum loss in wake, corrected for additional mass efflux of the jet
C_{drake}	Sectional drag coefficient as measured by the rake, uncorrected
C_l	Sectional lift coefficient
C_{lmax}	Maximum sectional lift coefficient obtainable within test limitations
C_p	Pressure coefficient, $(P_l - P_\infty)/q_\infty$
c	Chord length, ft
h	Slot height, inches
M_j	Mach number in the jet
$\dot{m}$	Jet mass efflux, slug/sec
P_d	Duct (plenum) total pressure, lb/ft^2
P_l	Local static pressure on the model, lb/ft^2
P_∞	Freestream static pressure, lb/ft^2
q_∞	Freestream dynamic pressure, lb/ft^2
R	Universal gas constant, 1715. $ft^2/sec^2\ °R$
T_d	Duct (plenum) total temperature, °R
V_∞	Freestream velocity, ft/sec
x	Chordwise distance from the leading edge, ft
α	Geometric angle of attack, degrees
γ	Ratio of specific heats

ABSTRACT

A circulation control (CC) elliptic airfoil section with a thickness-to-chord ratio of 0.17 and 1-percent circular arc camber, was experimentally evaluated to determine its low speed aerodynamic characteristics. The model profile is that of a previously tested single upper surface trailing edge slot airfoil, modified to incorporate an additional blowing slot on the lower surface. The main objective of this initial test was to determine if the control range, that is the range of lift coefficient available at a given angle-of-attack and momentum coefficient, could be increased without compromising the performance previously obtained with the single slot version. Test results show that the control range is more than doubled and there is no impact on upper surface only blowing performance. The range of lift coefficent produced at α = 0 degrees, using a combination of upper and lower slot only blowing is C_l from +3.6 to -4.0. Blowing efficiency when using the lower slot was found to be higher than that obtained when using the upper slot. This finding was somewhat unexpected, since lower surface blowing is equivalent to using CC on a negatively cambered airfoil. Data was aquired using either only the upper or the lower surface slot or with dual blowing, that is simultaneous upper and lower slot blowing.

ADMINISTRATIVE INFORMATION

The work herein was undertaken from 1986 - 1987 and was supported by the David W. Taylor Naval Ship Research and Development Center (now the Naval Surface Warfare Center Carderock Division) under the Independent Exploratory Development Program sponsored by the Space and Naval Warfare Systems Command (SPARWAR 05), and administered by the Research Coordinator (DTNSRDC, Code 012.3) under Program Element 62766N, Task Area RZ66300. DTNSRDC Work Unit 1-1690-107. This report was written under the auspices of the Office of Naval Research and Dr. R. Joslin.

INTRODUCTION

Research into the use of the Coanda effect as a form of boundary layer control to provide high lift has been the subject of extensive experimental investigation at the Naval Surface Warfare Center Carderock Division (NSWCCD) since the late 1960's. Application of this technology was both to fixed and rotary wing aircraft and to hydrodynamic vehicles (References 1 - 4).

Using Circulation Control (CC) high lift augmentation is obtained by tangentially ejecting a wall jet over the rounded

trailing edge of a wing or foil. The jet sheet, which provides a mechanism for boundary layer control, remains attached to the curved surface of the trailing edge due to the Coanda effect. The absence of a sharp trailing edge also removes the constraint of an enforced Kutta condition, allowing the effective trailing edge stagnation point to move and hence the wing circulation to freely change.

The lower surface blowing model (LSB17) was designed, built and tested in 1986 - 1987. The LSB two dimensional airfoil, shown in Figure 1a, was the first CC model designed at NSWCCD to incorporate both upper and lower trailing edge blowing slots. Previously using only upper surface slots the lift due to blowing could only increment, in a positive sense, the unblown lift. There are however applications where the ability to increase, decrease or produce a side force in either direction is desirable. In order to achieve such flexibility a lower surface slot was incorporated into an already existing CC model profile. The LSB17 model was designed for use at both subsonic and transonic speeds.

A limited experimental evaluation of the low speed characteristics of the LSB17 airfoil was undertaken in July-August 1987, as a prelude to a more extensive transonic test. The test at transonic speed, has not to this date, been undertaken.

Recently, however, a three dimensional low aspect ratio dual blowing CC wing suitable for hydrodynamic applications has been designed and tested at NSWCCD. The results of the experimental evaluation may be found in Reference 5.

MODEL AND TEST APPARATUS

The main objective of the design was to provide an expanded control range while maintaining performance comparable to a previously tested single, upper surface trailing edge slot model with the same basic profile, referred to as the "parent" airfoil (Figure 1b). A more complete discussion of the analysis, specifications, design objectives and design details of the LSB17 model may be found in DTNSRDC/TM-16-86/03 (the complete text of which is included in Appendix A).

The airfoil basic profile is an ellipse with a thickness ratio of 0.17 and 1.0 - percent circular arc camber. Since a design prerequisite for the LSB is for performance to remain comparable to that of the parent airfoil when the upper blowing slot is used, the lower slot is imbedded. Imbedding insures that when the lower slot is closed the contour in that region is smooth and remains virtually unchanged with respect to the original airfoil geometry. Such a design would reduce any tendency for the upper surface wall jet to separate prematurely due to the physical presence of the lower slot.

The LSB17 model is manufactured of aluminum with a 12 inch

chord and a 36 inch span. As shown in Figure 1a the model is constructed with two completely separate plenums to allow control of the pressure in each chamber independently of the other. Each slot exit is the throat of a converging nozzle whose height is adjusted through the use of pitch screws. The upper and lower blowing slots are located at x/c = 0.968 and 0.970 respectively. A listing of the coordinates of construction are given in Appendix B.

Testing was conducted with the model mounted between two - dimensional wall inserts installed in the NSWCCD 8- by 10-ft Subsonic Wind Tunnel[6]. Lift and pitching moment coefficients are obtained by numerical integration of surface pressure taps as recorded at center span using a multiple - port scanivalve system. These coefficients were corrected by the addition of jet reaction components. Standard solid blockage[7] and wall corrections[8] were also applied to the data. No wake blockage correction factor was used because of the varying effects of the jet. Drag is obtained from an integration of the wake momentum deficit as measured using a total head rake placed 3.0 chord lengths downstream of the model. The momentum deficit methods of Betz and Jones[9] were used to determine the drag coefficient. To account for the additional momentum from the Coanda jet, a correction was applied to the drag coefficient.

Normally a tangential wall blowing system is used to enhance the two dimensionality of the flow across the airfoil span. For this test the insert wall blowing system was unavailable, however the recorded model spanwise pressure distributions were examined. Data with either problematic spanwise or rake pressure distributions are presented for completeness but a hatch mark appears on the plots of lift as a function of momentum coefficient to indicate these points.

Performance of circulation control airfoils is characterized by the momentum coefficient, $C_\mu = \dot{m} \cdot V_j / (q_\infty \cdot S)$. Where S is the reference area and q_∞ is the freestream dynamic pressure. Mass flow rate, $\dot{m}$, through the Coanda slot was measured by a venturi meter inserted in the air supply line. Jet velocity (V_j) was calculated by assuming an isentropic expansion from duct stagnation pressure to the freestream static pressure as follows:

$$P_R = P_\infty / P_d$$

$$V_j = a_j \cdot M_j = \left[(2 \cdot R \cdot T_d) \cdot (\gamma - 1)/\gamma \right) \cdot \left(1 - (P_R)^{\gamma - 1/\gamma}\right)]^{1/2}$$

Testing of the LSB17 model included three blowing modes, (1) upper surface slot blowing only, (2) lower surface slot blowing only and (3) dual blowing (simultaneous upper and lower surface slots blowing). The test, out of necessity, was conducted using a single venturi to measure all the mass flow. For single slot blowing, either upper or lower, this arrangement presented no technical problems. Momentum coefficient is calculated using the

measured mass flow and the calculated jet velocity. When dual blowing was utilized the mass flow passing through each slot was calculated from the duct pressure and temperature and the slot exit area using the isentropic flow equation:

for $P_R > 0.5283$ (subsonic flow):

$$\dot{m} = A_j \cdot P_d \cdot [2\gamma/((\gamma-1)\cdot R\cdot T_d)\cdot[(P_R)^{2/\gamma} - (P_R)^{\gamma+1/\gamma}]]^{1/2}$$

for choked flow:

$$\dot{m} = A_j \cdot P_d \cdot [\gamma/(R\cdot T_d)^{1/2}]\cdot[2/(\gamma+1)]^{(\gamma+1)/2(\gamma-1)}$$

The mass flow computed for each slot are added together and compared to the total measured mass flow. Both calculated mass flows and the difference between the sum and measured mass flows were printed out and tracked as part of the data reduction and validation process.

A series of runs were made at freestream dynamic pressures from 20 to 60 psf, corresponding to a model Reynolds number range of 0.8×10^6 to 1.4×10^6 (Figure 2). Although there are some differences in performance as dynamic pressure changes most data was taken at $q_\infty = 40$ psf to allow for a wider range of C_μ. A limited number of points were recorded at $q_\infty = 20$ and 60 psf for each blowing and slot height configuration.

RESULTS AND DISCUSSION

Characteristics of a 17-percent cambered ellipse with both upper and lower surface trailing edge blowing slots were evaluated over a maximum incidence range of $-10 \leq \alpha \geq 10$ deg for three blowing modes. For upper and lower single slot blowing, the model was evaluated at two slot height-to-chord ratios, h/c = 0.0013 and 0.0020 and values of momentum coefficient ranging from $C_\mu = 0$ to 0.22 (for $q = 40$ lbs/ft^2). Figure 3 depicts the variation of momentum coefficient with duct pressure for both plenums. The expansion of the slots caused by the pressurization of the duct were also determined. Measurements taken by pressurizing each duct and measuring the resulting slot height with a thickness gage under quiescent tunnel condition showed less than 0.002" increment above the 0.025" height at $P_d = 10$ psig for both slots.

Techniques used for single and dual slot blowing differ somewhat from one another. For single slot blowing, the slot which is not being used is closed by releasing all tension in the pitch screws. Air supply lines are connected to both sides of the model, but only to the plenum in use (the inlet to the plenum not in use is temporarily capped off to prevent in/out drafts). The

momentum coefficient noted in the data and figures reflects the fact that all mass flow is exiting only from the slot indicated. For this test dual blowing was evaluated for only one combination of slot height settings; h/c = 0.0013 and 0.0002 for the upper and lower slots respectively. The two available air supply lines are connected one to each of the two plenum chambers. Such an arrangement results in each plenum being supplied from only one end of the model (a single end feed). The momentum coefficient on the figures for dual blowing mode reflect the combined mass flow ejected simultaneously out of both slots, unless otherwise noted.

LIFT

Sectional lift coefficients as determined by an integration of the midspan pressure taps for the LSB17 model and the single upper blowing slot parent airfoil are shown in Figure 4. Performance of the two models are virtually identical, and therefore the first major objective of the LSB17 design, to provide performance comparable to the parent airfoil, is met.

Figure 5 shows that the range of lift available at α = 0 deg is more than doubled when lower slot only blowing is used in conjunction with upper slot only blowing. This not only fulfills the second design objective, to provide an expanded control range, but also shows how a fixed surface can provide control authority using only blowing. Figure 5 also indicates that the augmentation of the airfoil with lower slot blowing (LSB) is higher than that achieved with upper slot blowing (USB). Augmentation is defined as the increment in lift achieved over the unblown value for a given momentum coefficient. Since the model is positively cambered in the conventional sense, lower surface blowing is equivalent to using CC on a negatively cambered airfoil. The augmentation obtained when using negative camber would usually be assumed to be less than that for a positively cambered foil. Although the reason for the increased augmentation could not be definitively determined within the scope of the current test, some possibilities include; (1) differences in the upper/lower surface upstream boundary layer due to differences in pressure distribution history, (2) details of the lower nozzle design or (3) some other heretofore unappreciated virtue of the pressure distributions developed when using negative camber or some combination thereof.

Lift coefficient as a function of momentum coefficient for upper surface blowing are shown in Figures 6a and 6b. In Figure 6a, for h/c = 0.0020, at $\alpha \geq 0$ deg the lift curves roll over at progressively lower values of C_μ as the angle increases. Examination of the pressure distributions indicates that a leading edge separation is occurring at each of the roll over points. These stall characteristics arise because the leading edge stagnation point moves not only in response to changes in incidence, but also in concert with the trailing edge stagnation

point as blowing is increased. For α = -5 and -10 deg, Figure 6a shows that either a reduction in the lift curve slope or a rollover precedes the maximum lift point. Examination of the pressure distributions show that this is not due to flow separation but rather to either a reduction in pressure or actual suction ($-C_p$) which develops on the lower trailing edge due to the influence of the Coanda jet. Figure 7, taken from Reference 10, illustrates the effects on the pressure distribution which can occur when the influence of the jet extends well onto the pressure side of the airfoil. For this slot height, a $C_{l_{max}}$ = 4.43 is produced at α = -5 degrees and C_μ = 0.22.

Lift data for h/c = 0.0013, shown in Figure 6b, indicate a $C_{l_{max}}$ = 4.17 is reached also at α = -5 degrees and a C_μ = 0.146; which represents the same maximum duct pressure of 21 psig used at the larger slot height. Data taken at a q = 20 lbs/ft^2 at this incidence (Figure 2a) show that a $C_{l_{max}}$ = 4.26 is obtained at C_μ = 0.199, before excessive suction on the lower trailing edge results in a reduction in the integrated lift. Leading edge separation is again noted near the roll over points at both α = 0 and 5 degrees (Figure 6b).

Data for both slot height-to-chord ratios are also plotted as a function of the square root of the momentum coefficient in Figure 8. The C_l,C_μ relationship is initially linear at low blowing, but becomes proportional to $C_\mu^{1/2}$ over most of the momentum coefficient range shown in the figure; except where either separation or suction are an issue (for a more detailed discussion see Ref. 5). A direct comparison of the lift produced at α = 0 and ± 5 degrees for h/c = 0.0013 and 0.0020 is made in Figure 9. For the upper surface slot, performance appears to be largely insensitive to h/c in the range tested.

Lift data for the lower surface blowing slot is presented in Figure 10 as a function of C_μ and as a function of $C_\mu^{1/2}$ in Figure 11. The angles-of-attack noted on all plots for lower surface blowing are physically the same as those for USB. For h/c = 0.0013 the maximum C_l = -4.27 is obtained at α = 5 deg and a C_μ = 0.136, despite a large region of suction which develops on the upper aft region of the trailing edge (Figure 10a). For lower surface blowing large regions of suction, which reduce the integrated lift, are noted at $\alpha \geq 0$ deg for higher values of C_μ (symbols are on Fig.10 for these points). For each of the negative angles in Figure 10 the loss in lift correlates with leading edge separations as determined by examining the surface pressure distributions.

At an h/c = 0.0020 (Figure 10b) maximum lift still occurs at 5 deg., however the coefficient has increased to -4.77. The reduction in the lift curve slope at α = 0 deg. which begins at C_μ = 0.1 is due to upper trailing edge suction, while the roll over in the curve at C_μ = 0.13 is due to flow separation along the lower leading edge. A comparison of the performance at the two slot heights tested for the LSB configuration is shown in

Figure 12.

For the dual blowing mode (h/c_{upper} = 0.0013 and h/c_{lower} = 0.0002) lift as a function of momentum coefficient for the upper slot is found in Figure 13. Also plotted on this figure are the lift data for upper slot only blowing. The accompanying ratio of slot momentum coefficients for these data are shown in Figure 14. The C_μ ratios examined in this test ranged from approximately 20 to 30 percent, which is very high compared to the data of Ref. 5 and probably account for the reduction in lift. Within the constraints of the current test it was not possible to make use of the separate valving system for each plenum. Such a system would permit a complete assessment of the impact of the C_μ ratio on overall dual blowing performance, including possible reduction in the loss of lift due to the excessive turning of the Coanda wall jet.

Augmentation ratio data are presented in Figures 15a - 15d. The highest augmentation, in excess of 70, is achieved with LSB at h/c = 0.0013, for $10 \leq \alpha \geq -2.5$ degrees. Using USB, ratio's greater than 50 are produced over a range of incidence angles. The augmentation ratio depicted in this figure are not those resulting from a determination of a "local slope", but rather calculated numerically using the definition $\Delta C_l/C_\mu$. In general for a given slot height the higher augmentation is obtained with lower rather than upper slot blowing.

The value of the minimum pressure coefficient as a function of lift coefficient are shown in Figures 16a - 16e for each blowing configuration. Minimum pressure has implications for both aerodynamic and hydrodynamic applications, governing either critical Mach number or cavitation onset. Minimum pressure usually occurs in the vicinity of the trailing edge, particularly at the higher blowing coefficients and is mainly a function of C_l, α and the local radius of curvature.

To complete the discussion of lift characteristics, the effect of spanwise nonuniformity must be considered. Even when wall blowing is used to supress seperation of the insert wall boundary layer (thereby assuring model spanwise two-dimensionality), the high lift coefficients still produce induced downwash. For this test the insert wall blowing system was unavailable and a determination of the effective incidence angle was made. For the cases selected, potential flow pressure distributions for several incidence angles and the experimental C_l were produced. The resulting distributions were then compared to the experimental pressure distribution until leading edge characteristics coincided. A further requirement for the match was that the delta C_p at midchord for both the experimental and potiential distribution (delta C_p being uniquely related to C_l) were the same. The effective incidence correction was determined to be 0.5 degrees per C_l.

DRAG

The variation of a modified drag coefficient with momentum coefficient are presented in Figures 17a - 17e for upper, lower and dual blowing, respectively. These data result from an integration of the wake deficit using the method of Betz[9] which was modified to account for the additional momentum of the jet thereby becoming $C_d = C_{drake} - \dot{m} \cdot V_\infty / (q_\infty \cdot S)$. The initial unblown drag levels are high due to the nature of bluff trailing edge airfoils. Negative drag levels are achieved and maintained at zero and negative incidence for USB. For LSB the initial drag level is reduced for most of the angles and become negative for positive incidence. The secondary drag rise which occurs for both USB and LSB configurations is associated with either leading edge separation or trailing edge suction on the surface opposite the blowing slot. This is the case whether or not there is a degradation observed in the lift curve. An increase in drag often begins before changes in the lift curve slope are noted.

Drag for the dual blowing mode is shown and compared to that obtained with USB in Figure 17e. For dual blowing drag becomes and remains negative as the momentum coefficient increases. The drag rise seen at $\alpha = 0$ degrees for USB, which is due to a leading edge separation, does not occur with dual blowing because the lift coefficient produced at a given C_μ is reduced.

The drag as presented does not include the energy expended to produce blowing, which is usually equated to an equivalent drag term. An equivalent drag can be computed using:

$$d_e = d + P_{comp}/V_\infty + \dot{m}V_\infty$$

The first term d is the momentum deficit as measured by the wake rake (corrected for jet efflux); the second term is the compressor power and the third term is an intake momentum flux. The compressor power required may be expressed as:

$$P_{comp} = 0.5 \cdot \dot{m} \cdot R \cdot T_d \cdot (2\gamma/\gamma - 1) \cdot [(1 - (P_{t\infty}/P_t)^{\gamma - 1/\gamma})]$$

For subsonic flows with $M_\infty \leq 0.2$, $P_{t\infty} \approx P_\infty$ and the above becomes:

$$P_{comp} = 1/2 \cdot \dot{m} \cdot V_j^2$$

Substituting for P_{comp}, the coefficient form becomes:

$$C_{de} = C_d + C_\mu \, V_j/(2V_\infty) + C_\mu \, V_\infty/V_j$$

The equivalent lift-to-drag ratio as a function of C_l is shown in Figure 18 for USB at an h/c = 0.0013.

PITCHING MOMENT

The pitching moment about the midchord (C_{m50}) as a function of momentum coefficient is depicted in Figures 19a - 19e, for upper, lower and dual blowing respectively. In the absence of other phenomena, the relatively high trailing edge suction peak tends to produce a nose down moment for USB and a nose up moment for LSB. Abrupt changes in moment can signify either leading edge separation or the development of suction on the trailing edge of the surface opposite the blowing slot. For USB, leading edge separation can also produce a negative increment in moment, while a positive increment can signify that there is suction (a loss of stagnation pressure) on the lower trailing edge due to the influence of the Coanda jet. For LSB the sign of the moment trends is reversed.

For the LSB configuration presented in Figure 19d, the nose down moment generated at α = 0 deg for $C_\mu > 0.1$ is due to excess suction on the upper trailing edge. Suction is also noted on the pressure plots at α = 5 deg, however the pitching moment does not become more negative. For this case changes in the pitching moment appear to be mitigated by an imbalance between the lower surface leading and trailing edge suction peaks developed on the airfoil.

For USB the data at α = 10, 5 and 0 deg in Figure 19a represents the pitching moments which may result from a number of flow phenomena. At α = 10 deg there is both a leading edge separation and excessive suction on the lower trailing edge for $C_\mu \geq 0.13$. After examining the available airfoil pressure distributions, the governing factor for the moment is the balance between leading and trailing edge suction peaks. The trailing edge suction peak continues to rise throughout the C_μ range while the pressure coefficient at the leading edge becomes relatively constant at a fairly small, negative value of C_p (due to leading edge separation). Suction which develops along the lower trailing edge is not sufficient to change the moment.

At α = 5 deg both upper surface leading edge separation and suction on the lower trailing edge (beginning at $C_\mu = 0.07$) are still both present. Pressure levels on the upper surface at both ends of the chord are more similar at 5 deg then at α = 10 deg; however the trailing edge suction peak does begin to dominate as C_μ increases. The combined effect of the upper surface pressure distribution and lower trailing edge suction is that the pitching moment remains virtually unchanged over the blowing range.

The resultant pressure distributions at α = 0 deg also show a combination of upper leading edge separation and lower trailing edge suction (which begins at a $C_\mu = 0.10$). At this incidence the moment curve becomes more positive with the onset of lower trailing edge suction.

CONCLUSIONS

An initial evaluation of a cambered 17-percent thick circulation control elliptic airfoil with both upper and lower trailing edge blowing slots was undertaken. The objective was to determine whether an expanded control range could be obtained by incorporating a lower surface blowing slot, while maintaining the performance previously achieved using the single slot parent airfoil. The following conclusions were drawn from an examination of the data:

1. A lower trailing edge slot can be incorporated into an airfoil without compromising the lift produced using upper surface trailing edge blowing.

2. The airfoil control range, that is the ΔC_l available at a given angle-of-attack and momentum coefficient, was more than doubled for the cambered profile of the LSB17 solely by changing the blowing slot which is being used, from upper to lower or vice versa.

3. A loss in the maximum integrated lift due to a loss in positive pressure and/or suction produced by the excessive turning of the Coanda jet was noted for both slots, but occurred at lower blowing coefficients for lower surface slot blowing. Such excessive turning has been shown in subsequent testing to be controllable using a low rate of bleed air from the opposing slot, with an attendant increase in lift.

4. For USB a maximum lift coefficient of 4.4, which is a ΔC_l due to blowing of 4.8, is achieved at α = -5 degrees and a C_μ = 0.22. A C_l = 4.2 (ΔC_l = 4.6) is obtained at the same incidence for a C_μ = 0.15. Using LSB at α = +5 degrees produces a $C_{l_{max}}$ = -4.3 (ΔC_l = 5.0) at a C_μ = 0.14. Also at α = +5 degrees for a C_μ = 0.1 a C_l = 3.5 (ΔC_l = 4.2) is obtained.

5. Lift augmentation ratios, as computed using $\Delta C_l/C_\mu$, in excess 70 are noted for lower surface blowing for a number of combinations of incidence and blowing. Somewhat lower augmentation ratios, in excess of 50, are produced using the upper surface slot.

6. The reason for the comparative increase in blowing efficiency when using the lower rather than the upper slot is not definitively known. Determining why the efficiency is higher would be best approached using computational methods.

ACKNOWLEDGMENTS

The author wishes to thank Mr. Ernest Rogers for his contributions during both the design and testing phases of this project.

REFERENCES

1. Englar, R.J., and C.A. Applegate, "Circulation Control - A Bibliography Of DTNSRDC Research and Selected Outside References (Jan 1969 - Dec 1983)," DTNSRDC Report 84/052, Sept 1984.

2. Abramson, J. and E.O. Rogers, "Optimization Theory Applied To Higher Harmonic Control Of Circulation Controlled Rotors" VERTICA, Vol. 6, No. 2, 1982, pp. 77 - 88.

3. Rogers, E.O., A.W. Schwartz and J. Abramson, "Applied Aerodynamics Of Circulation Control Airfoils And Rotors," AHS 41st Annual Forum, May 1985.

4. Englar, R.J. and R.M. Williams, "Design Of A Circulation Control Stern Plane For Submarine Applications," NSRDC, TN AL-200, March 1971.

5. Rogers, E.O. and M.J. Donnelly, "Characteristics Of A Dual-Slotted Circulation Control Wing Of Low Aspect Ratio Intended For Naval Hydrodynamic Application," AIAA Paper 2004-1244, Jan 2004.

6. Englar, R.J. and J. Ottensoser, "Calibration of Some Subsonic Wind Tunnel Inserts For Two-Dimensional Airfoil Experiments," TN AL-275, Sept 1972.

7. Rae, W.H. and A. Pope, "Low Speed Wind-Tunnel Testing," Second Edition, John Wiley and Sons, Inc. New York, 1984, pp. 349-355.

8. Garner H.C., Rogers, E.W.E., et al, "Subsonic Wind Tunnel Wall Corrections," AGARDOGRAPH 109, Paris, Oct 1966 .

9. Schlicting, Hermann, "Boundary Layer Theory," Sixth Edition, McGraw-Hill Book Company, New York, 1968, pp. 708-713.

10. Abramson, J., "Two-Dimensional Subsonic Wind Tunnel Evaluation Of Two Related Cambered 15-Percent Thick Circulation Control Airfoils," DTNSRDC ASED-373, Sept 1977.

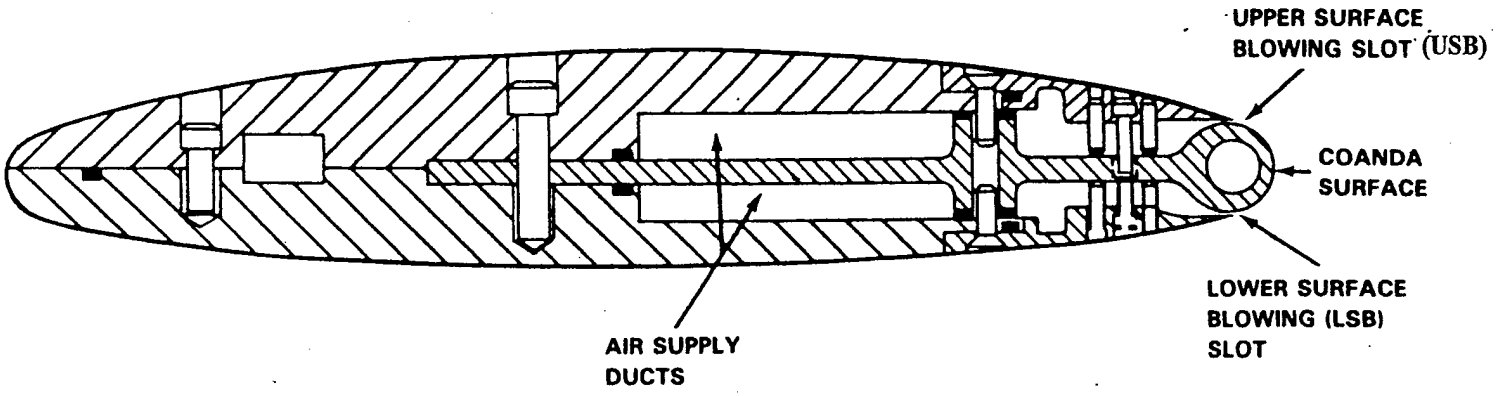

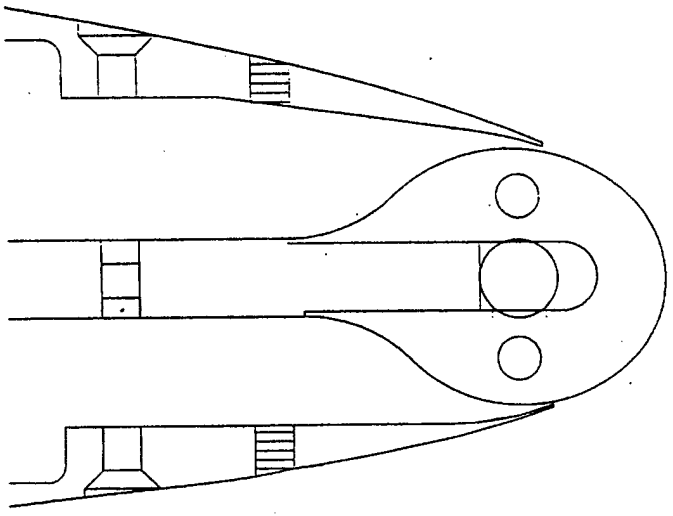

Figure 1a. LSB17 mechanical layout and Coanda trailing edge details.

Figure 1. LSB17 and "parent airfoil" contours.

Figure 1. (Continued)

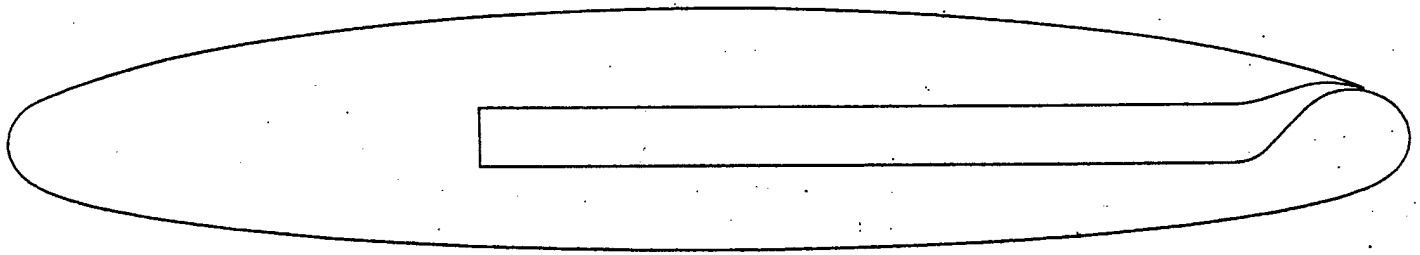

Figure 1b. LSB "parent airfoil" contour, the RB17.

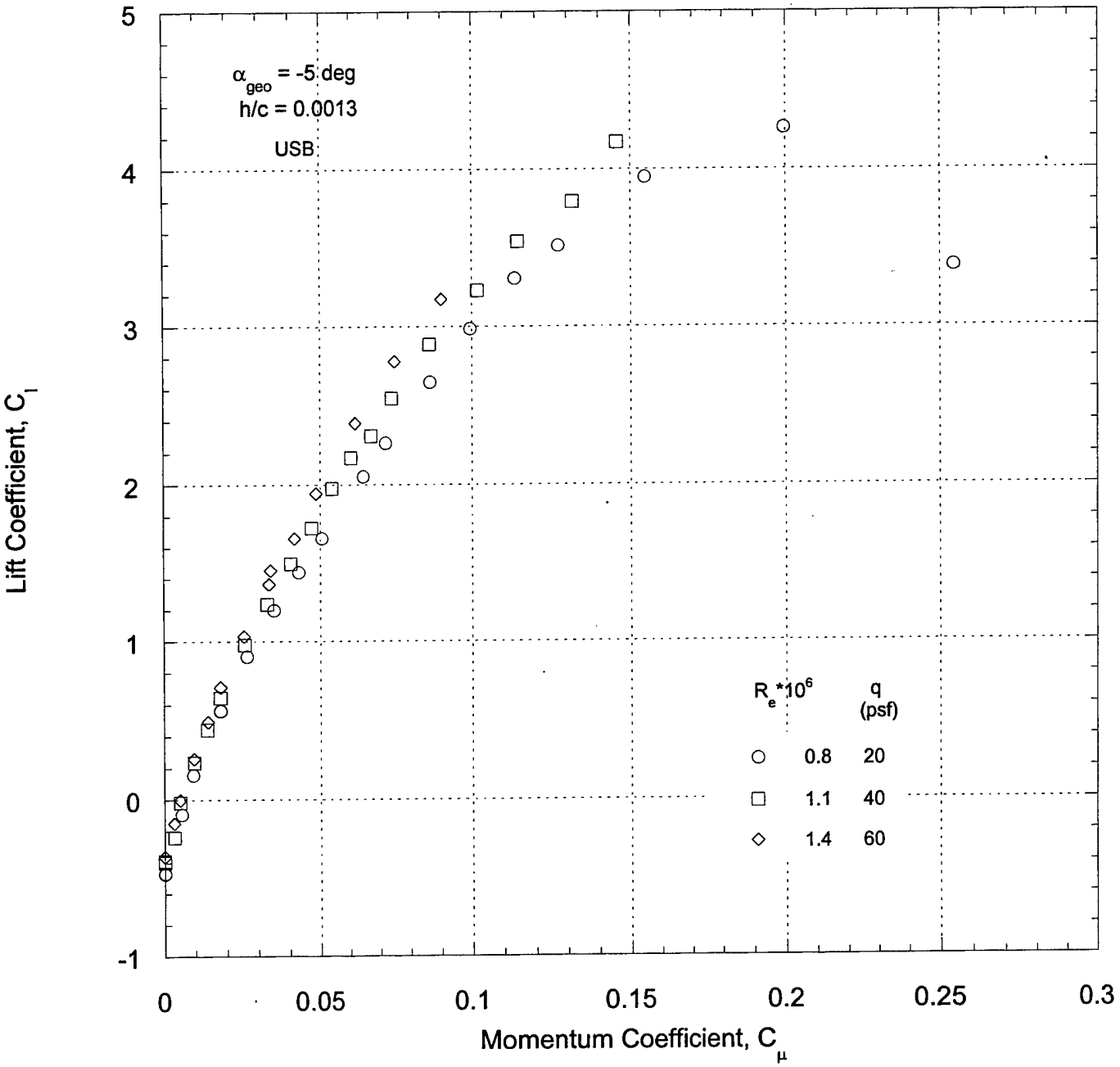

Figure 2a. Upper surface blowing.

Figure 2. Lift variation with Reynolds number.

Figure 2. (Continued)

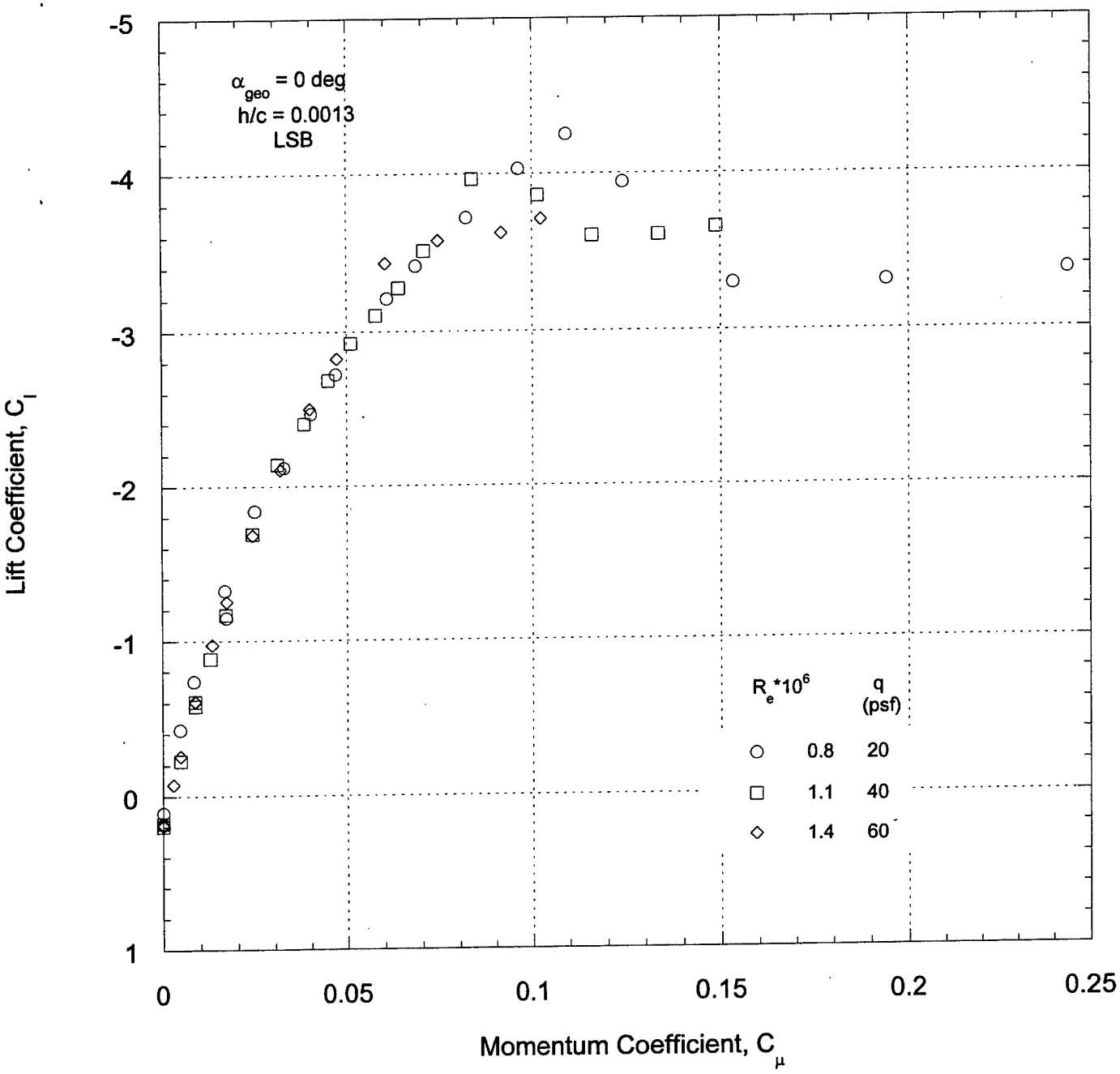

Figure 2b. Lower surface blowing.

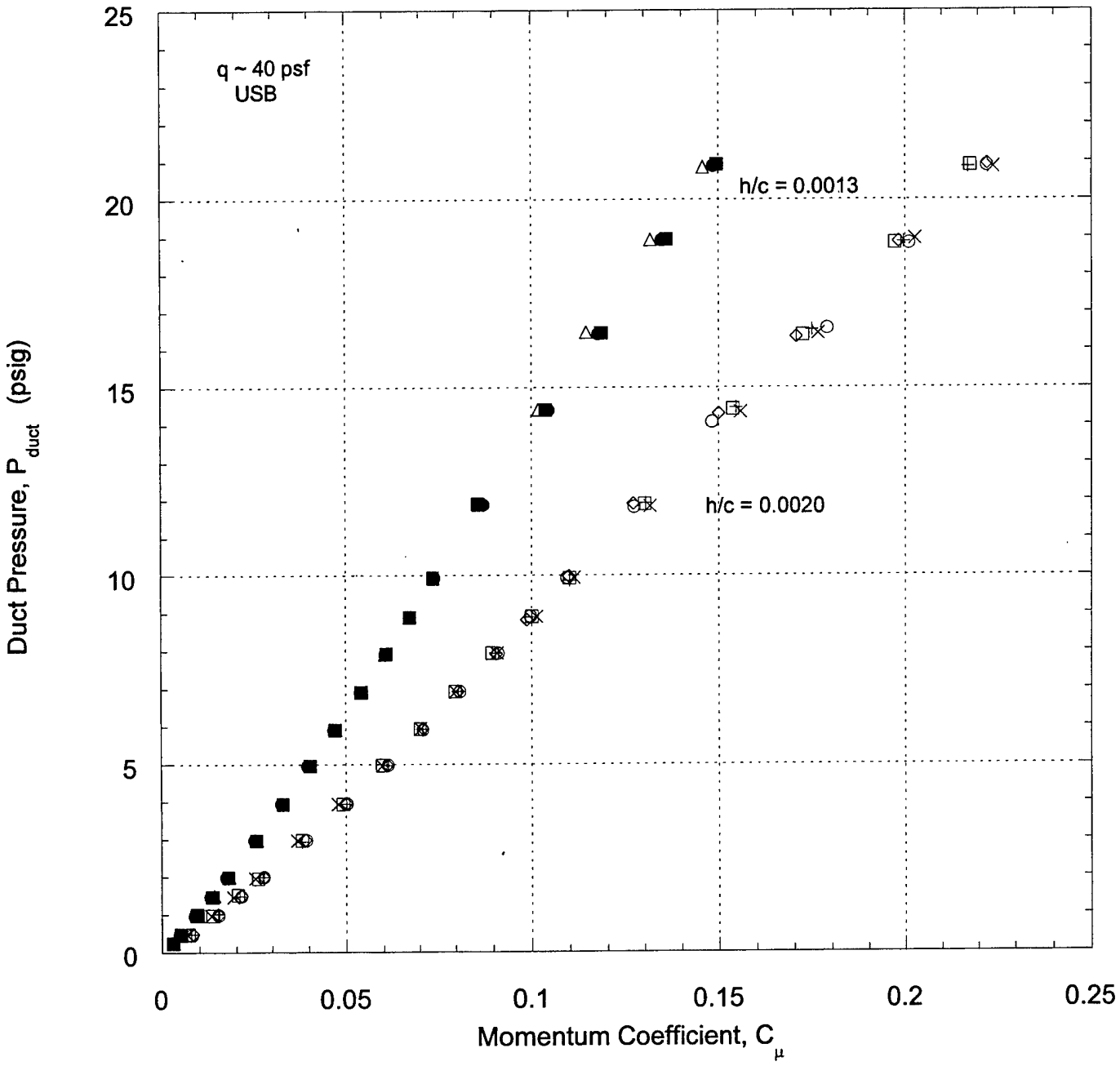

Figure 3a. Upper surface blowing.

Figure 3. Variation of momentum coefficient with duct pressure and slot height.

Figure 3. (Continued)

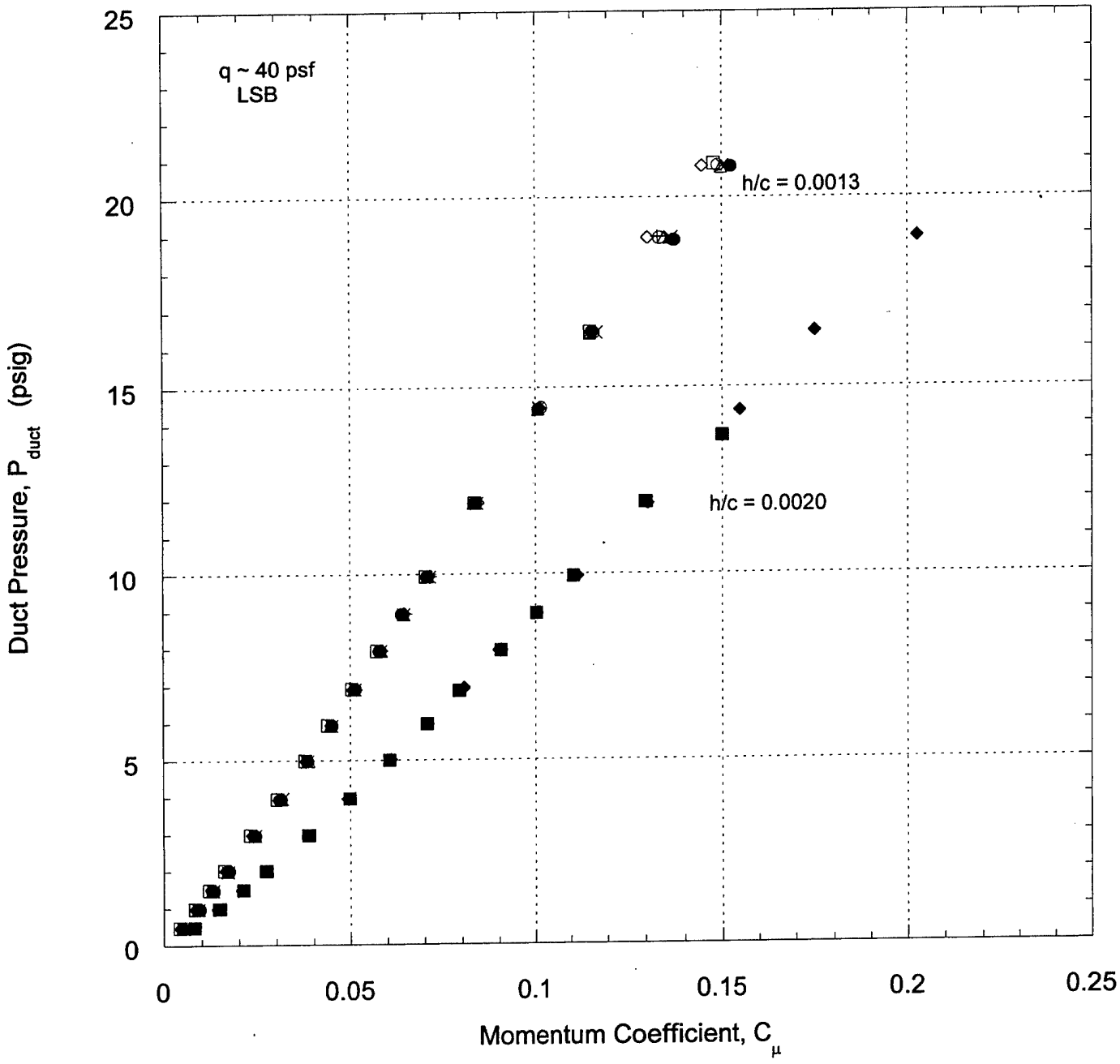

Figure 3b. Lower surface blowing.

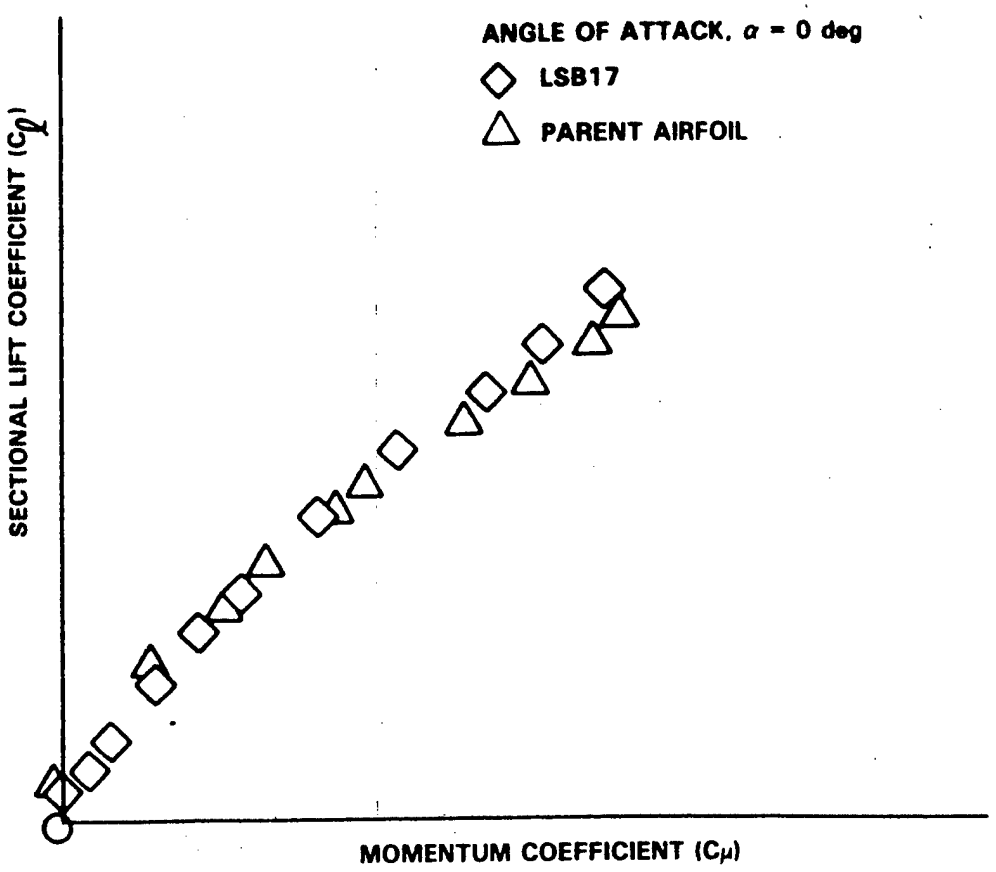

Figure 4. Comparison of the lifting efficiency of the LSB17 and parent airfoil.

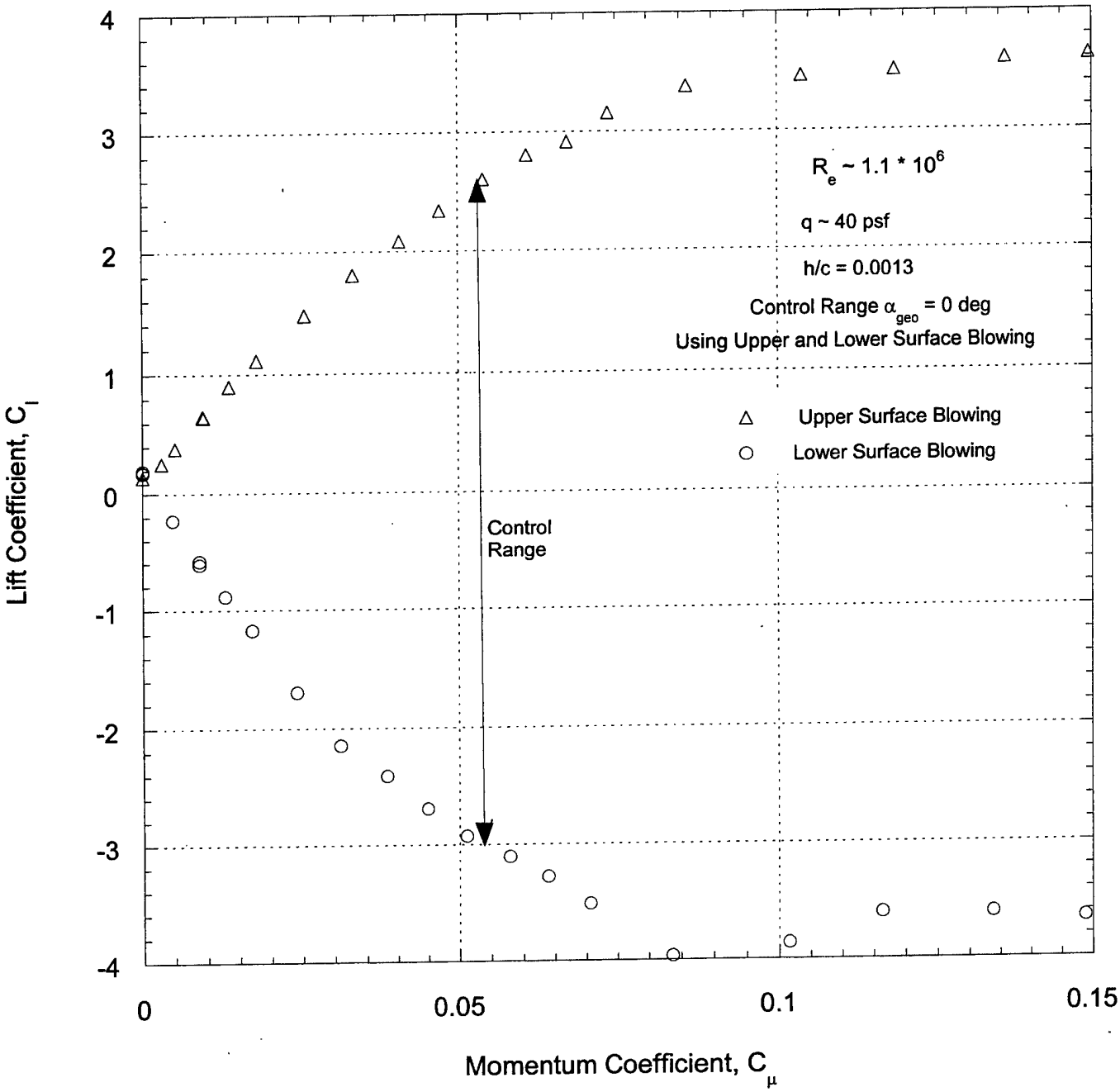

Figure 5. Airfoil control range at a fixed angle-of-attack.

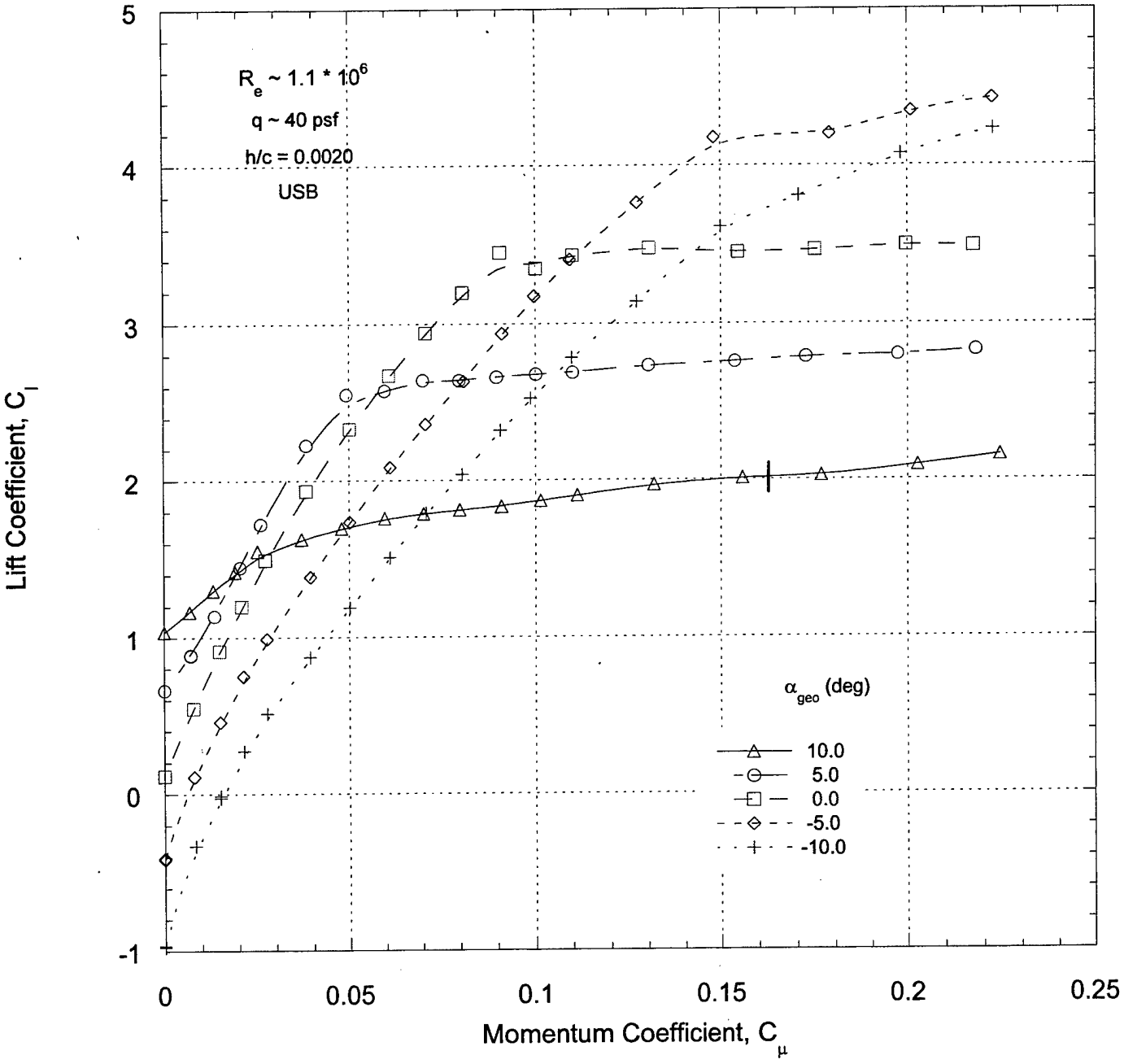

Figure 6a. USB, h/c = 0.0020.

Figure 6. Lift variation with momentum coefficient.

Figure 6. (Continued)

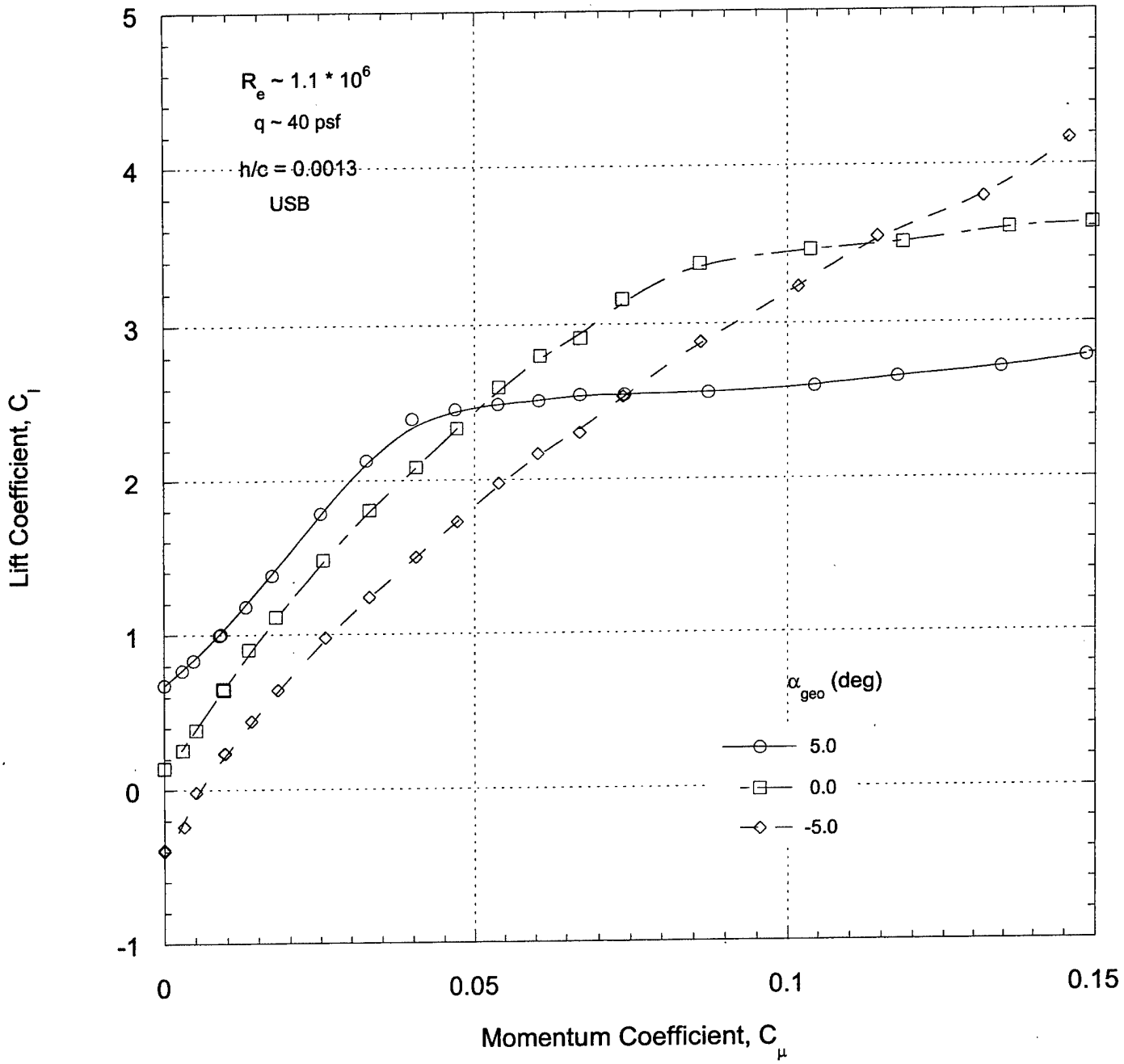

Figure 6b. USB, h/c = 0.0013.

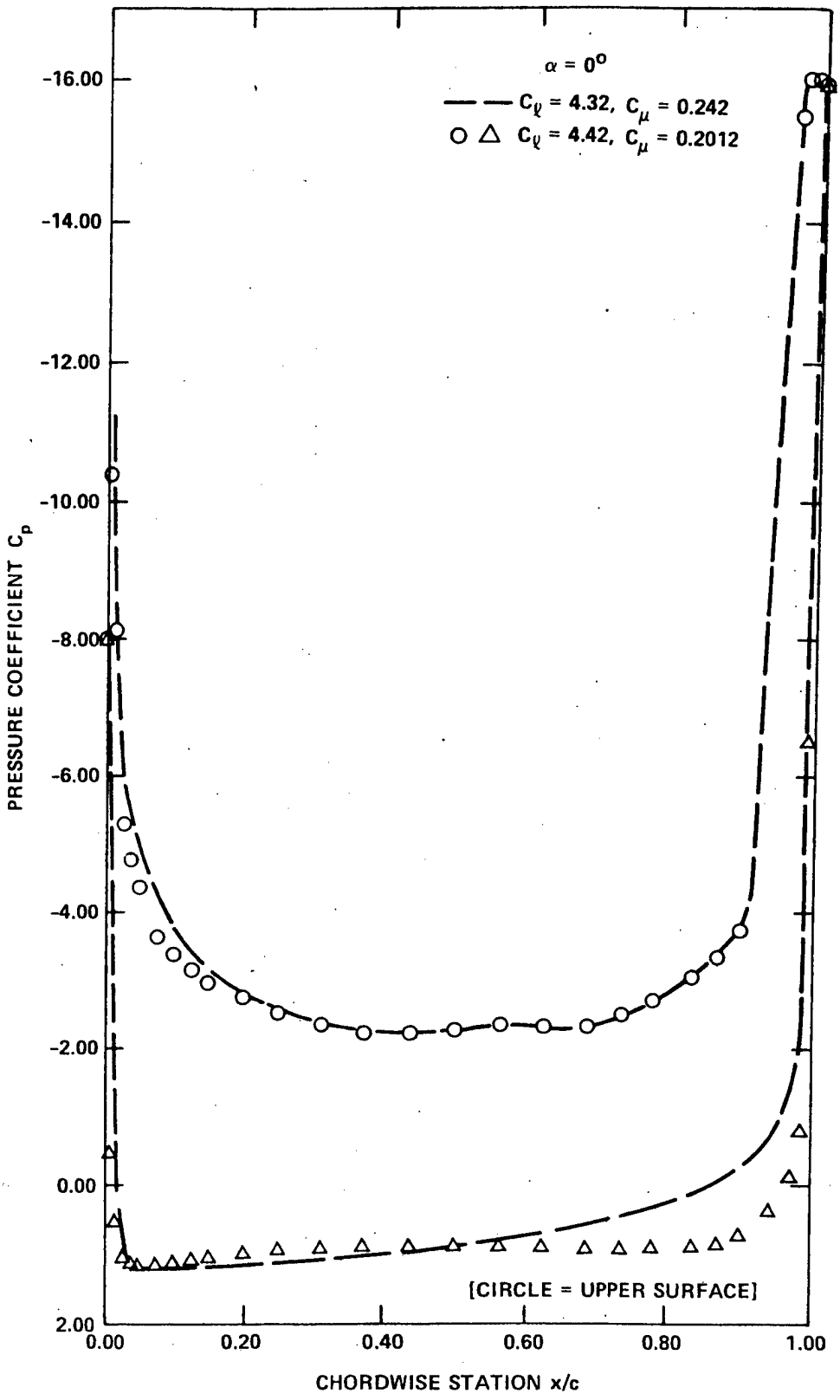

Figure 7. Model NCCR 1510-7067N, experimental pressure distributions from Reference 10.

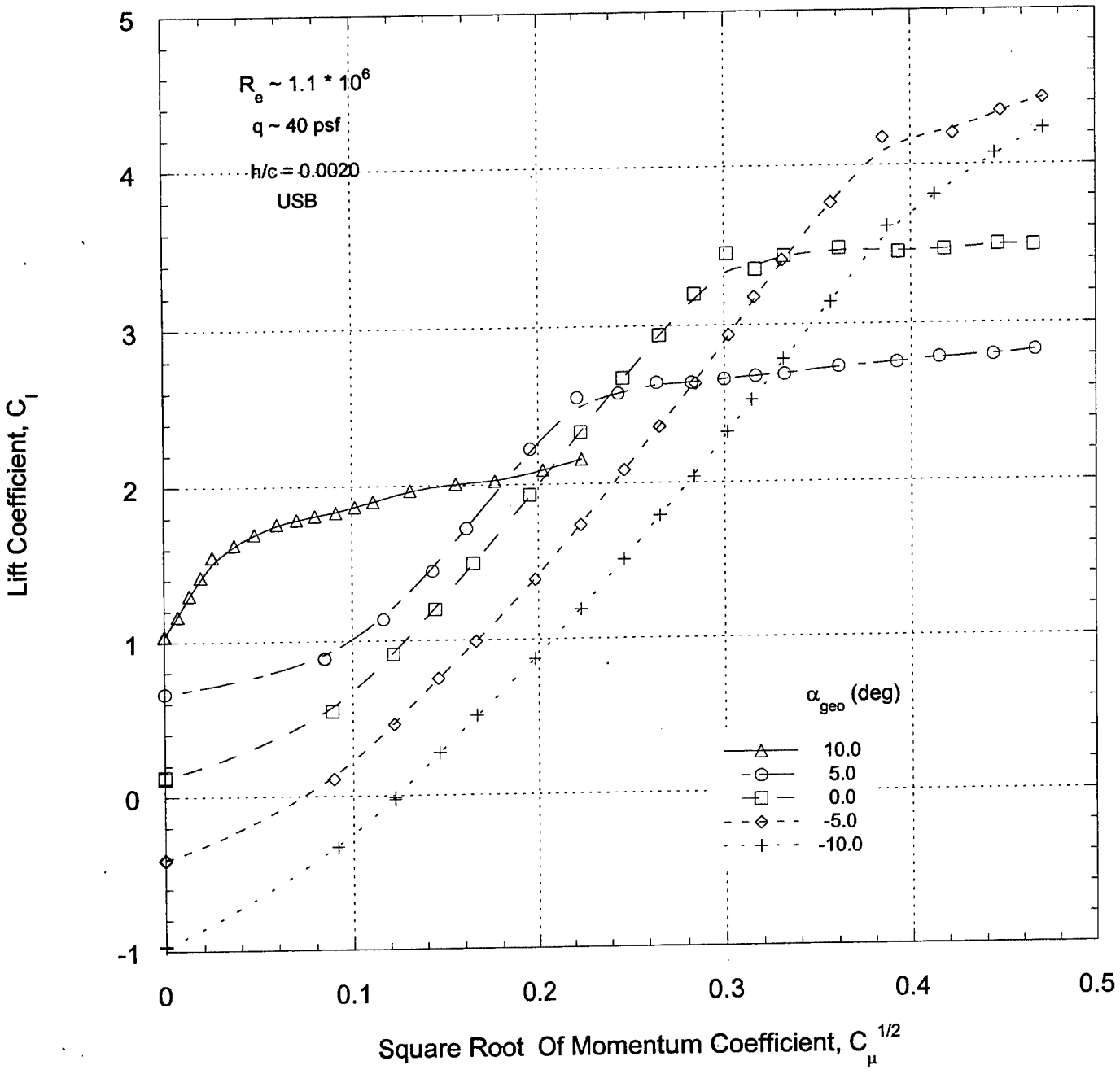

Figure 8a. USB, h/c = 0.0020.

Figure 8. Lift variation with the square root of momentum coefficient.

Figure 8. (Continued)

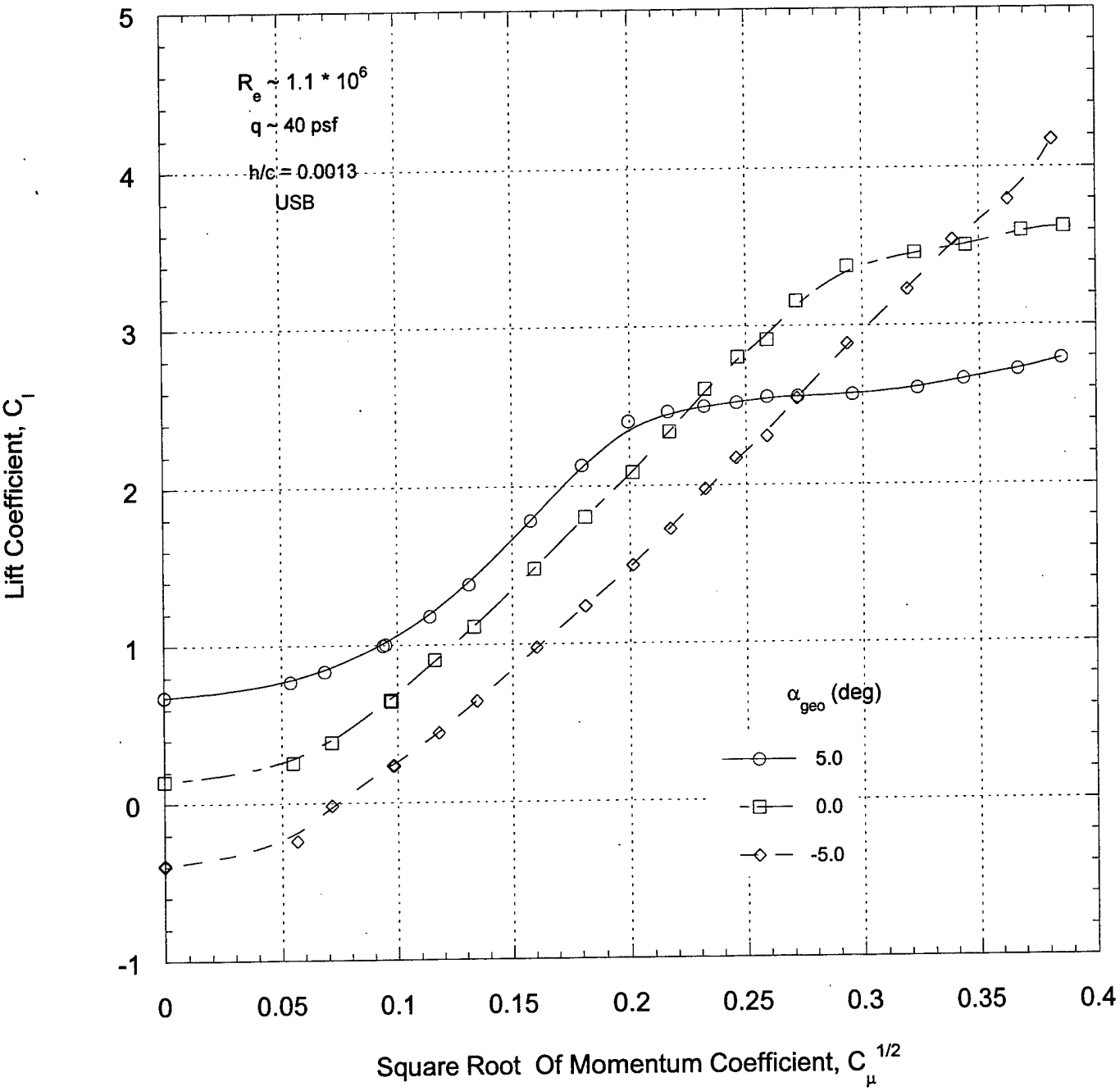

Figure 8b. USB, h/c = 0.0013

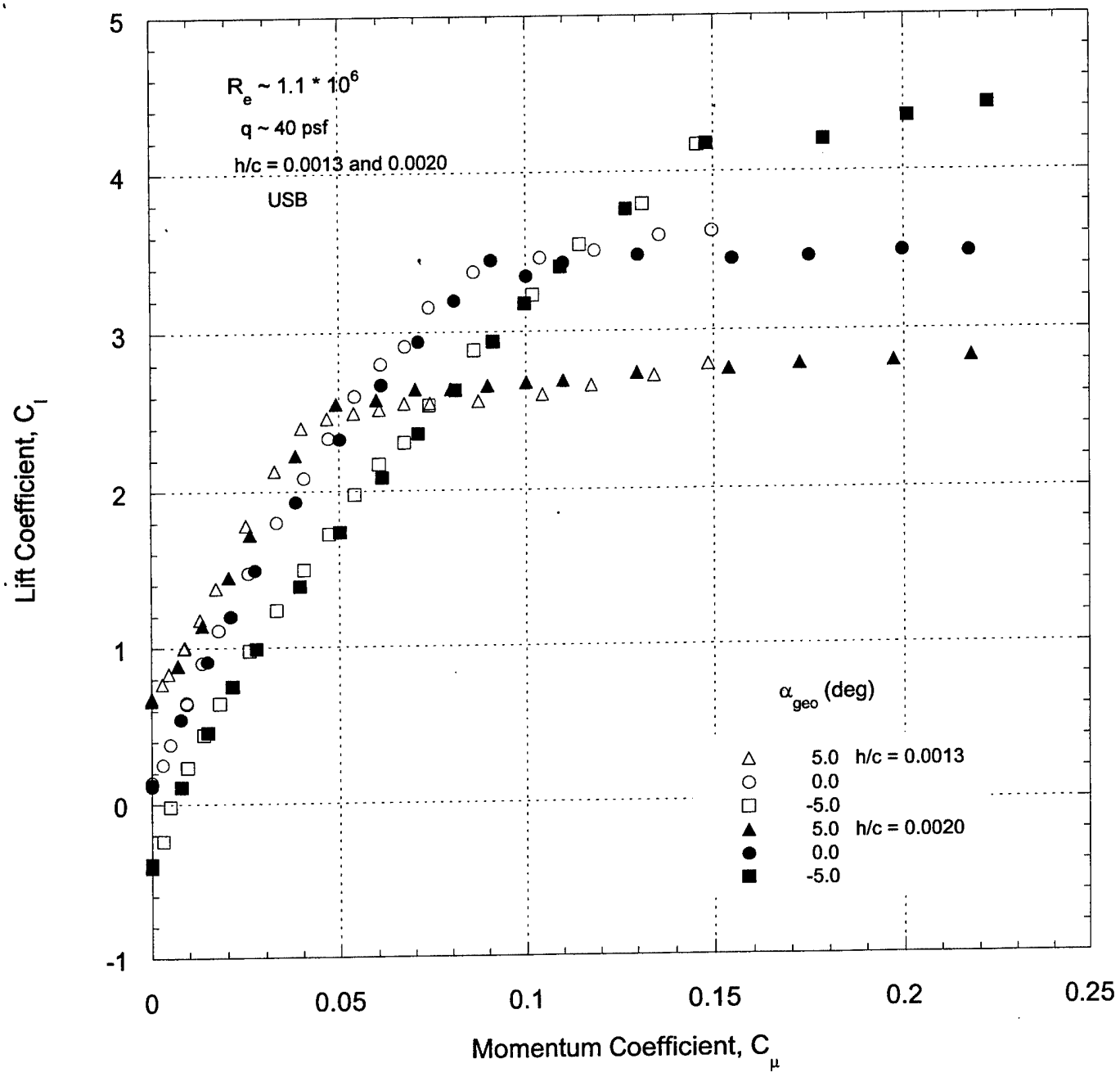

Figure 9. Lift variation as a function of momentum coefficent and slot-height-to-chord ratio for USB.

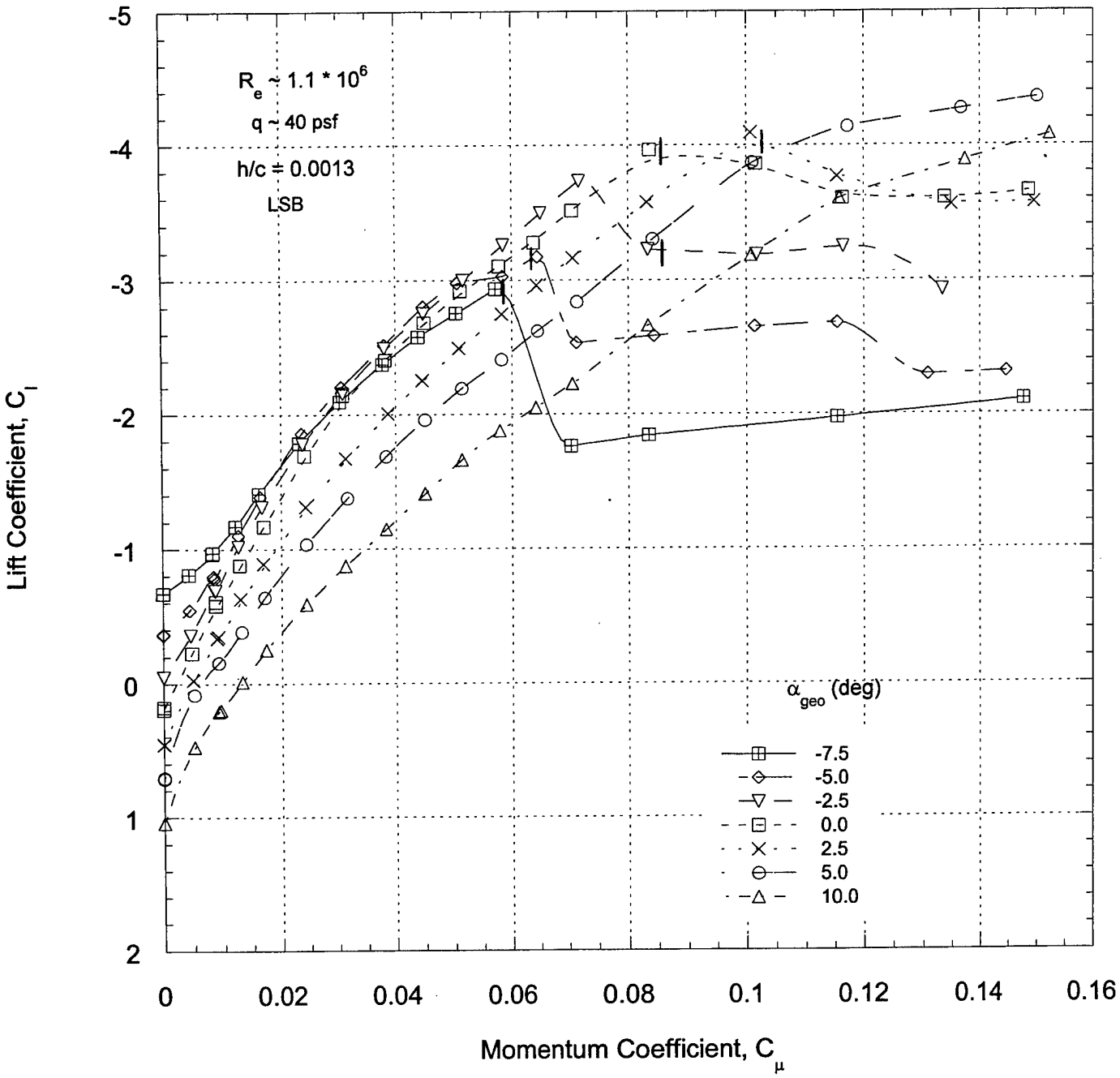

Figure 10a. LSB, h/c = 0.0013.

Figure 10. Lift variation with momentum coefficient.

Figure 10. (Continued)

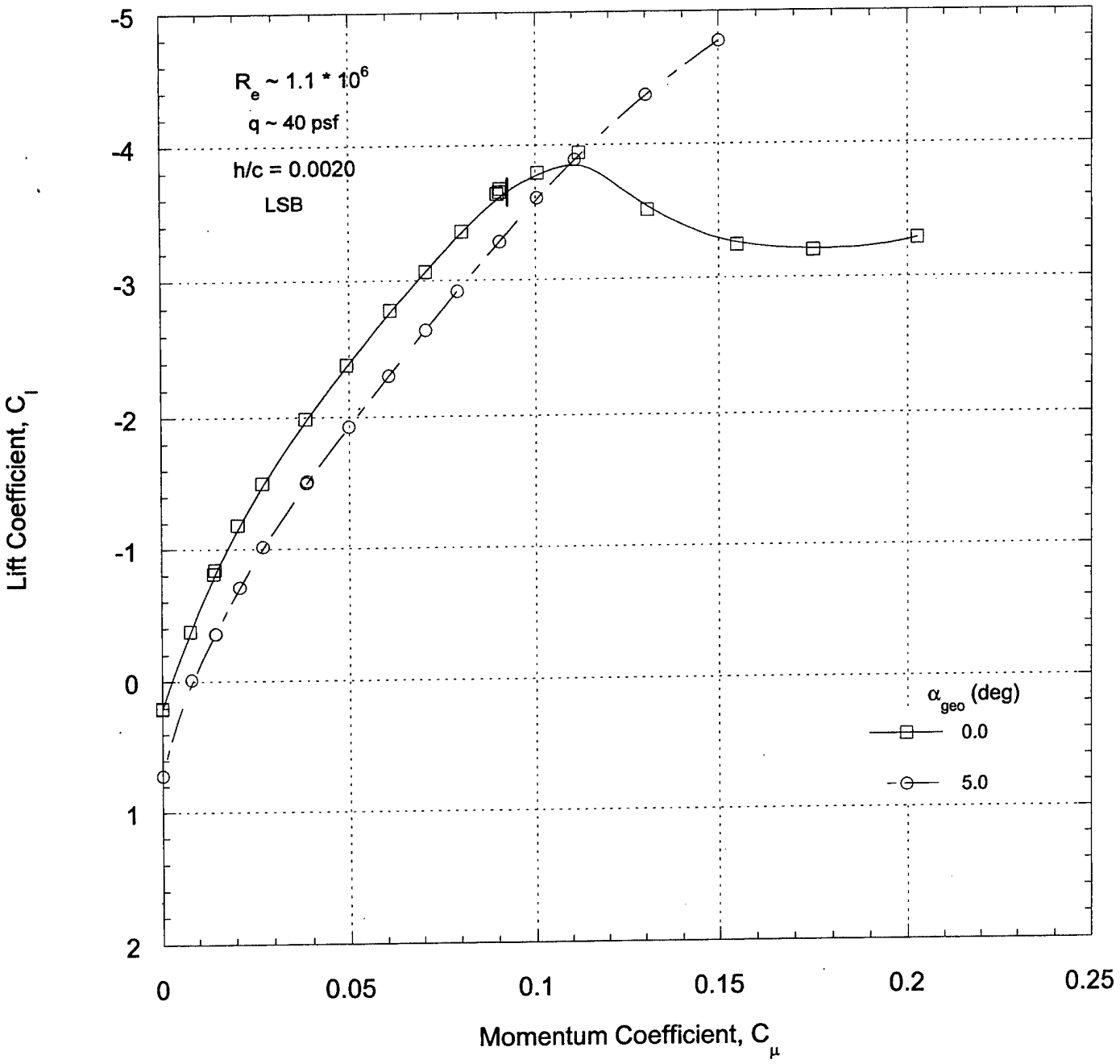

Figure 10b. LSB, h/c = 0.0020.

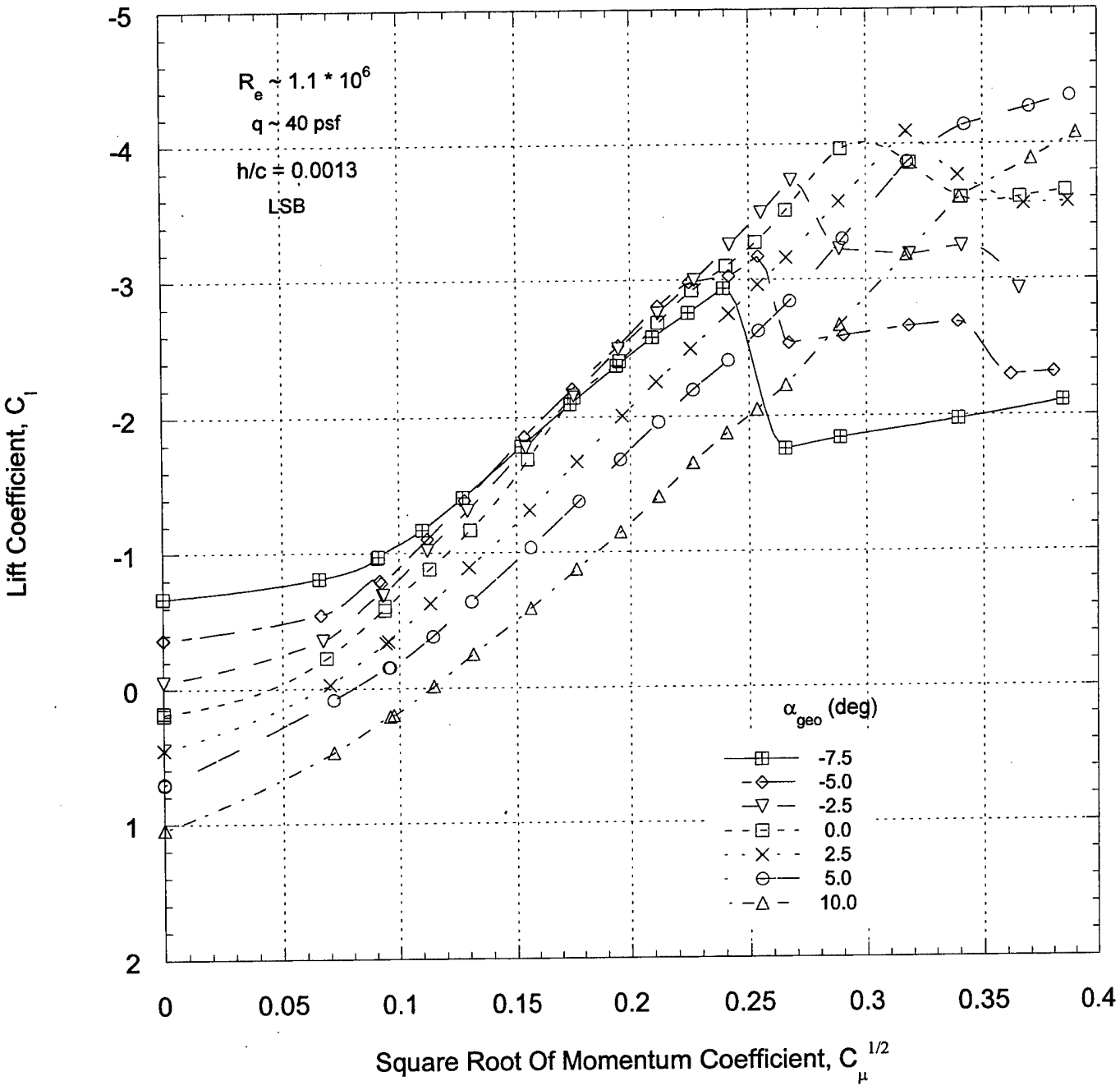

Figure 11a. LSB, h/c = 0.0013.

Figure 11. Lift variation with the square root of momentum coefficient.

Figure 11. (Continued)

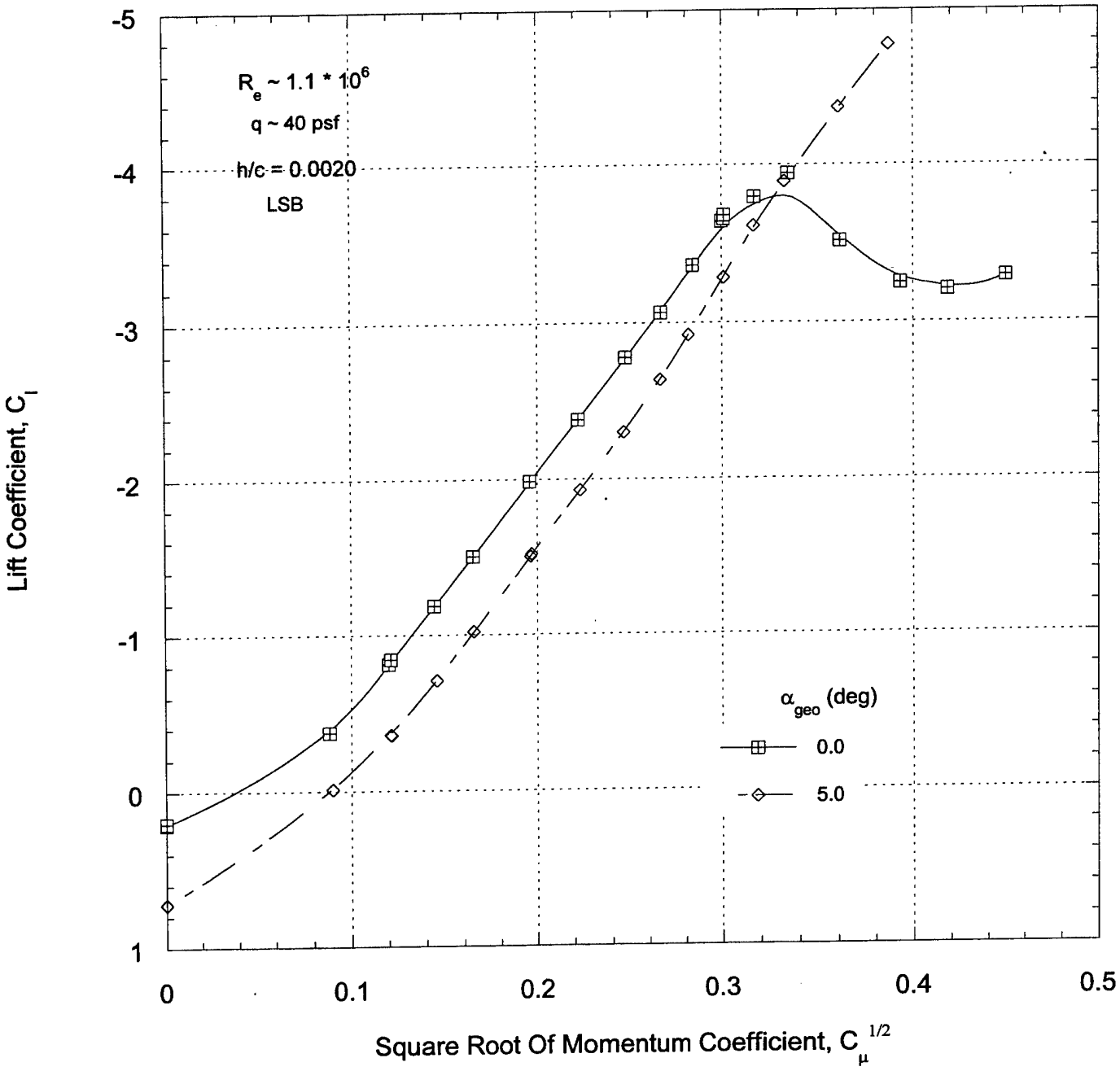

Figure 11b. LSB, h/c = 0.0020

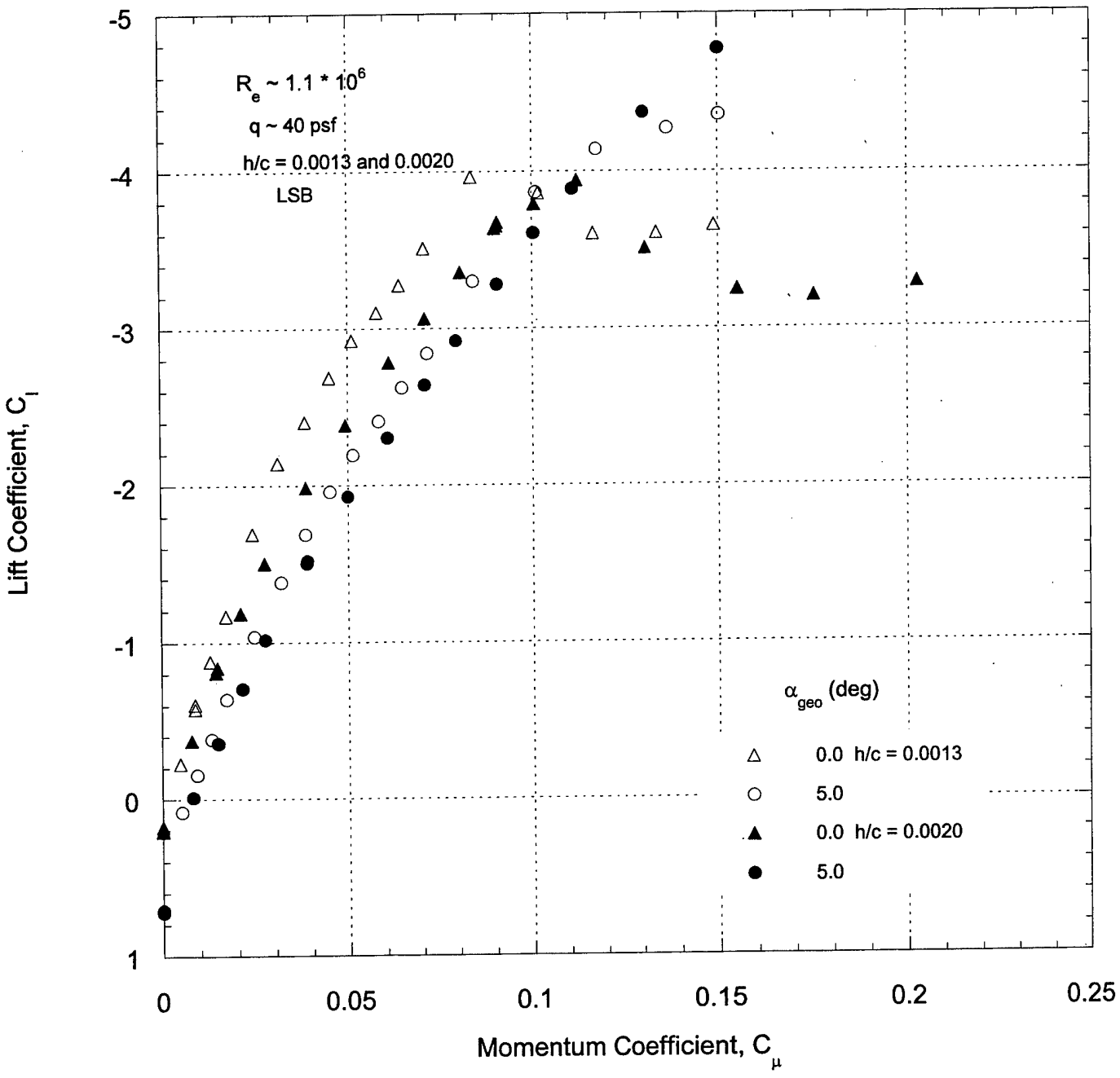

Figure 12. Lift variation as a function of momentum coefficent and slot height-to chord ratio for LSB.

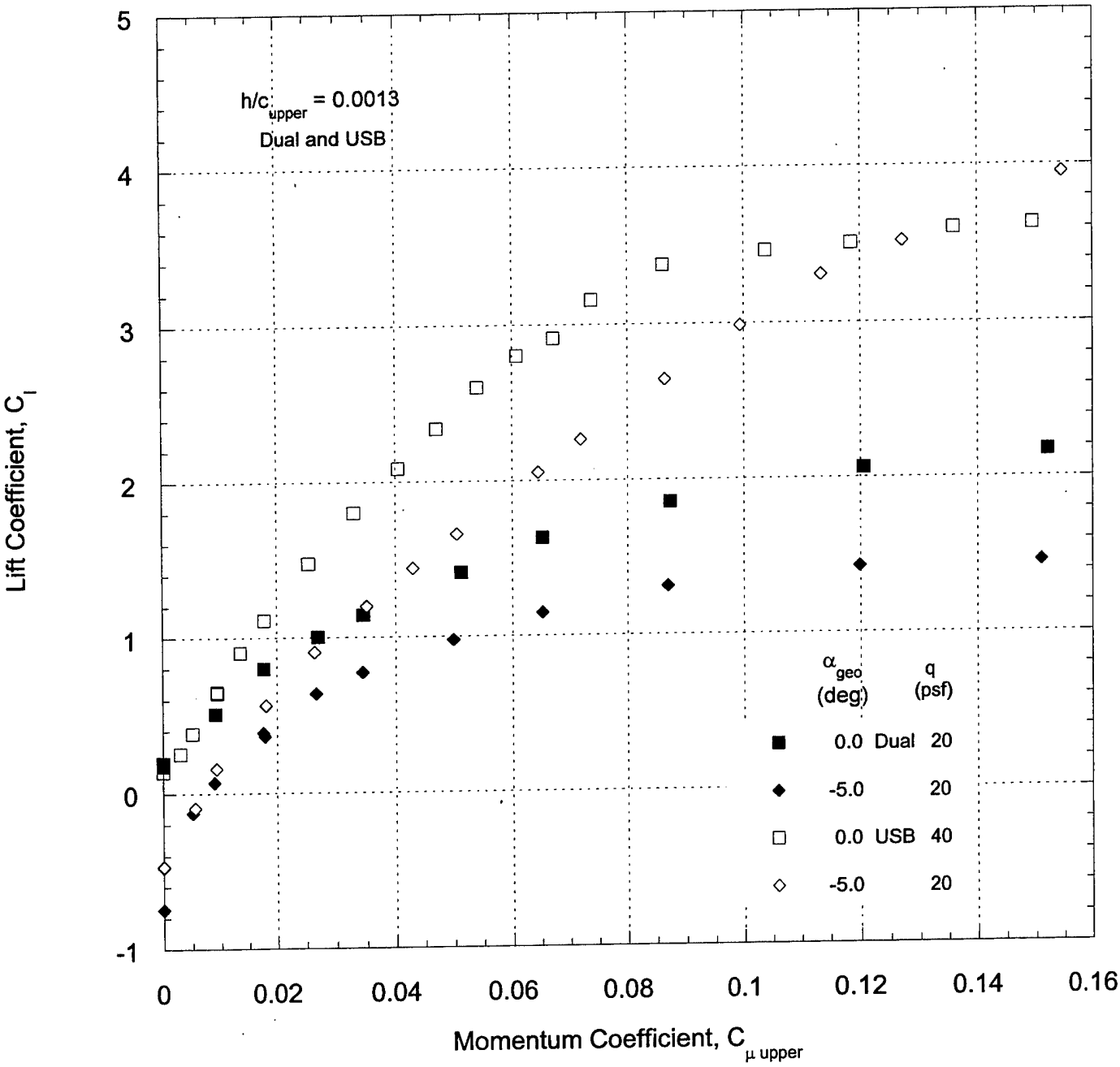

Figure 13. Lift coefficient for dual and upper surface blowing.

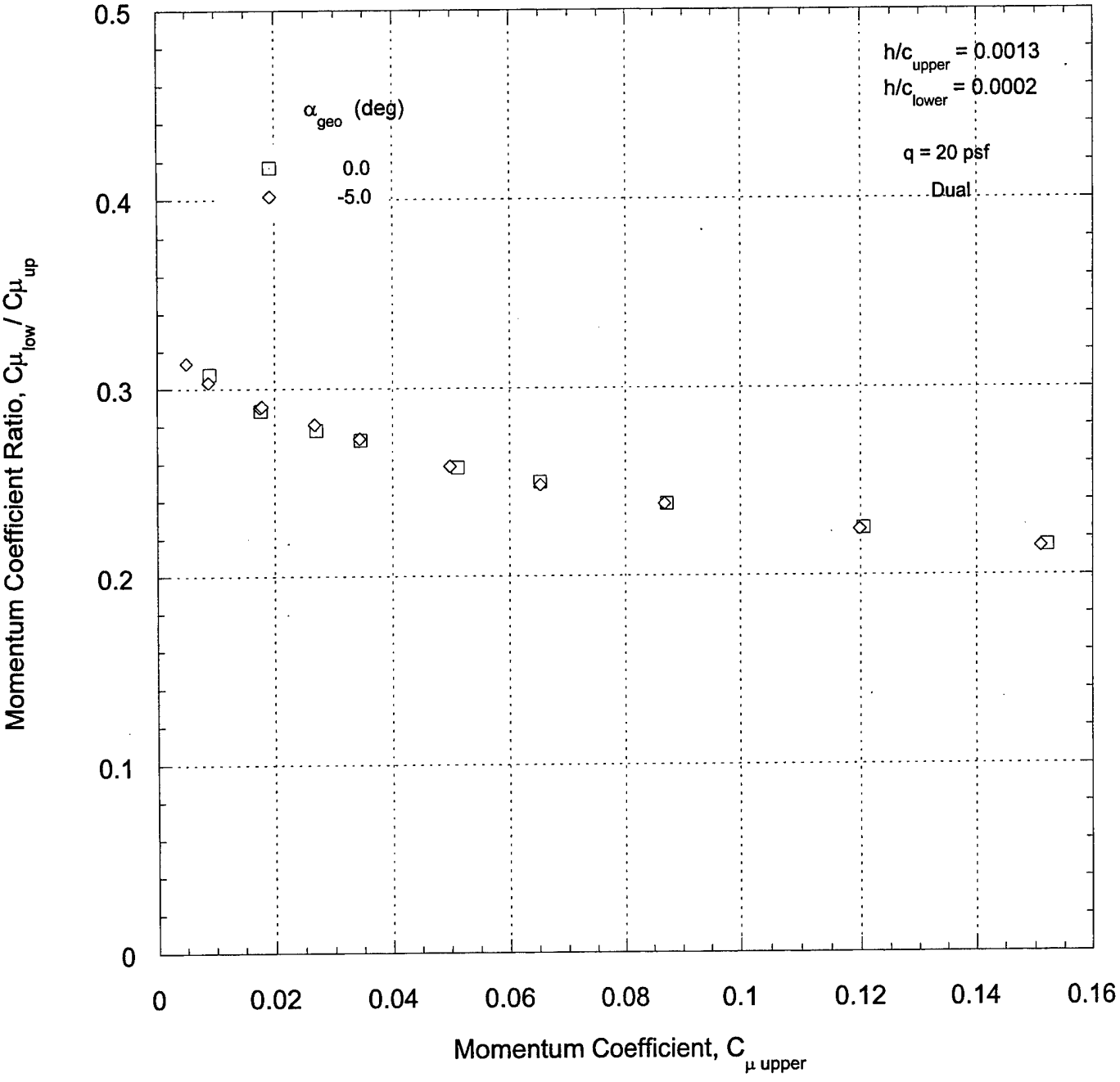

Figure 14. Ratio of upper to lower slot momentum coefficient when using dual blowing.

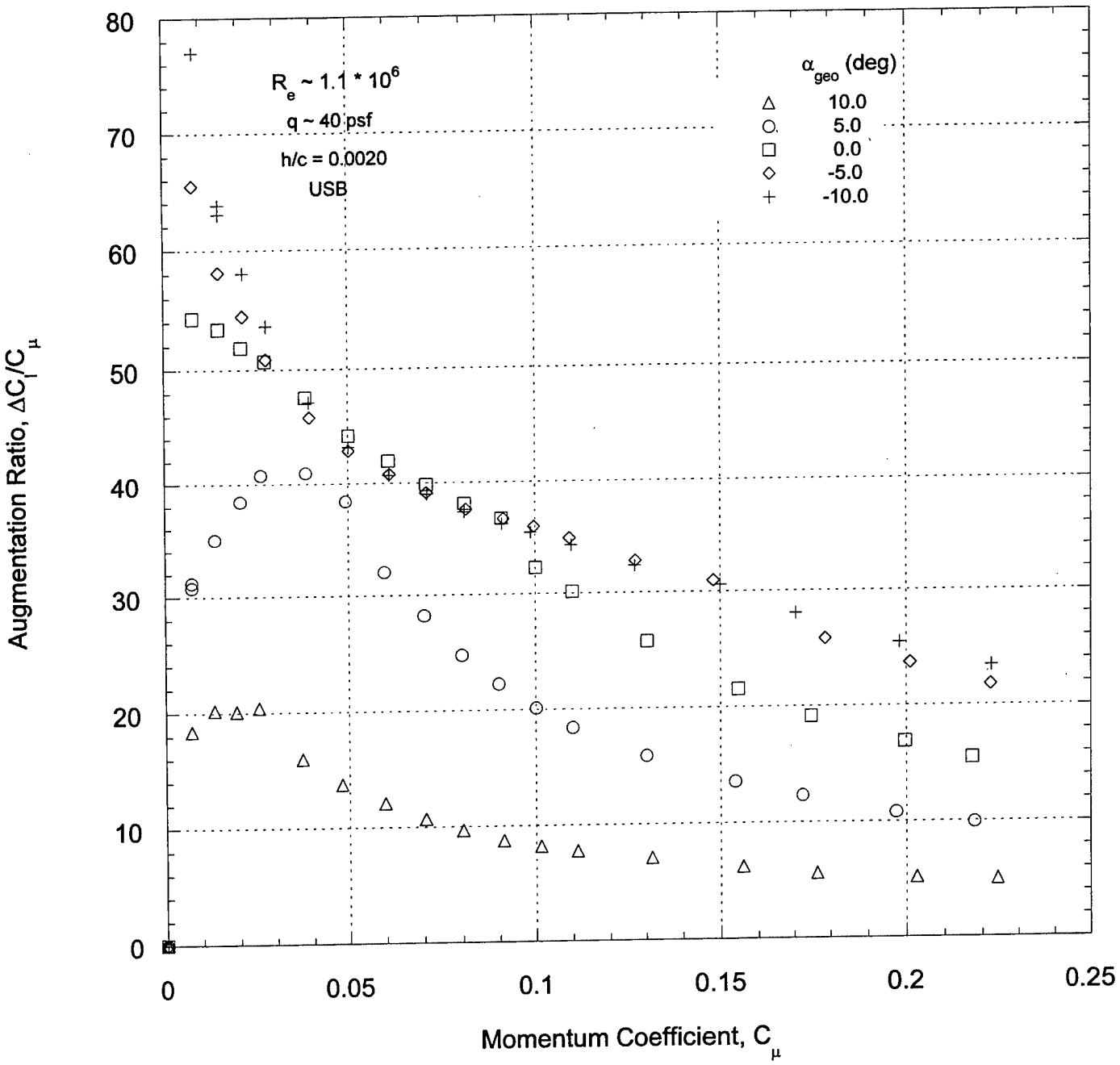

Figure 15a. USB, h/c = 0.0020

Figure 15. Lift augmentation ratio.

Figure 15. (Continued)

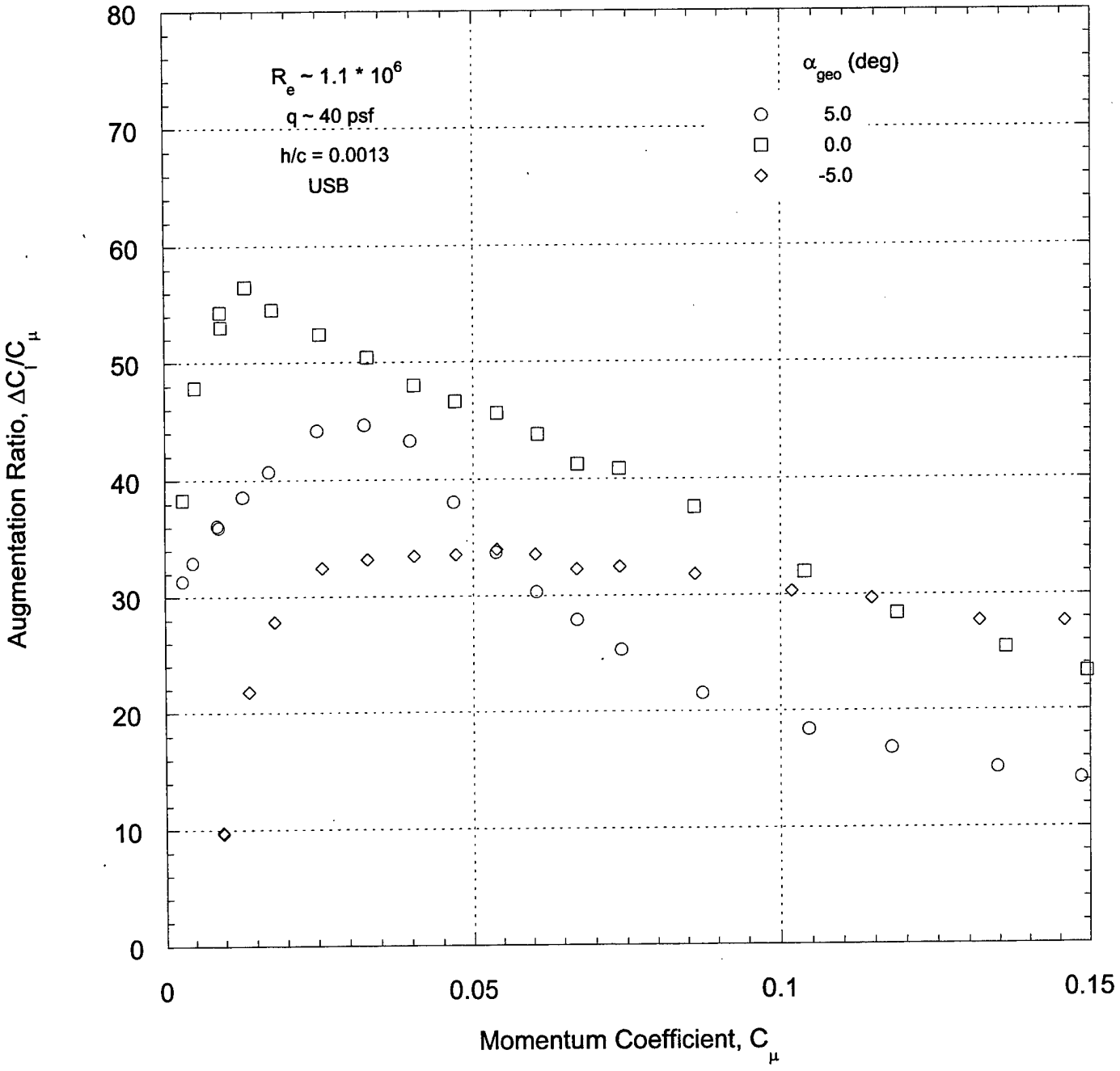

Figure 15b. USB, h/c=0.0013

Figure 15. (Continued)

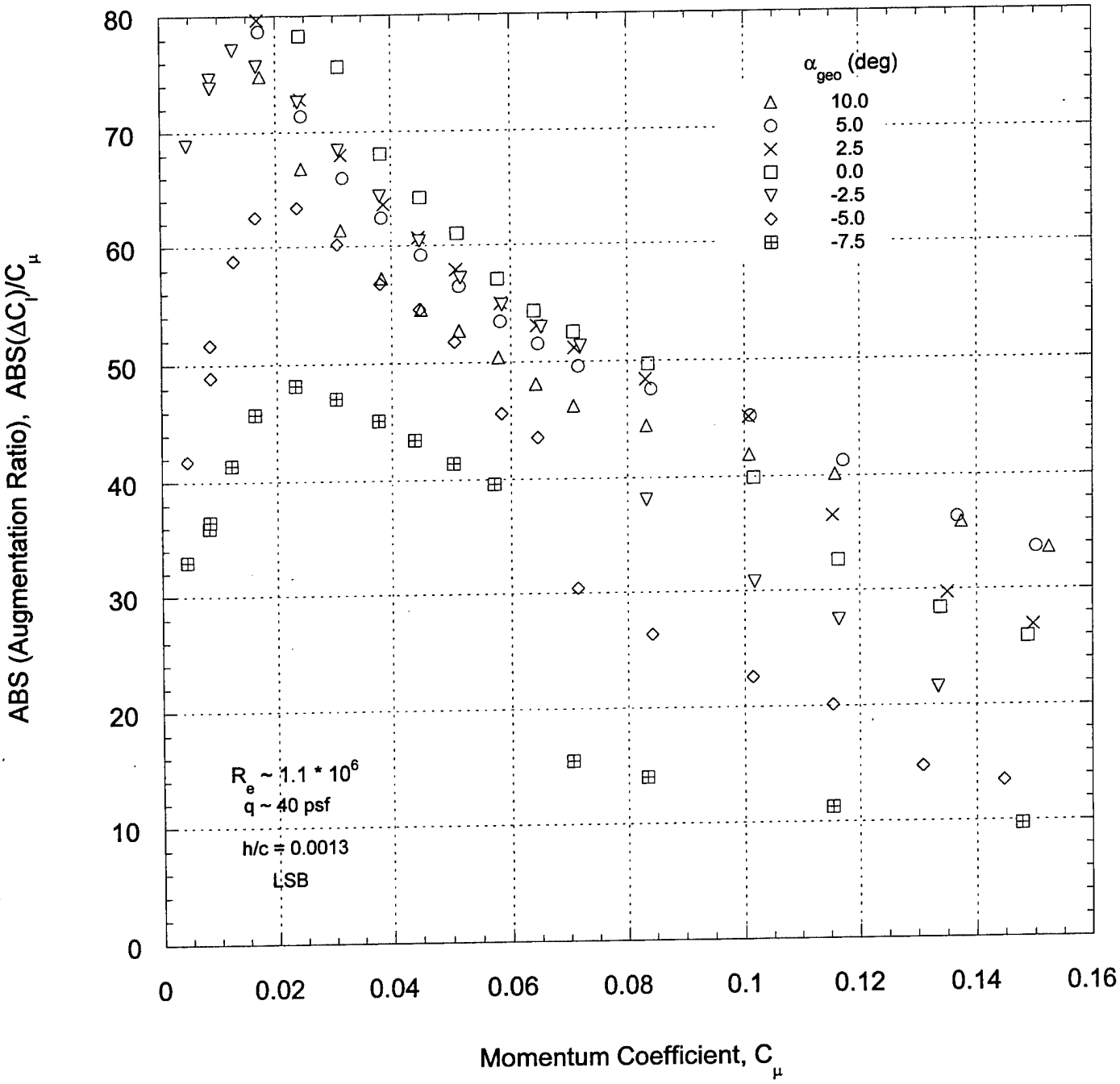

Figure 15c. LSB, h/c = 0.0013

Figure 15. (Continued)

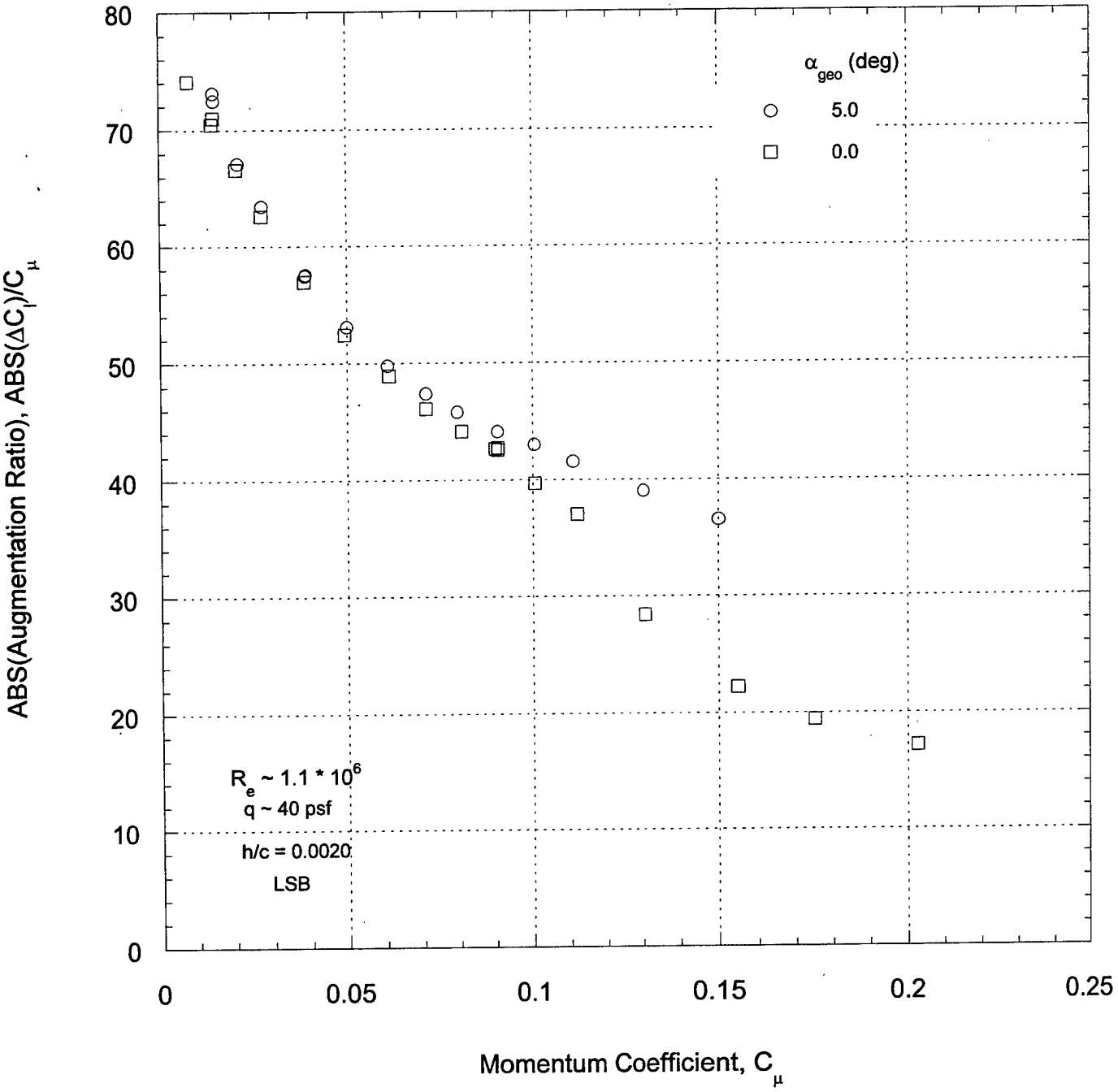

Figure 15d. LSB, h/c = 0.0020.

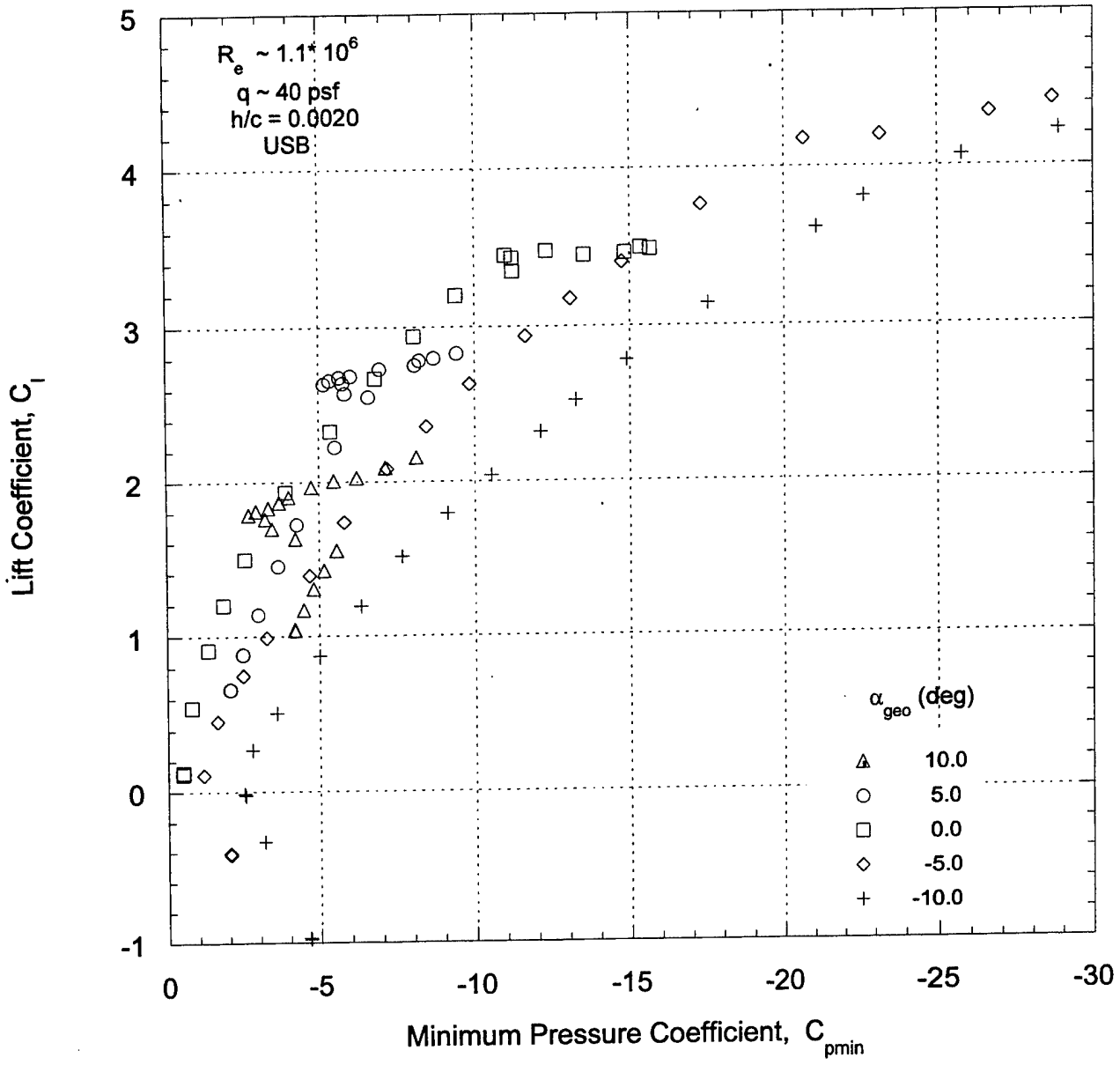

Figure 16a. USB, h/c = 0.0020.

Figure 16. Minimum pressure coefficient as a function of lift.

Figure 16. (Continued)

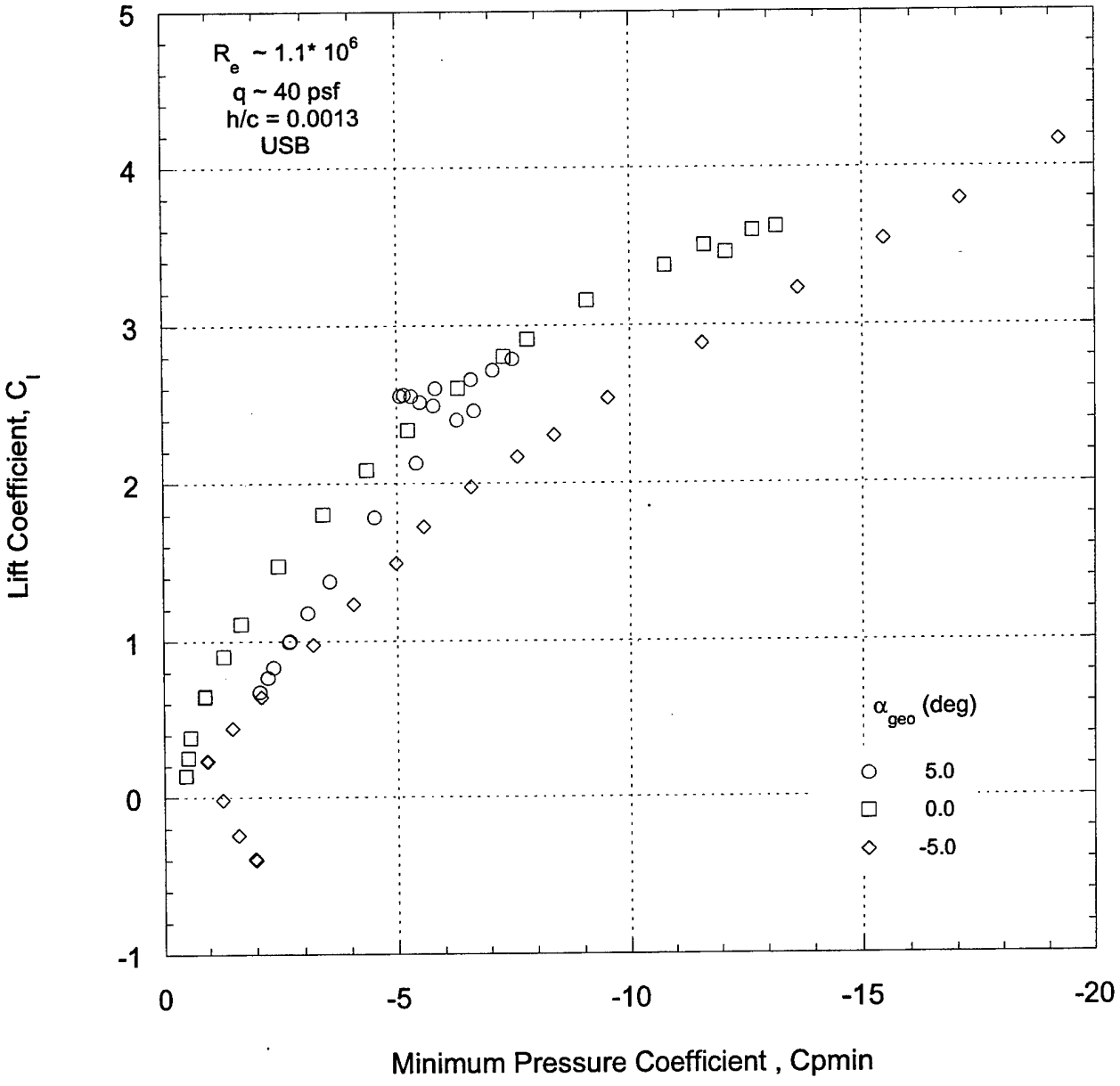

Figure 16b. USB, h/c = 0.0013.

Figure 16. (Continued)

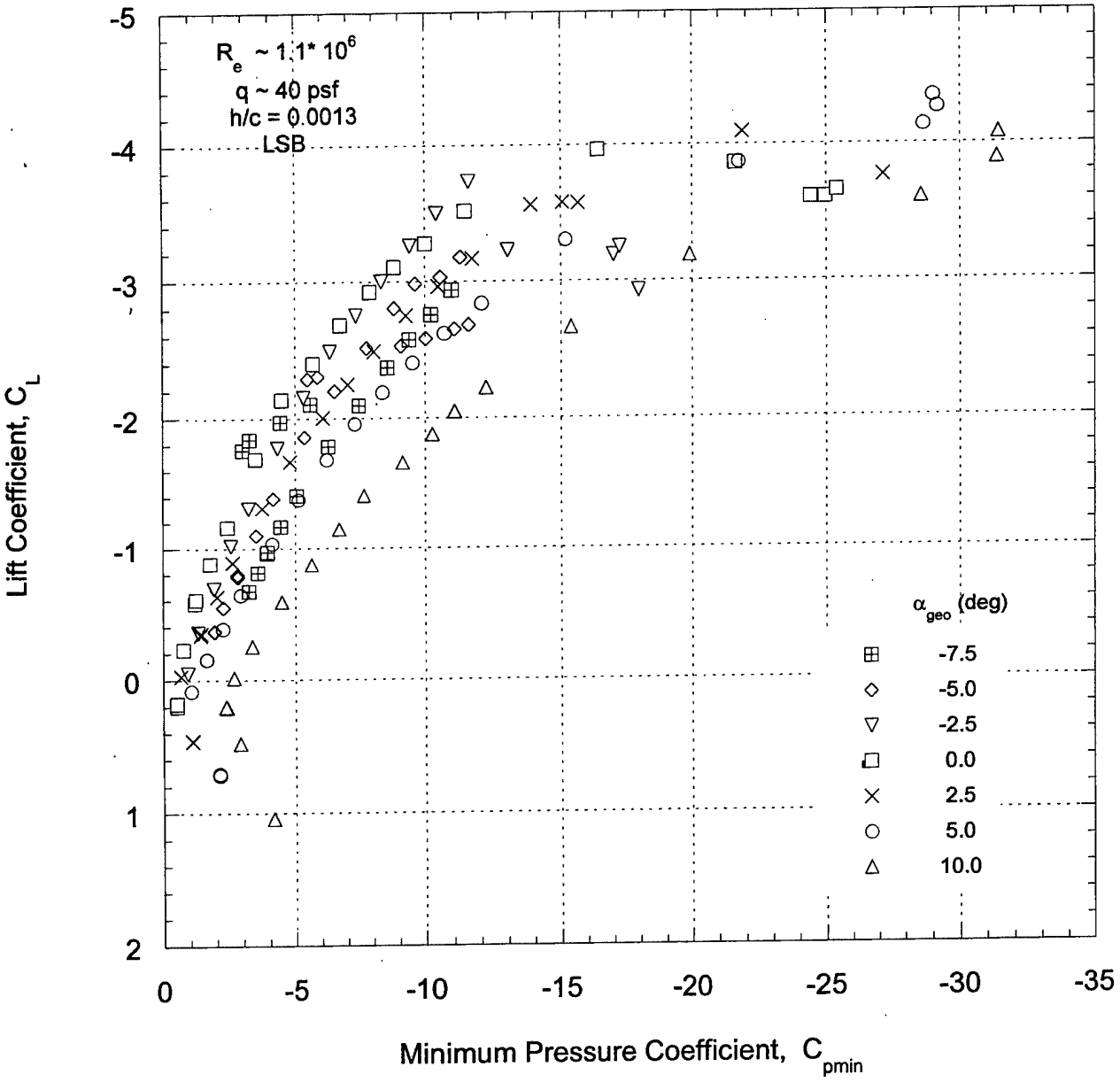

Figure 16c. LSB, h/c = 0.0013

Figure 16. (Continued)

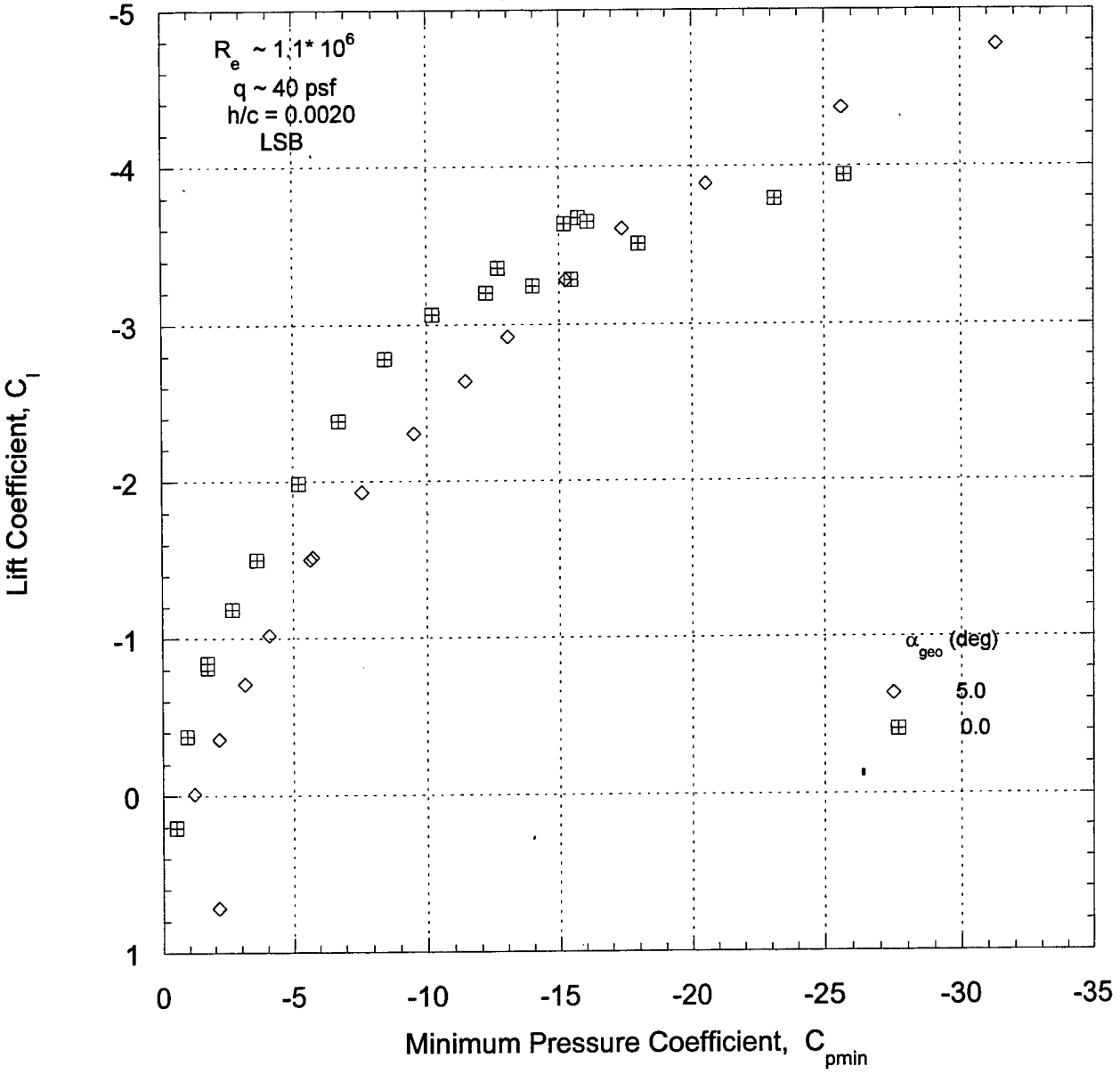

Figure 16d. LSB, h/c = 0.0020

Figure 16. (Continued)

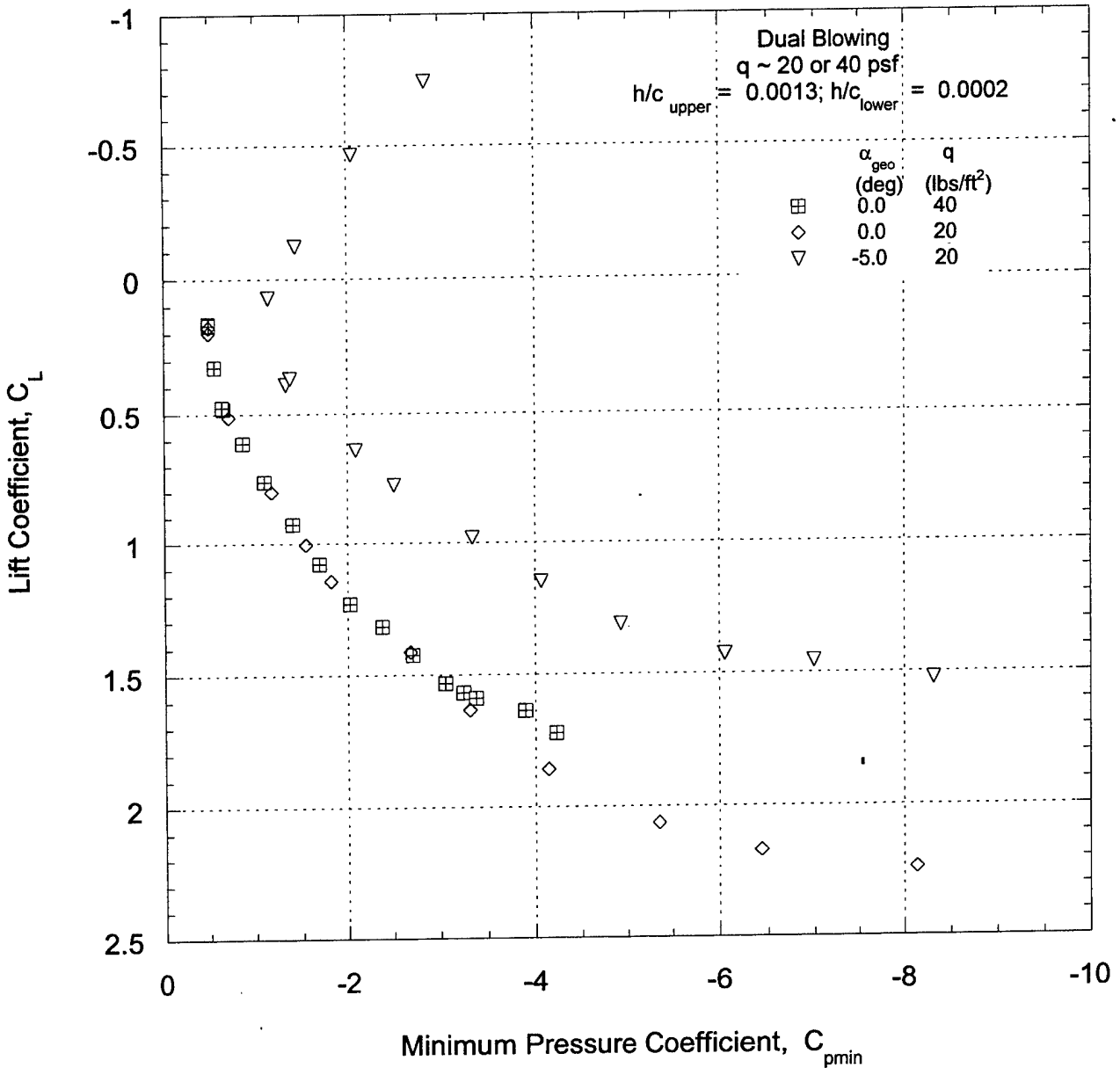

Figure 16e. Dual blowing.

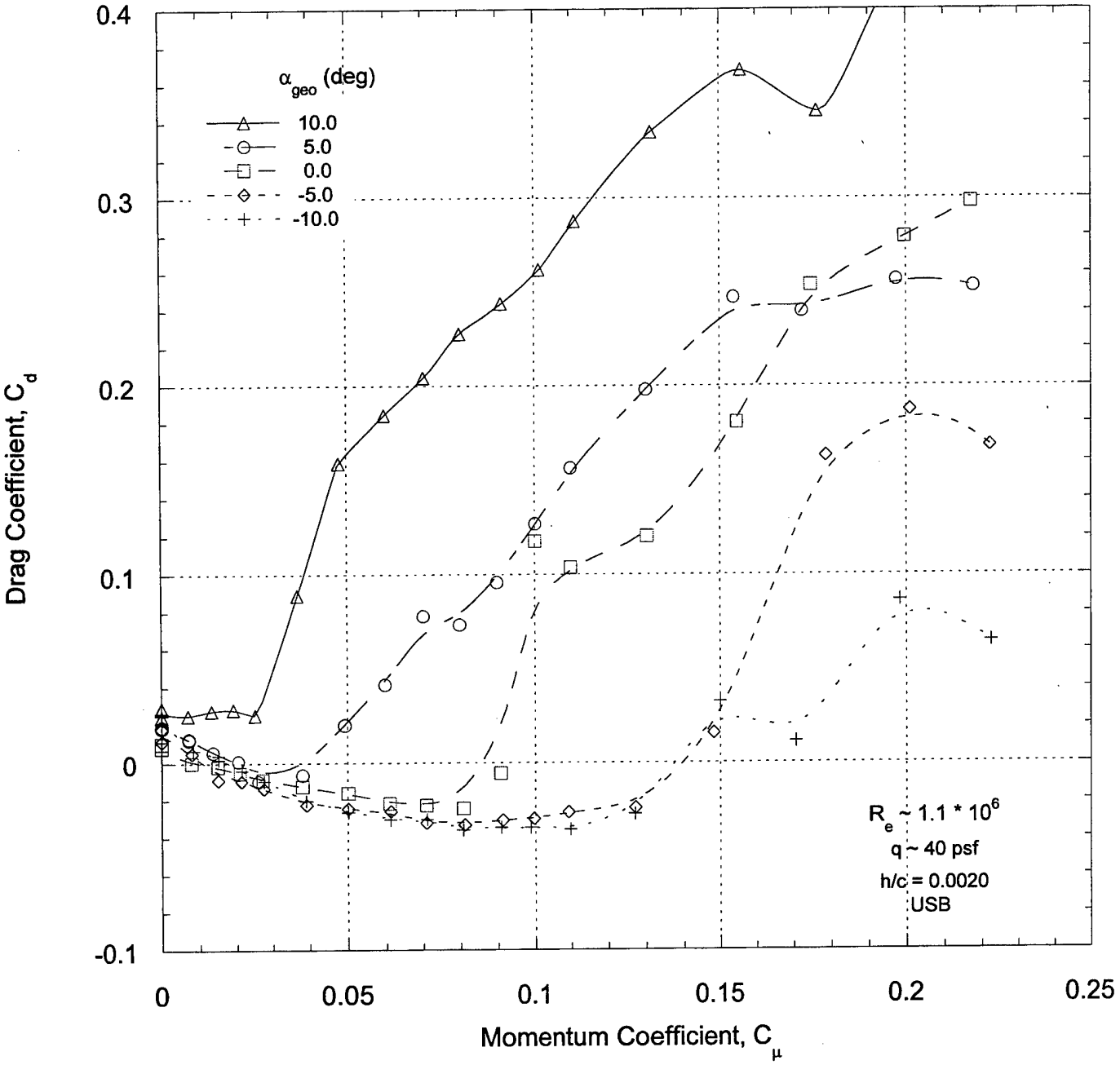

Figure 17a. USB, h/c = 0.0020.

Figure 17. Drag coefficient variation with momentum coefficient.

Figure 17. (Continued)

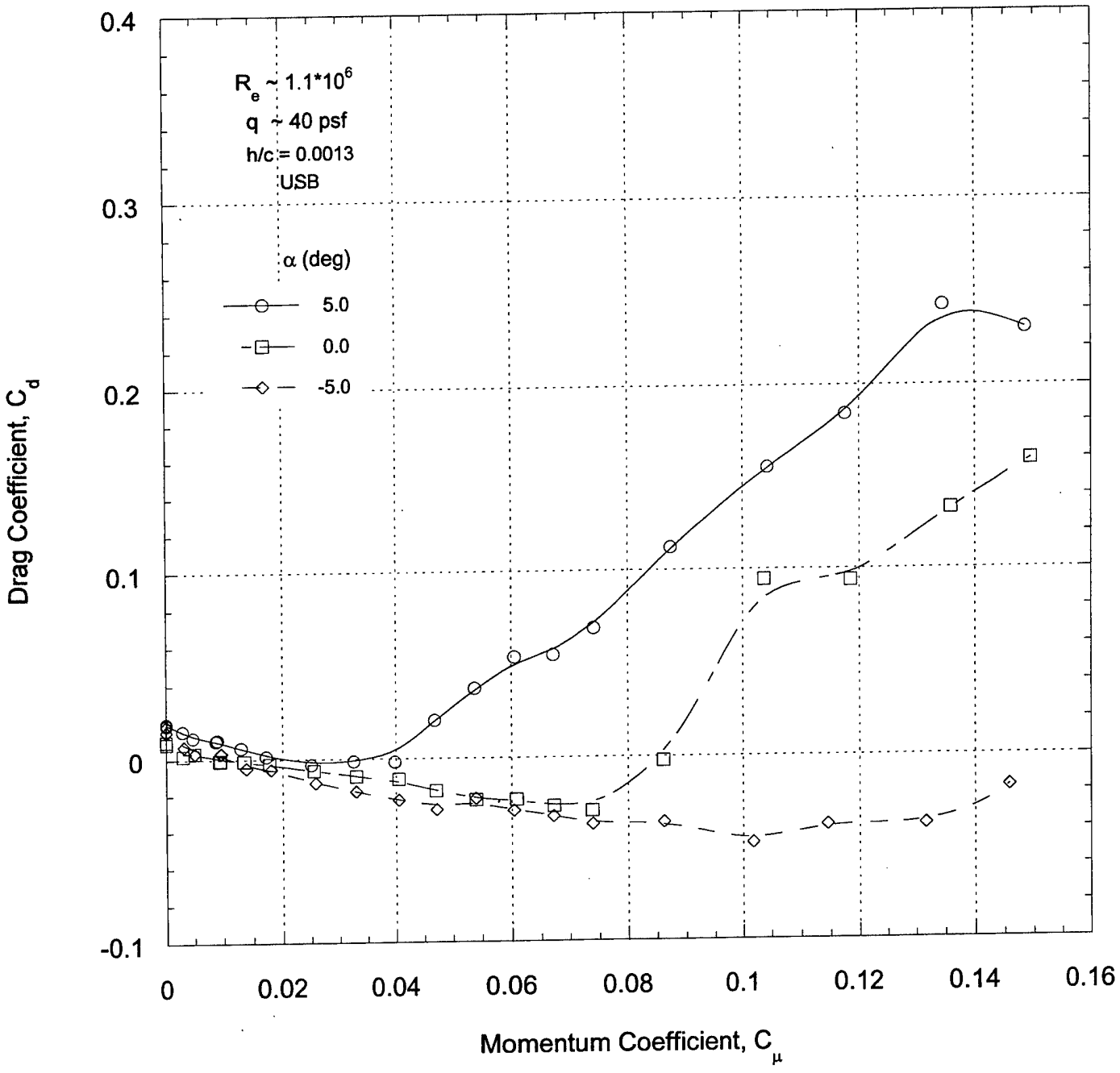

Figure 17b. USB, h/c =0.0013.

Figure 17. (Contrinued)

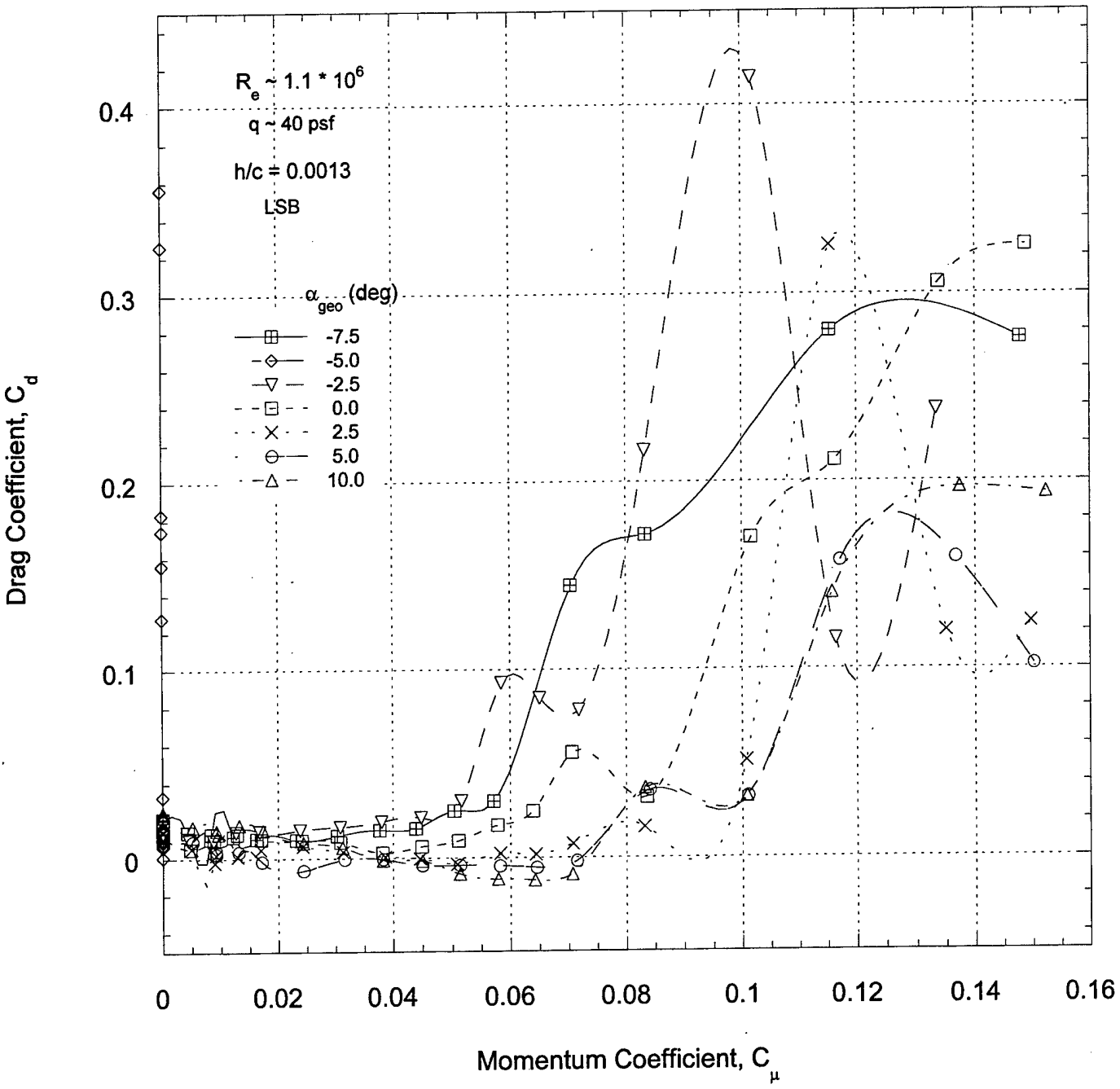

Figure 17c. LSB, h/c = 0.0013.

Figure 17. (Continued)

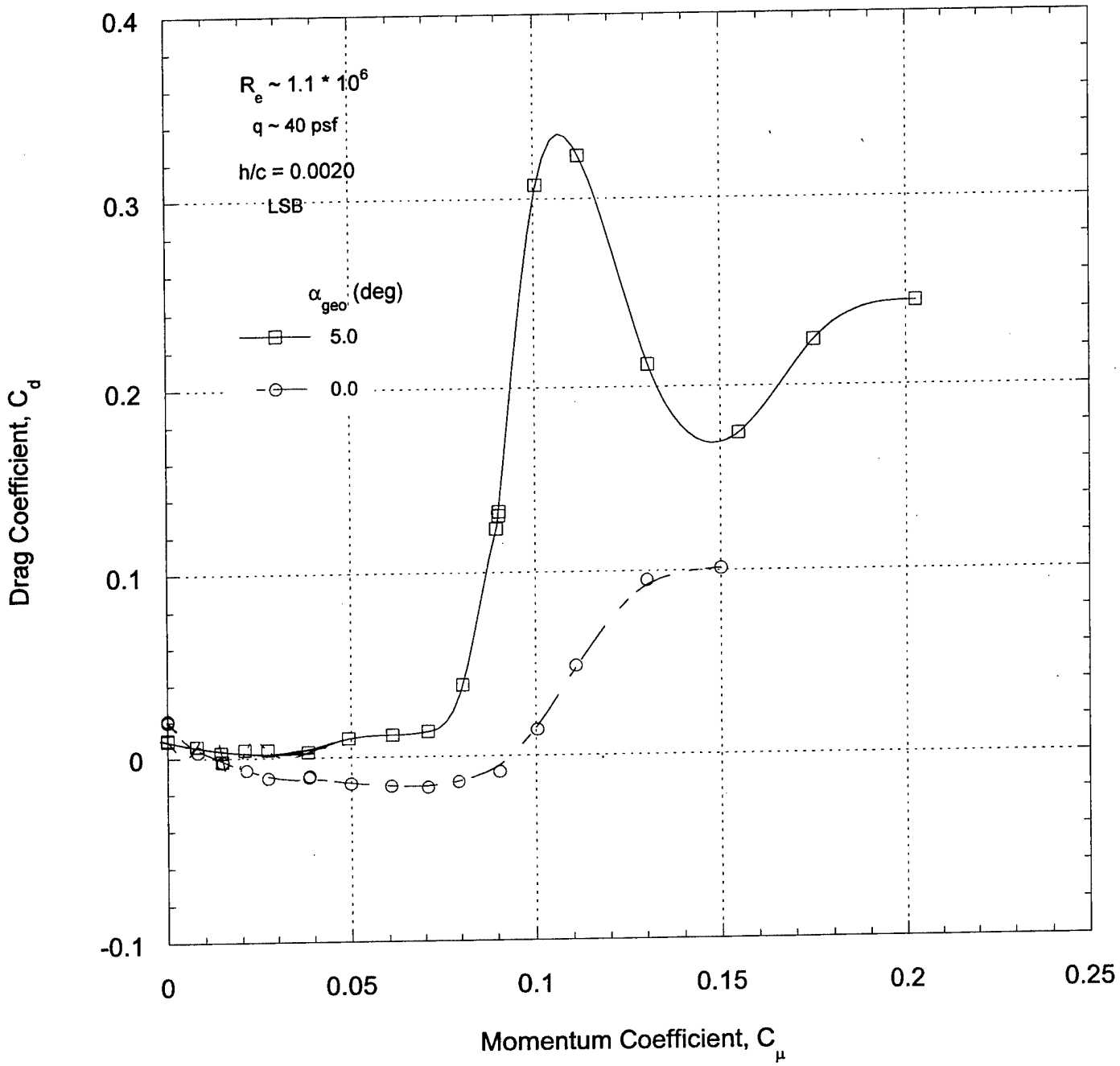

Figure 17d. LSB, h/c = 0.0020.

Figure 17. (Continued)

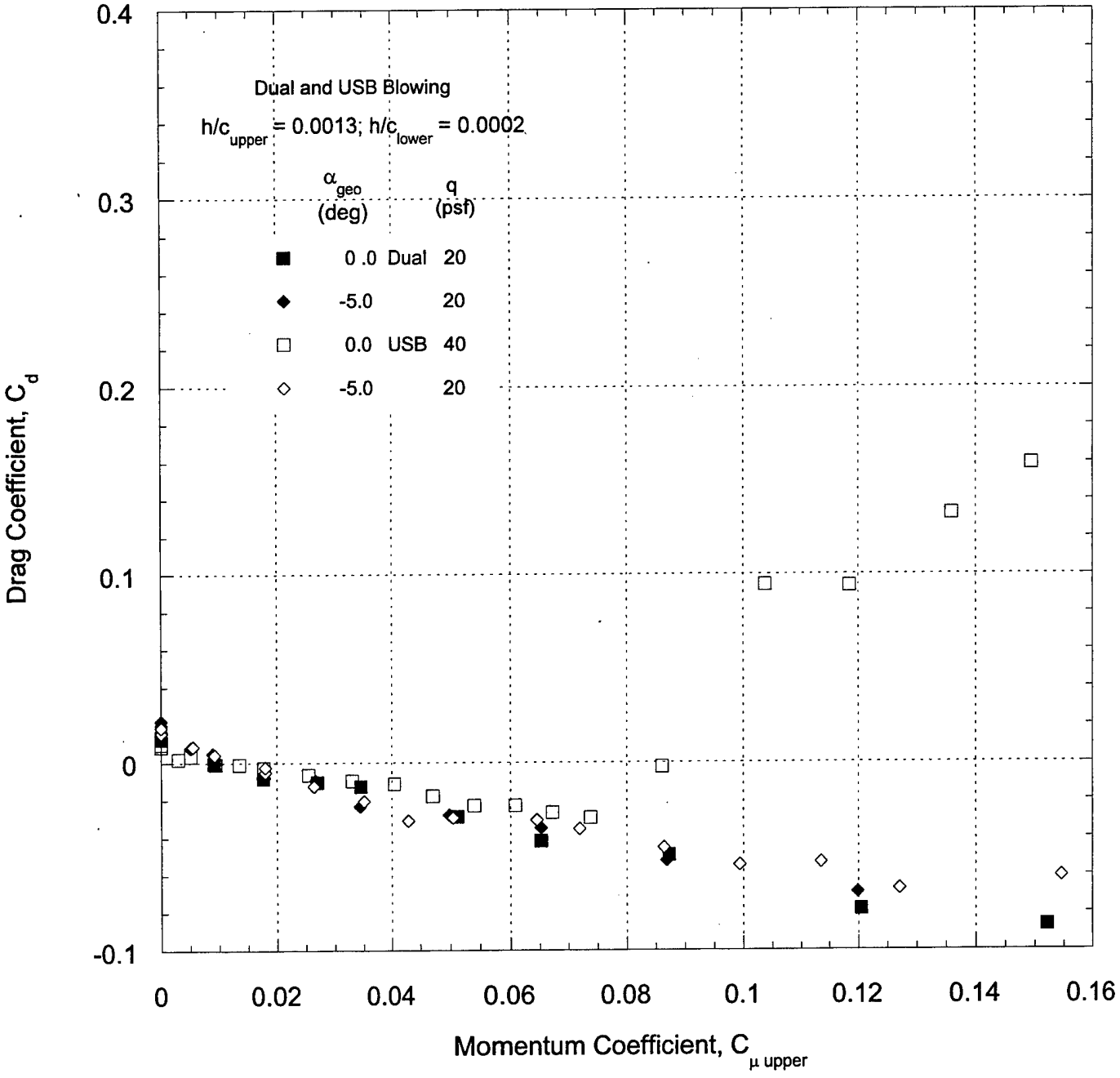

Figure 17e. Dual Blowing, h/c_{upper} = 0.0013 and h/c_{lower} = 0.0002.

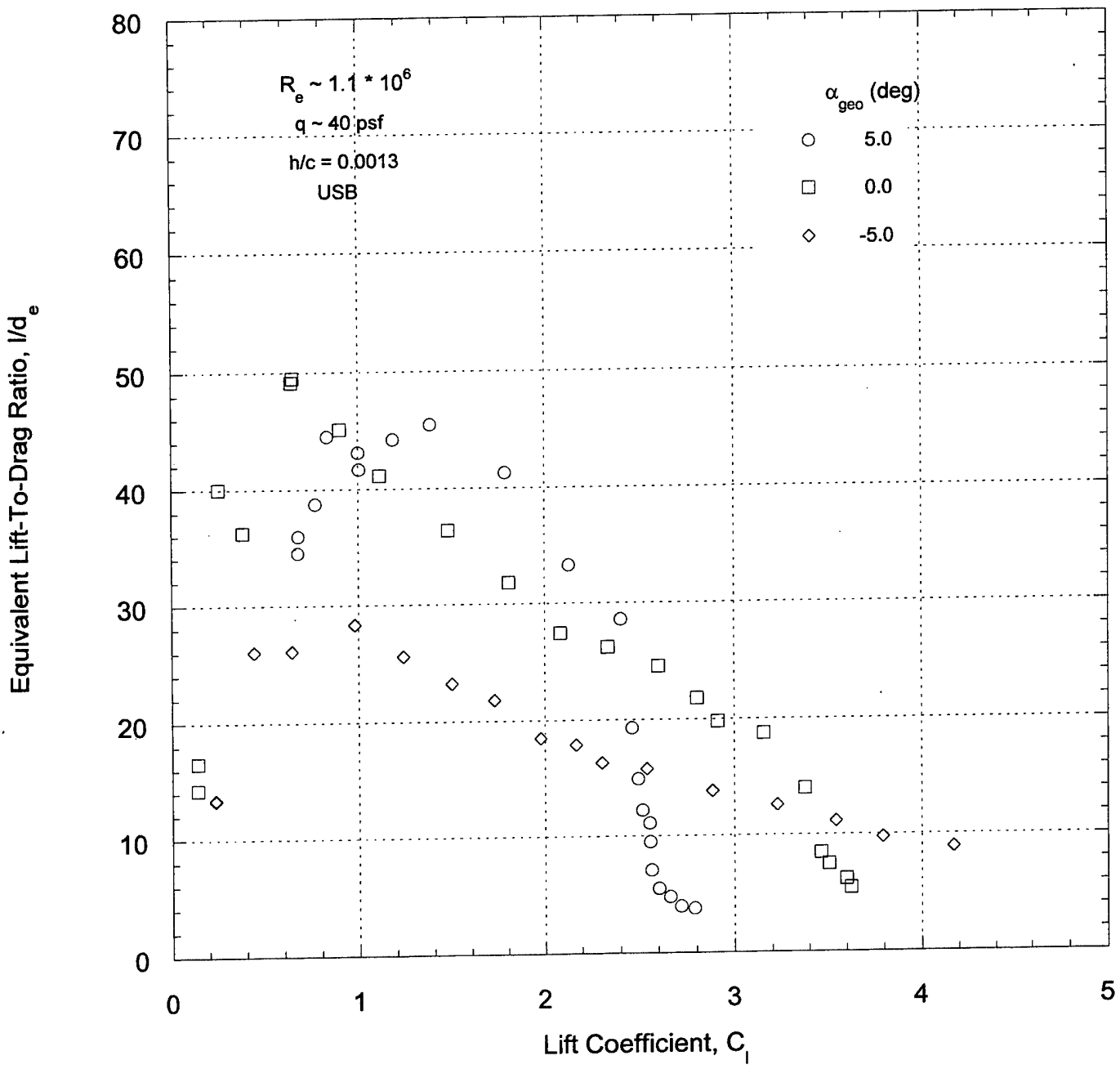

Figure 18. Equivalent lift-to-drag ratio for USB at h/c = 0.0013.

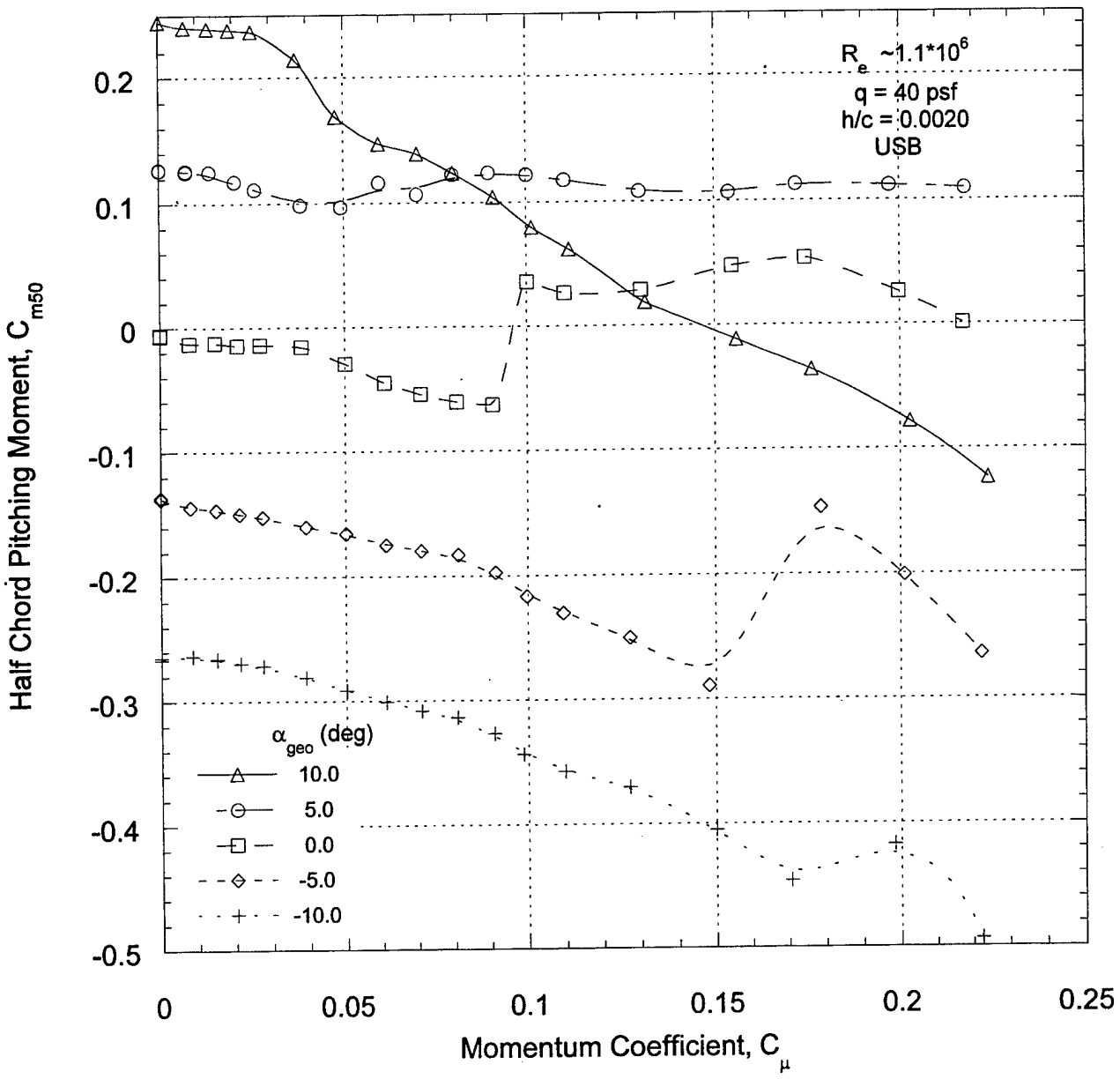

Figure 19a. USB, h/c = 0.0020.

Figure 19. Variation in half-chord pitching moment as a function of momentum coefficient.

Figure 19. (Continued)

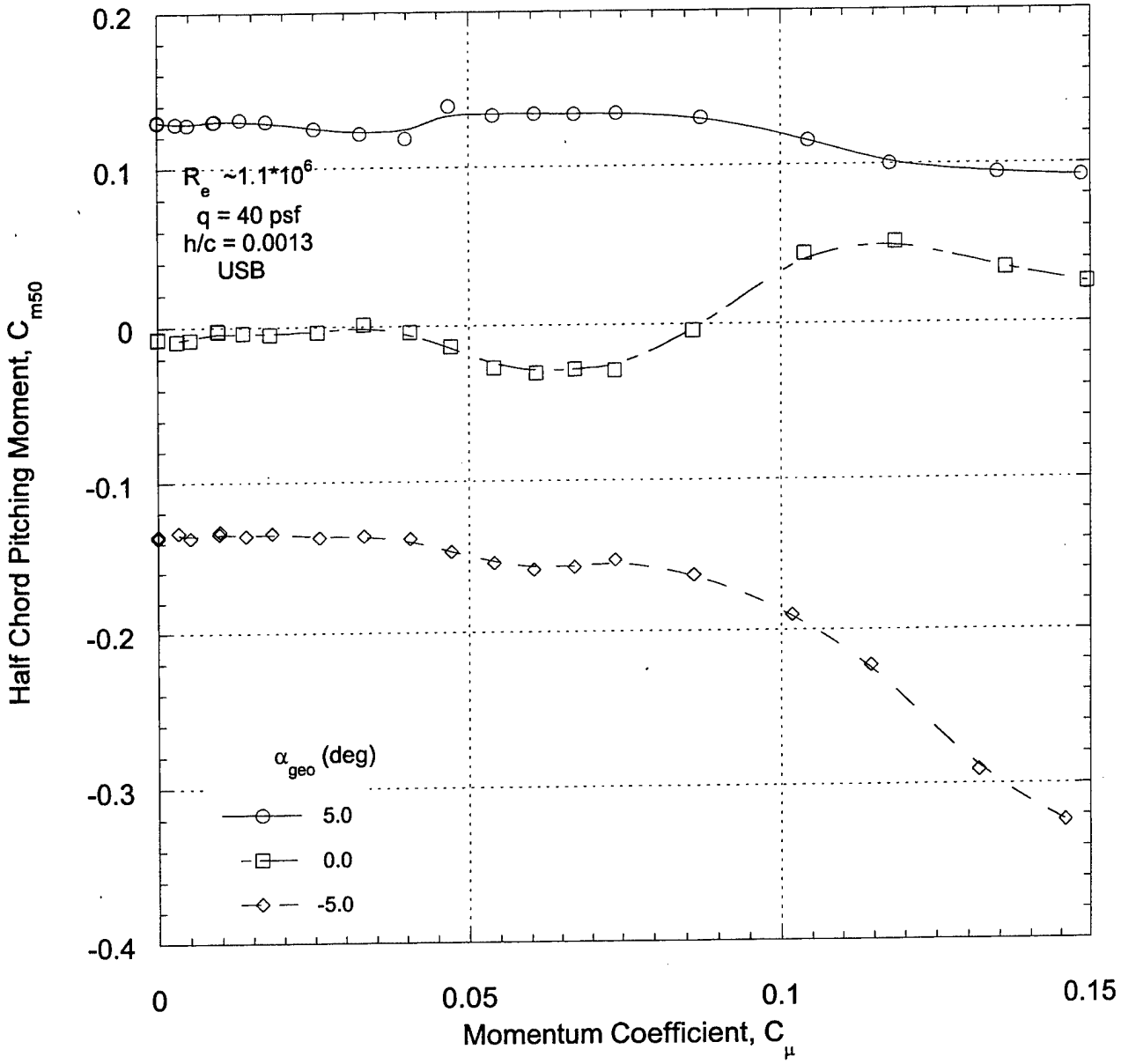

Figure 19b. USB, h/c = 0.0013.

Figure 19. (Continued)

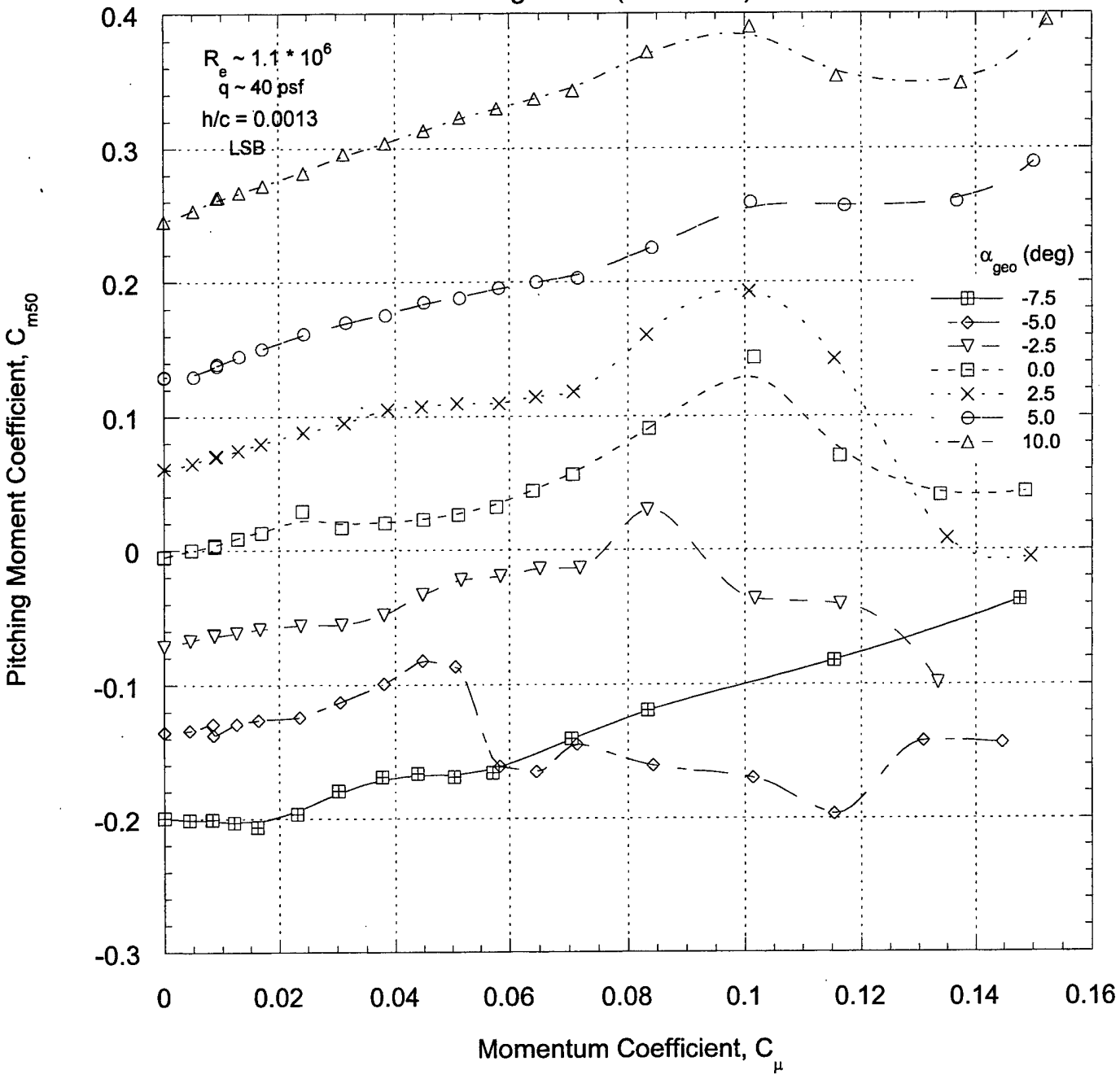

Figure 19c. LSB, h/c = 0.0013.

Figure 19. (Continued)

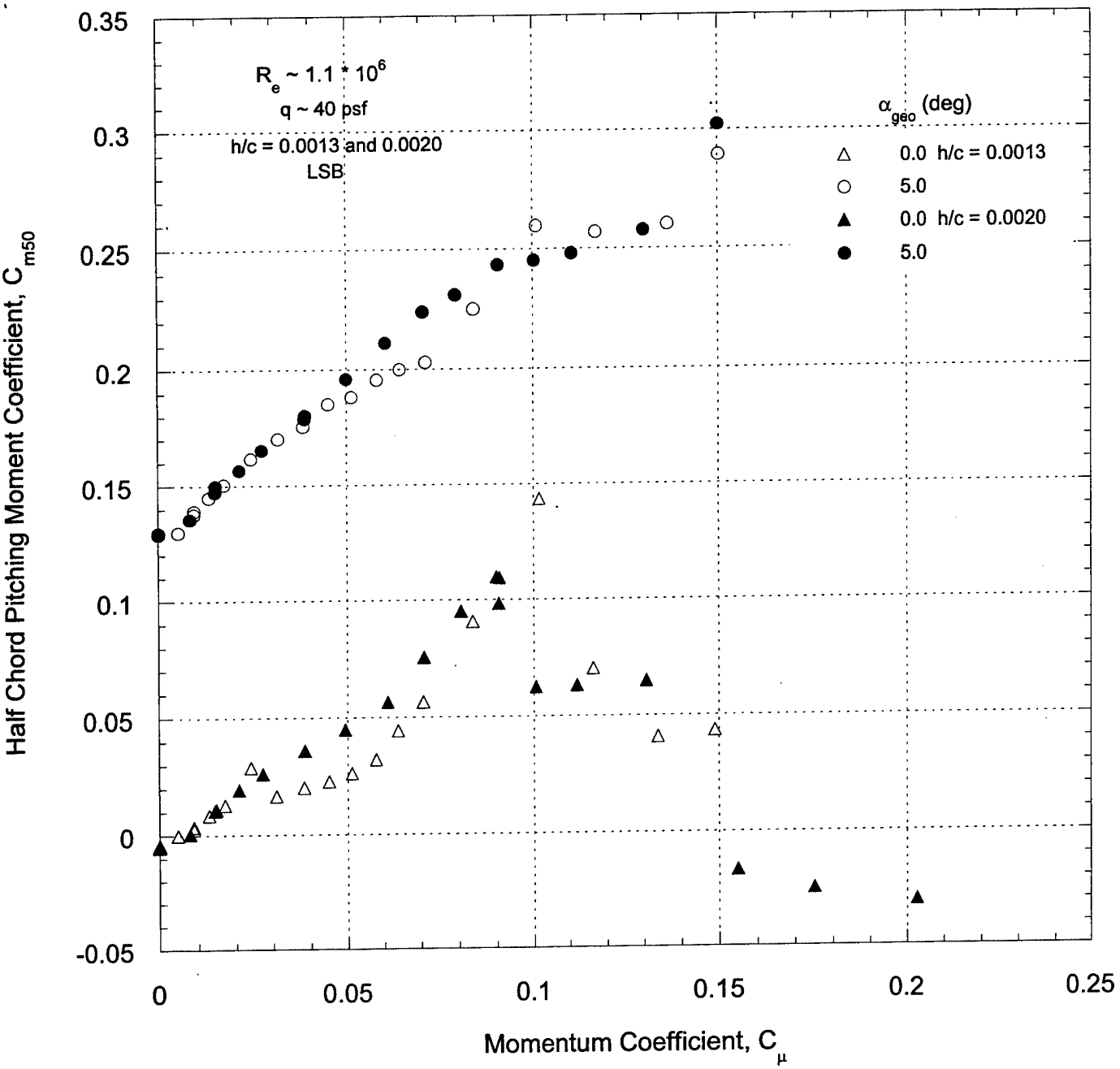

Figure 19d. LSB comparision of moments at h/c = 0.0020 and 0.0013.

Figure 19. (Continued)

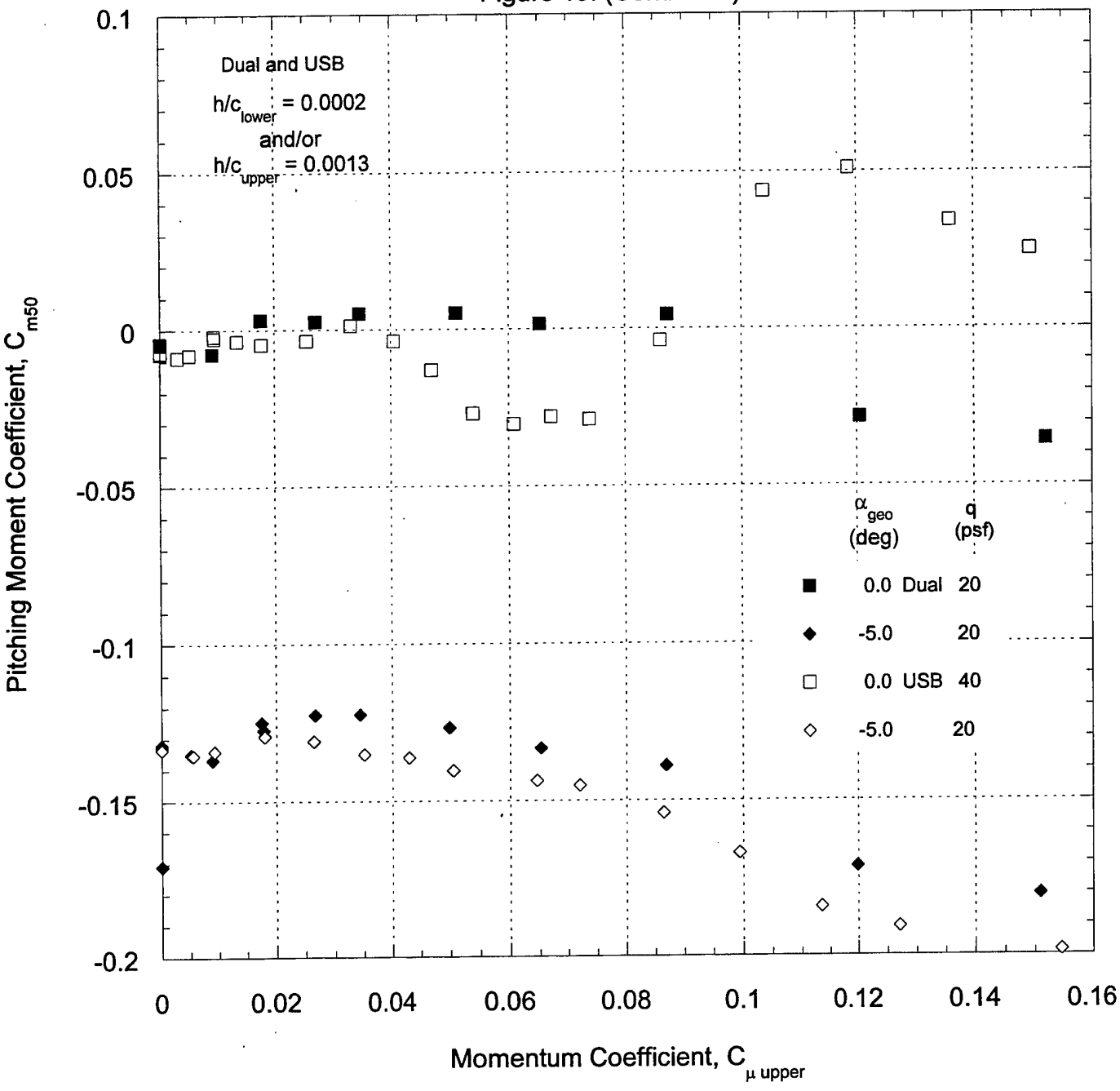

Figure 19e. Comparision of moments for dual and upper surface blowing.

APPENDIX A

THIS PAGE INTENTIONALLY LEFT BLANK

DESIGN OF A CIRCULATION CONTROL AIRFOIL HAVING BOTH UPPER AND LOWER SURFACE TRAILING EDGE SLOTS (MODEL LSB17)

by
Jane S. Abramson
Ernest O. Rogers

DTNSRDC/TM-16-86/03 September 1986

TABLE OF CONTENTS

	Page
ABSTRACT	1
ADMINISTRATIVE INFORMATION	1
INTRODUCTION	1
ANALYTICAL METHODS	2
MODEL CONTOUR SELECTION	2
DESIGN DETAILS	3
WIND TUNNEL MODEL SPECIFICATIONS AND REQUIREMENTS	4
SUMMARY	5

FIGURES

1.	Rotor angle of attack distribution, Θ_c = 0 degrees	6
2.	Rotor lift coefficient distribution, Θ_c = 0 degrees	7
3.	Predicted maximum lift coefficient as a function of Mach number	8
4.	Airfoil pressure distributions for identical absolute lift levels (typical)	9
5.	LSB Coanda contour	10
6.	Radius of curvature of LSB Coanda surface	11
7.	LSB nozzle details (model inverted)	12
8.	LSB17 model	13

ABSTRACT

A circulation control (CC) airfoil wind tunnel model with both upper and lower surface blowing slots has been designed for use in performance evaluations. Previously all CC airfoils designed at the David W. Taylor Naval Ship Research and Development Center have had slots placed only on the upper surface. In such a configuration the lift due to blowing can only increase the unblown lift. With the addition of a lower surface slot, lift either can be increased or decreased, which effectively doubles the airfoil control range. One major application of this airfoil is to circulation control rotorcraft where the collective pitch angle mechanism can be eliminated thereby potentially reducing the lifting system weight.

ADMINISTRATIVE INFORMATION

The work presented herein was supported by the David W. Taylor Naval Ship Research and Development Center (DTNSRDC) under the Independent Exploratory Development Program sponsored by the Space and Naval Warfare Systems Command (SPARWAR 05), and administered by the Research Coordinator (DTNSRDC, Code 012.3) under Program Element 62766N, Task Area RZ66300. DTNSRDC Work Unit 1-1690-107.

INTRODUCTION

To date all DTNSRDC circulation control (CC) airfoils have been designed with blowing slots placed only on the upper surface. In this configuration the lift due to blowing can only increment (increase in a positive sense) the unblown lift. The objective of this project has been to provide an airfoil where lift can be increased or decreased with respect to the unblown value. Such an objective can be achieved with an airfoil incorporating both an upper and lower surface blowing (LSB) slot. One specific purpose of LSB airfoils is to eliminate the variable mechanical collective mechanism (blade pitch angle) required for roll moment trim at high speed on circulation control rotors. The current task, therefore, has been

to design a wind tunnel model of an LSB airfoil for use in performance evaluations.

ANALYTICAL METHODS

Before designing the actual airfoil, it was necessary to establish operational requirements for an LSB airfoil. The CRUISE4 rotor performance code was used to ascertain the local angle of attack and the lift-due-to-blowing (ΔC_ℓ) required for rotor trim with a fixed-blade (zero) collective pitch angle. The results are shown in Figs. 1 and 2. Potential flow theory was then used to predict the maximum lifting capability in both the upper and lower surface blowing modes of several airfoil sections on the RBCCR† blade; see Fig. 3. Maximum lift is predicted using a C_p* stall criteria; that is, a stall phenomenon which occurs when critical (sonic) pressure is reached in the vicinity of the Coanda surface. A comparison of the rotor requirements for CRUISE4 with the analytically predicted maximum lift capability showed that the LSB concept is feasible.

Potential flow theory was also used to determine the placement of the lower blowing slot. The slot is usually placed ahead of the onset of adverse pressure gradients for typical combinations of lift and angle of attack. Predicted pressure distributions for identical absolute lift levels for both upper and lower surface blowing are shown in Fig. 4. The substantial difference in the distributions is due to the presence of camber.

MODEL CONTOUR SELECTION

Several factors were considered in selecting a basic contour for implementation of LSB. The state of the art in CC airfoil design has not reached the point where an entirely new contour can be devised with confidence. Thus an existing

† Reader, K.R. and J.B. Wilkerson, "Circulation Control Applied to a High Speed Helicopter Rotor," DTNSRDC-77/0824 (Feb 1977).

profile, the RB17, was selected with a thickness ratio of 0.17 and a 1.0-percent camber. The basic performance properties of the RB17 are well suited to the needs of a follow-on rotor design where it might be applied to the blade outboard region. The outboard region is where the LSB feature is most beneficial for roll control due to the large moment arm. Also, an extensive performance data base already exists for direct comparison of this airfoil with the LSB variant.

DESIGN DETAILS

A design prerequisite was that the performance of the LSB17 be comparable to its parent airfoil when using upper surface blowing. Thus the new slot was imbedded, and the existing trailing-edge radius was maintained as completely as possible. Imbedding the slot means that when lower surface blowing is not being used (the slot is closed) the contour in the slot exit area will be as smooth as possible. A requirement that the second derivative of the modified Coanda surface be continuous was also placed on the design.

Several analytic functions were applied in an attempt to modify the lower surface of the RB17 airfoil to accommodate a lower slot/nozzle/Coanda. None of the functions could simultaneously satisfy the derivative requirements for the Coanda surface while providing appropriate clearances for a closed (imbedded) slot nozzle design. Due to time constraints, a decision was made to use a computer aided design (CAD) system. The available CAD system could use only circular arcs to modify existing surfaces; therefore, by an iterative process, the existing trailing edge was modified using a circular arc whose radius matched that of the original Coanda surface at the break point. Figure 5 shows the final LSB Coanda contour. The modifying arc with an $r/c = 0.0417$ [$(x/c)_c = 0.9614$, $(y/c)_c = 0.00808$] intersects the RB17 trailing edge at $x/c = 0.987$, $y/c = -0.02486$. Results of a

radius of curvature analysis of the LSB Coanda surface are presented in Fig. 6. The design slot height to radius ratio (0.0015 ÷ 0.0417 = 0.036) is consistent with the value used on the upper slot; therefore, premature jet detachment would not be expected. The slot nozzle, shown in Fig. 7, was designed using straight line segments, as had previously been the practice at DTNSRDC. The interior of the upper (RB17) nozzle design also required modification to provide a larger duct area. However, the original nozzle contour was preserved for 10 slot heights (based on h/c = 0.0020) upstream of the slot exit.

WIND TUNNEL MODEL SPECIFICATIONS AND REQUIREMENTS

The proposed wind tunnel model has a 12-in. chord and a span of 36 in. The chord length is based on two criteria. First, there is the necessity of having a Reynolds number (R_e) of at least 1×10^6 (based on chord) at the low-speed test condition of $M_\infty = 0.12$. Performance properties unrepresentative of full-scale conditions are believed to occur below a model Reynolds number of one million. Also, the test results would then be at essentially the same R_e as that of the original RB17 model, thereby permitting more certainty in identifying LSB effects on basic performance. Second, the selected chord length should not be so large as to cause excessive wall effects during the proposed high-speed tests in the NASA 6-ft wind tunnel. Physically the model must be compatible with the inserts in both the DTNSRDC 8- by 10-ft and the NASA Ames 6-ft wind tunnels.

The LSB model will be constructed with two plenum chambers to allow pressure control of each chamber independently of the other for investigating differential blowing. In the past, closing down a slot on a model to eliminate blowing during single slot testing has been unsatisfactory due to leakage. Figure 8 shows a partially completed mechanical layout of the actual model.

SUMMARY

The aerodynamic and mechanical design of a circulation control airfoil with both an upper and lower surface blowing slot have been completed. The basic profile, taken from an existing airfoil, will allow assessment of the effect of a lower surface blowing slot on the overall aerodynamic performance. An experimental evaluation of performance at low speed will be undertaken in the DTNSRDC subsonic wind tunnel upon completion of model construction.

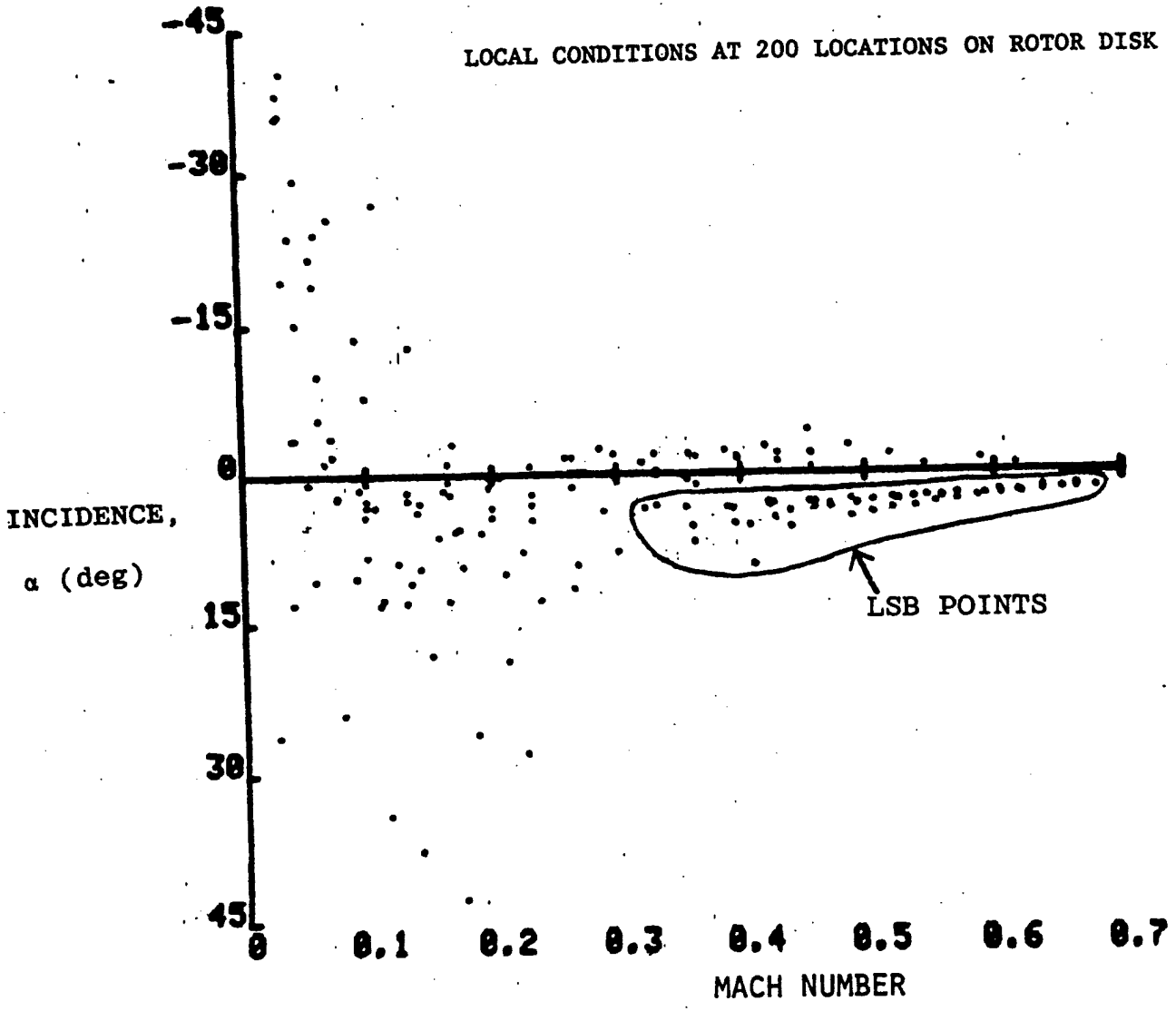

Figure 1 - Rotor Angle of Attack Distribution, Θ_c = 0 Degrees

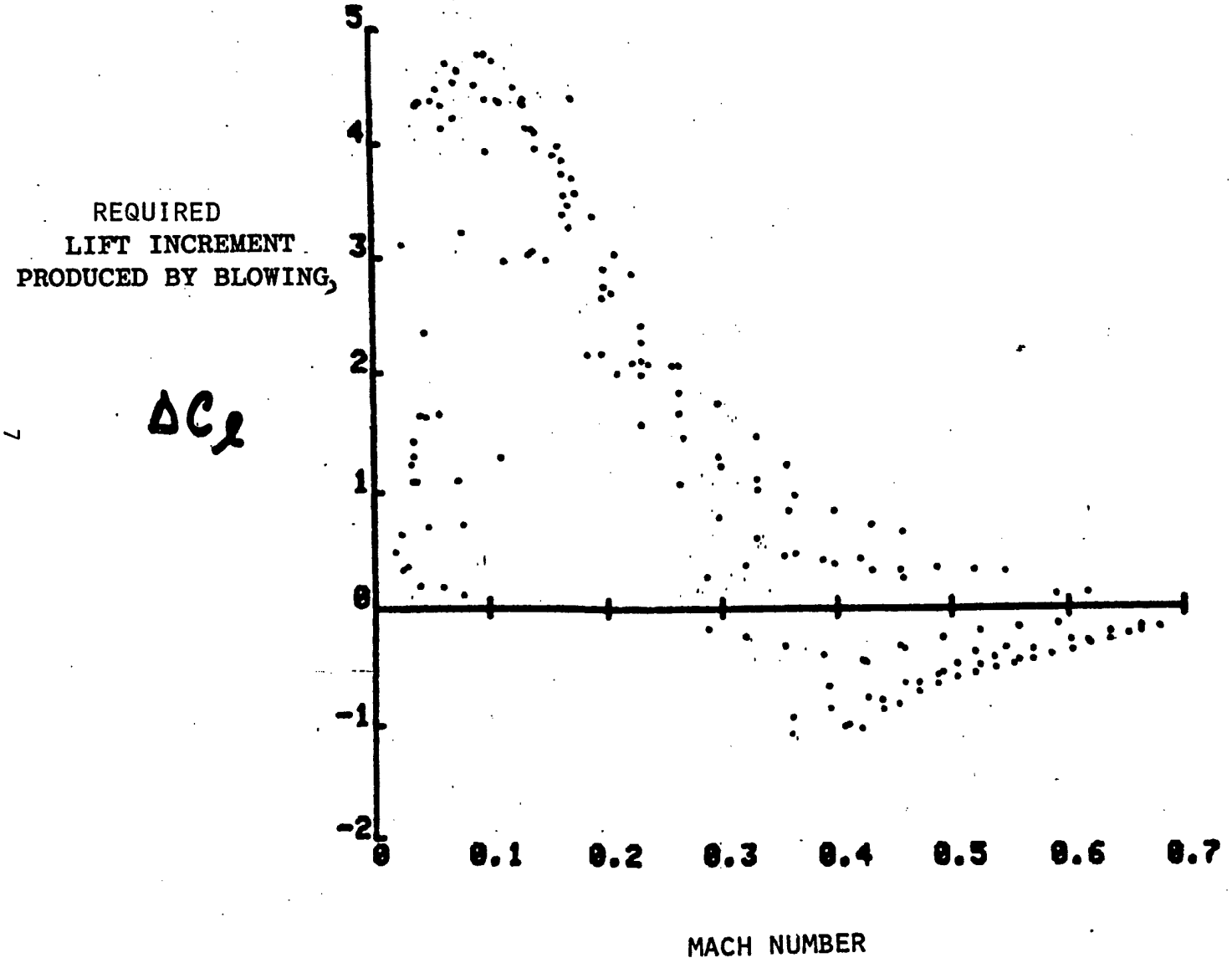

Figure 2 - Rotor Lift Coefficient Distribution, Θ_c = 0 Degrees

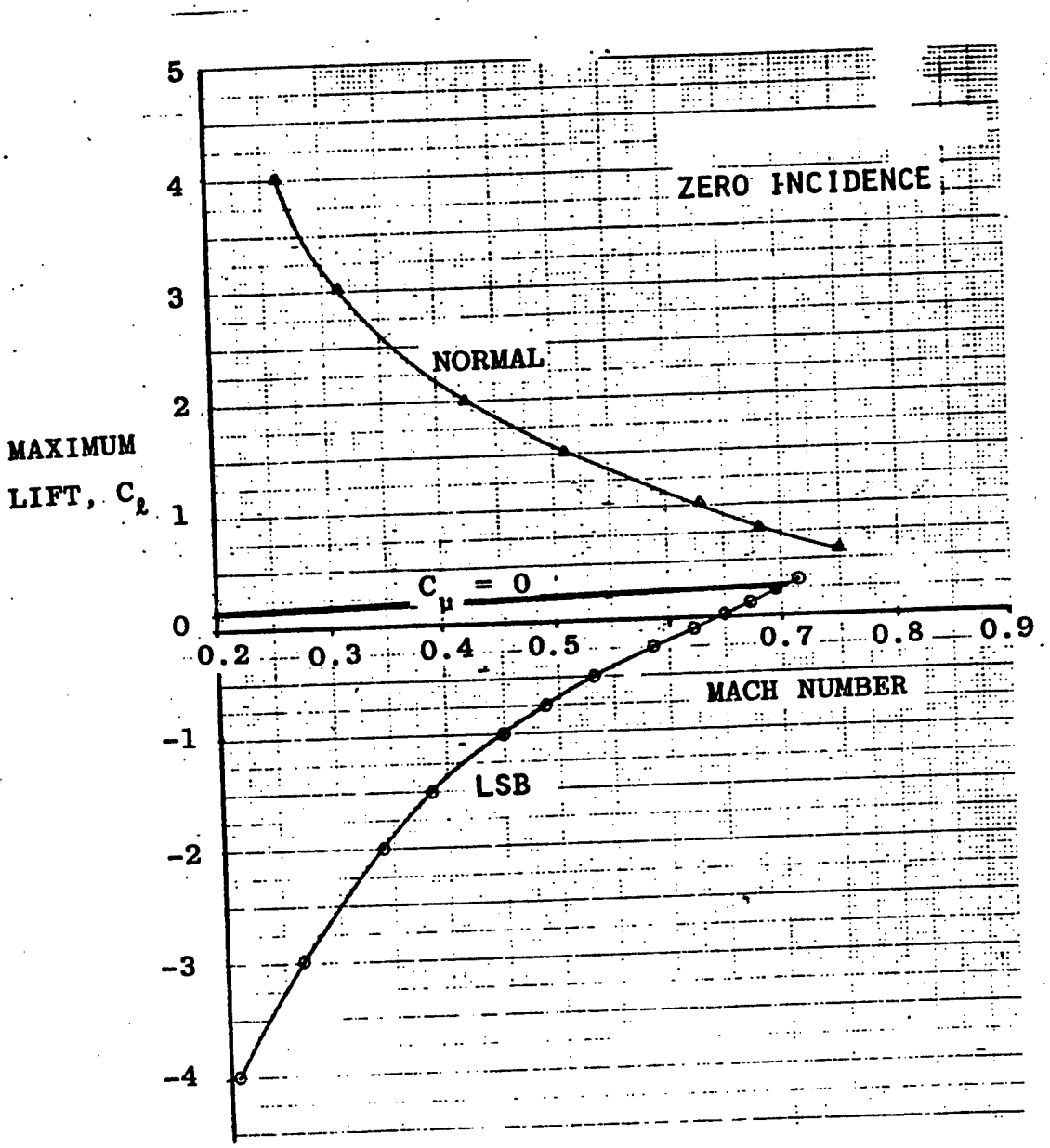

Figure 3 - Predicted Maximum Lift Coefficient as a Function of Mach Number

MID-SPAN AIRFOIL (2.5% CAMBER)

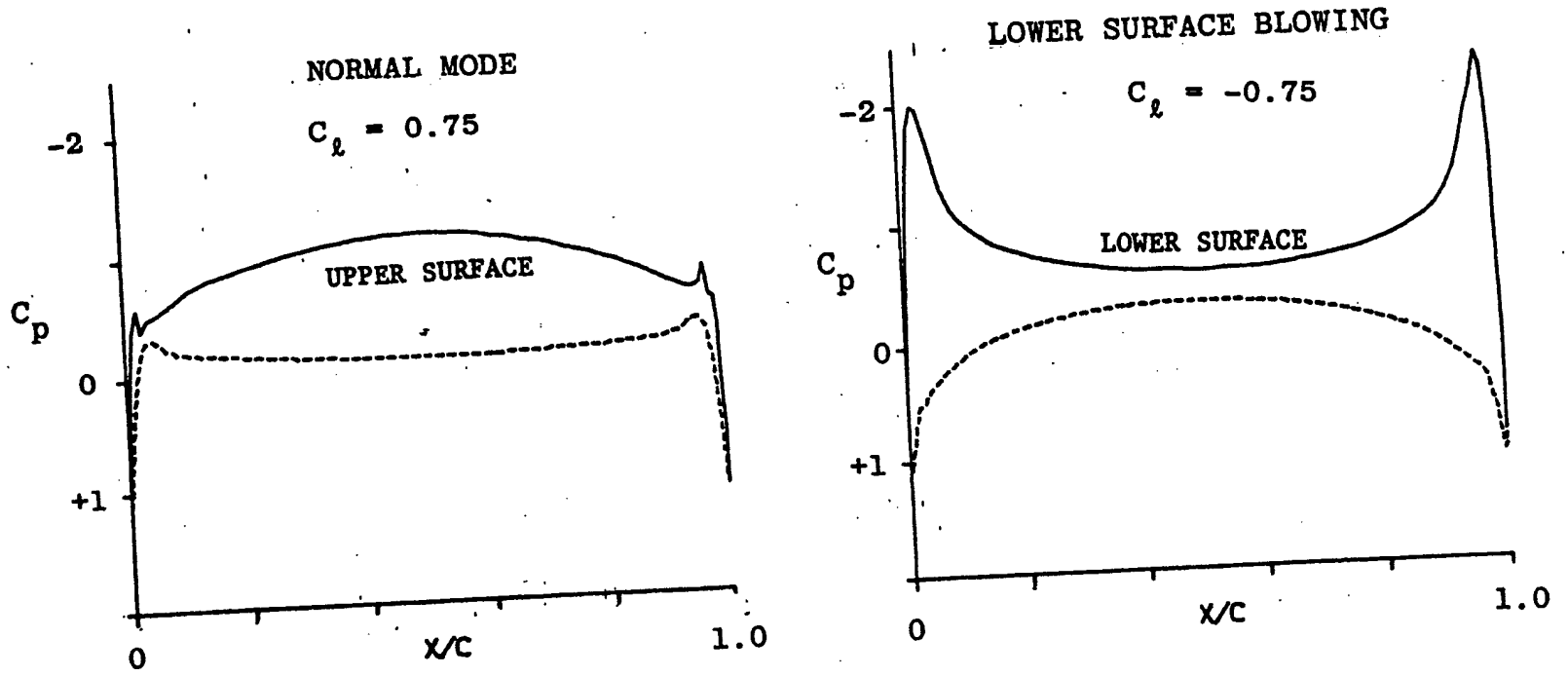

Figure 4 - Airfoil Pressure Distribution for Identical Absolute Lift Levels (Typical)

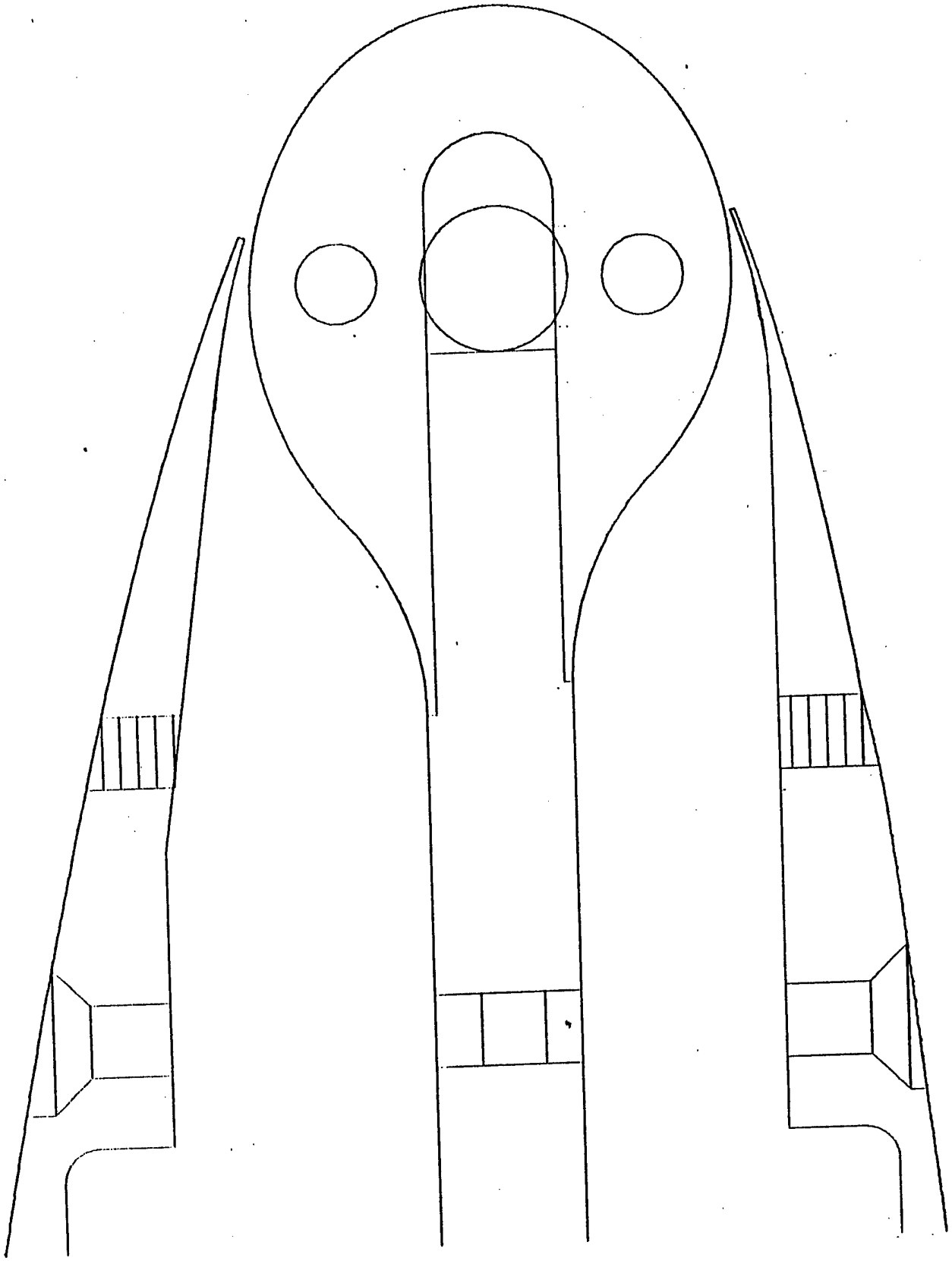

Figure 5 - LSB Coanda Contour

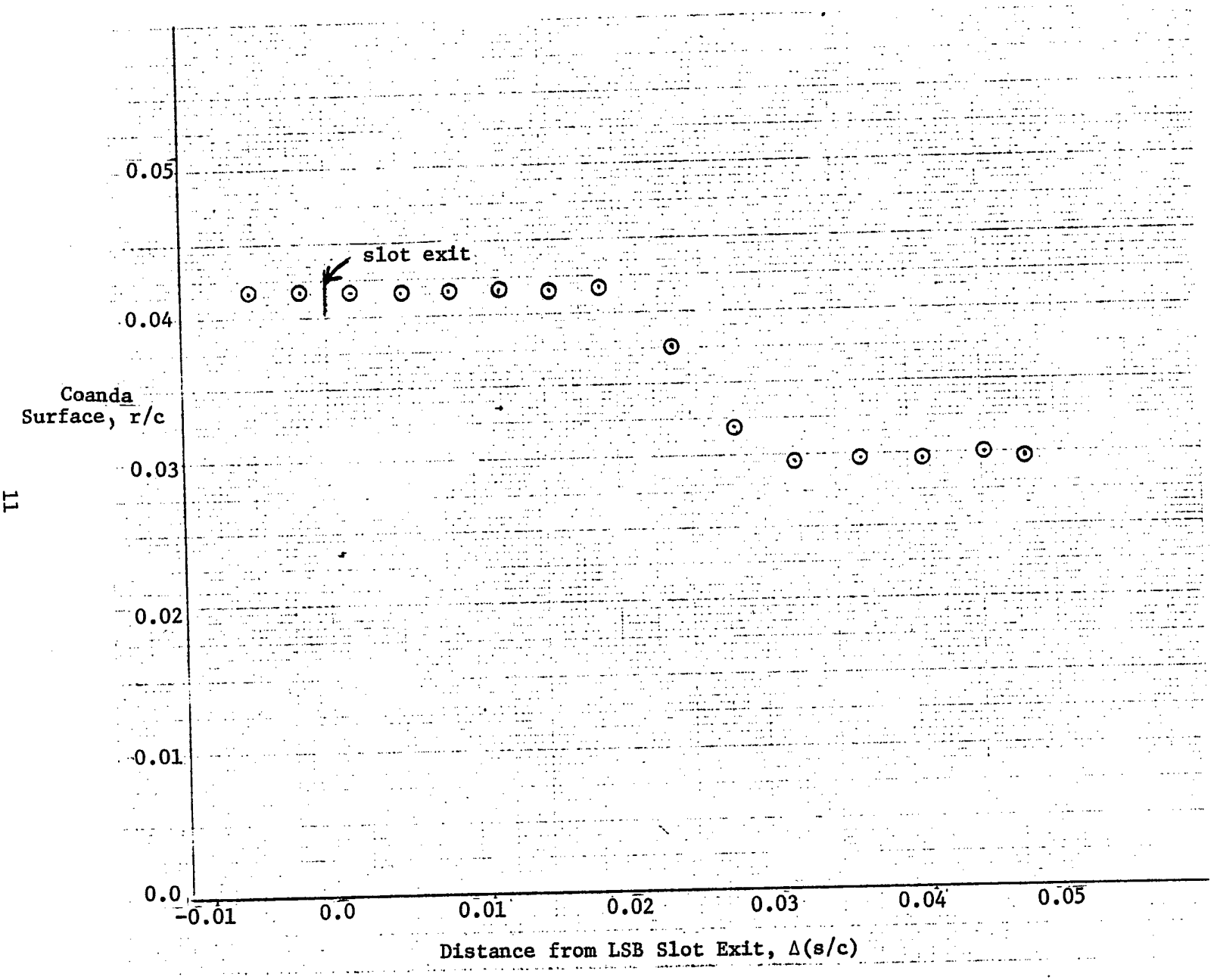

Figure 6 - Radius of Curvature of LSB Coanda Surface

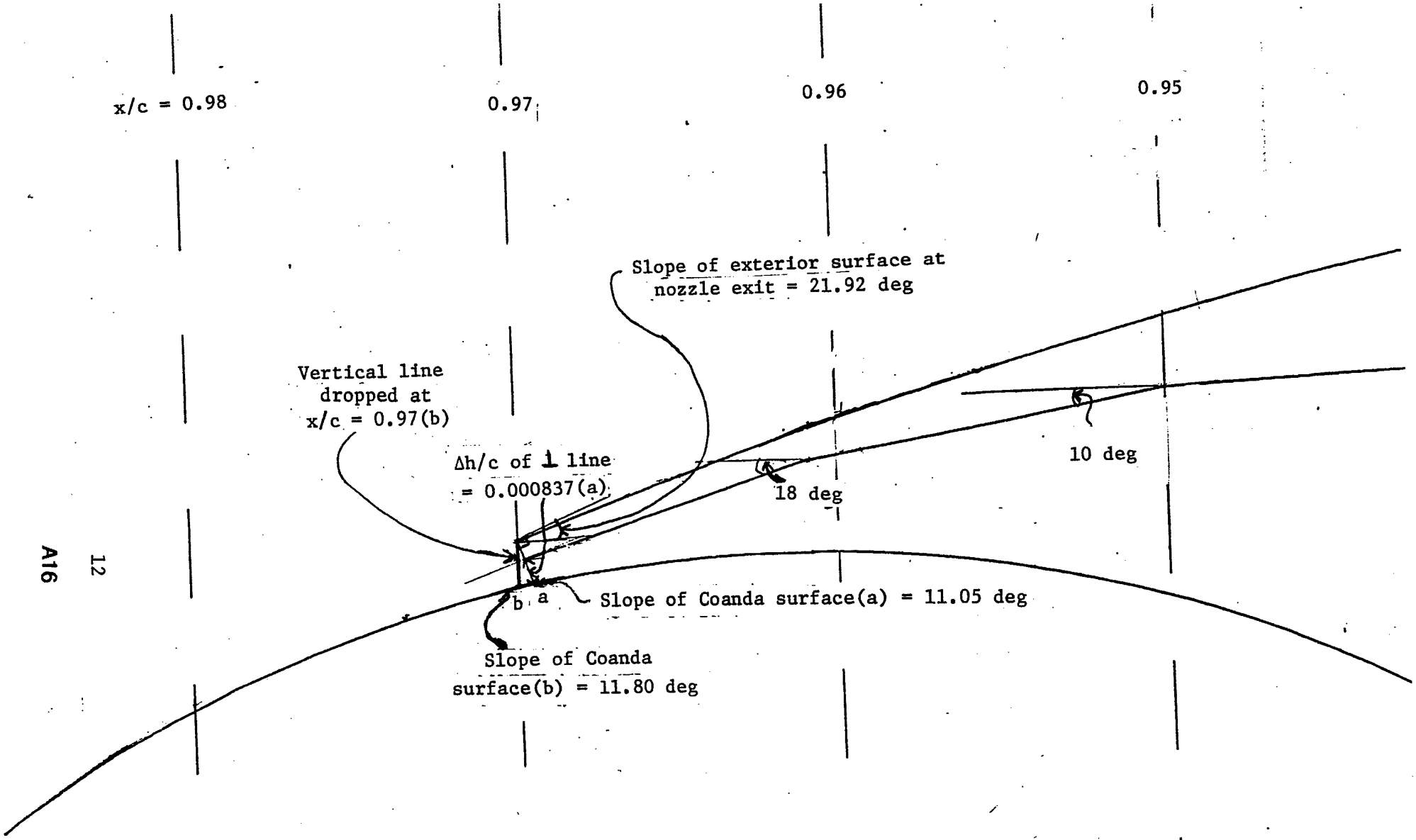

Figure 7 - LSB Nozzle Details (Model Inverted)

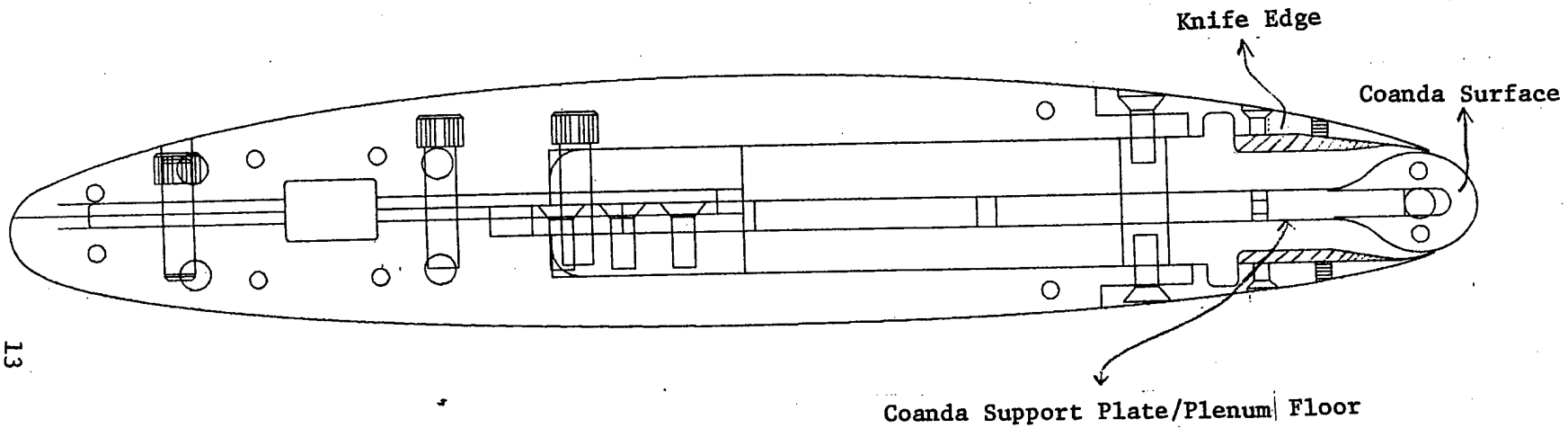

Figure 8 - LSB17 Model

APPENDIX B

THIS PAGE INTENTIONALLY LEFT BLANK

Table B1. Coordinates of construction for the LSB17 model.

X (inches)	Y(inches)	
6.00000000	-.46766880	lower plenumn floor
10.050000	-.46766880	
10.050000	-.36380000	
10.800000	-.36380000	
11.280000	-.44866000	lower nozzle
11.340000	-.45390000	
11.400000	-.45390000	
11.460000	-.45078000	
11.53200000	-.43810560	
11.63732040	-.40388400	interior nozzle point slot exit
11.64000000	-.41056680	exterior nozzle point
11.62380360	-.41694360	
11.57538240	-.43479960	
11.52647400	-.45129000	
11.47718760	-.46660800	
11.42758920	-.48089040	
11.37773280	-.49423800	
11.32766160	-.50675160	
11.27741160	-.51853800	
11.22702480	-.52971240	
11.17652640	-.54039360	
11.12594760	-.55066800	
11.07529680	-.56059440	
11.02458720	-.57019560	
10.97381640	-.57949440	
10.92299640	-.58849560	
10.87212360	-.59721600	
10.82120880	-.60567240	
10.77025440	-.61387200	
10.53950640	-.64808400	
10.30819920	-.67825560	
10.07646960	-.70503840	
9.84442440	-.72893040	
9.61213920	-.75030960	
9.37965360	-.76947360	
9.14701920	-.78666240	
8.91425640	-.80206800	
8.68139160	-.81583800	
8.44844520	-.82811160	
8.21542680	-.83898960	
7.98235200	-.84856560	
7.74923160	-.85691640	
7.51607040	-.86409840	
7.28287680	-.87016800	
7.04965680	-.87516480	
6.81642120	-.87912360	
6.58316880	-.88207200	
6.34990680	-.88402680	
6.11663640	-.88499760	
5.88336480	-.88499760	
5.65009440	-.88402680	

LOWER SURFACE

Table B1. (Continued)

5.41683240	-.88207200
5.18358000	-.87912360
4.95034320	-.87516480
4.71712320	-.87016800
4.48393200	-.86409840
4.25077080	-.85691640
4.01764800	-.84856560
3.78457320	-.83898960
3.55155600	-.82811160
3.31860840	-.81583800
3.08574360	-.80206800
2.85298200	-.78666240
2.62034520	-.76947360
2.38786440	-.75030960
2.15557440	-.72893040
1.92353160	-.70503840
1.69180440	-.67825560
1.46049360	-.64808400
1.22974800	-.61387200
1.18109400	-.60604800
1.13247600	-.59799240
1.08390000	-.58969560
1.03536840	-.58114440
.98688240	-.57232440
.93844800	-.56322960
.89007000	-.55384560
.84175200	-.54415200
.79350600	-.53411160
.74534760	-.52365840
.69730200	-.51269640
.64940040	-.50112240
.60167640	-.48883800
.55416360	-.47576040
.50690400	-.46179360
.45994560	-.44685000
.41335560	-.43079400
.36723240	-.41344440
.32173560	-.39451440
.27708240	-.37368000
.23357160	-.35055840
.19159800	-.32475240
.15171960	-.29582160
.11461440	-.26342400
.08120760	-.22723440
.05263560	-.18713040
.02986800	-.14346960
.01334400	-.09708240
.00333360	-.04887000
0.00000000	0.00000000 — leading edge
.00341400	.04945440
.01350240	.09765000

.03010200	.14400960
.05277360	.18772440
.08084160	.22819200
.11358360	.26498400
.15029160	.29782560
.19028640	.32658000
.23292840	.35124360
.27765840	.37188960
.32398560	.38864400
.38399040	.41559960
.49855440	.46225560
.61445760	.50547840
.73148760	.54555360
.84939240	.58298040
1.08712200	.65146800
1.32683640	.71265600
1.56827040	.76665600
1.81103760	.81429840
2.05464360	.85748760
2.29890720	.89679840
2.54371560	.93257760
2.78897400	.96510600
3.03461760	.99460440
3.28058760	1.02125160
3.52683120	1.04520000
3.77331720	1.06656960
4.02000000	1.08546480
4.26685920	1.10196240
4.51386000	1.11613800
4.76098200	1.12804800
5.00820000	1.13773680
5.25549480	1.14524040
5.50284360	1.15058760
5.75023080	1.15379640
5.99763720	1.15487760
6.24504480	1.15383600
6.49243320	1.15066800
6.73978200	1.14536160
6.98708040	1.13790000
7.23429840	1.12825440
7.48142280	1.11638640
7.72842840	1.10225400
7.97528880	1.08579960
8.22197520	1.06695360
8.46846360	1.04563200
8.71471800	1.02173400
8.96069040	.99513840
9.20633880	.96569640
9.45160560	.93322800
9.69642240	.89751360
9.94069920	.85827360
10.18431840	.81516240
10.42713360	.76772400
10.66893360	.71535840
10.73595360	.69982200
10.81735200	.68027400
10.89857280	.65999760
10.97959320	.63894240
11.06038440	.61703160

UPPER SURFACE

Table B1. (Continued)

Table B1. (Continued)

11.14092720	.59421360	
11.22118560	.57041640	
11.30111520	.54553200	
11.38065840	.51945000	
11.45974200	.49199160	
11.49907440	.47767440	
11.53824360	.46292040	
11.57722920	.44768760	
11.61601200	.43194000	slot
11.61206280	.42140640	
11.54372640	.44181960	
11.47395600	.45674160	
11.40360360	.46865400	underside of upper nozzle
11.340000	.47304000	
11.280000	.47304000	
11.220000	.47094400	
11.182000	.46762000	
10.960000	.45329000	
10.745000	.44850000	
10.050000	.44850000	end nozzle
10.050000	.58236000	
6.00000000	.58236000	
-6.000000	-.1176400	Coanda support plate lower surface
-10.83690	-.1176400	
10.89222	-.1207059	
10.94682	-.1298600	
11.00008	-.1450040	
11.05134	-.1659390	
11.09997	-.192410	
11.14537	-.2241000	
11.16729600	-.24018120	
11.19650760	-.26970720	
11.22806520	-.29671320	
11.26175280	-.32100960	
11.29733760	-.34243200	Lower Coanda Surface
11.33457360	-.36083160	
11.37320760	-.37608240	
11.41297200	-.38807880	
11.45359440	-.39673920	
11.49479520	-.40200360	
11.53628880	-.40383600	
11.57779200	-.40222440	
11.61901920	-.39717840	
11.65968720	-.38873400	
11.69951520	-.37694760	
11.73822960	-.36190200	
11.77556400	-.34370040	
11.81126160	-.32246760	
11.84507640	-.29835000	
11.88852120	-.26037000	
11.92299360	-.22200360	

fairing of support plate into lower Coanda Surface

Table B1. (Continued)

11.95199760	-.17936400	
11.97451200	-.13297200	
11.99010480	-.08381760	
11.99848680	-.03293400	
12.00000000	0.00000000	trailing edge point
11.99951400	.01869360	
11.99315520	.06987000	
11.97953280	.11960640	
11.95894560	.16688760	
11.93206680	.21090840	
11.89971720	.25107960	Upper Coanda Surface
11.86271040	.28701360	
11.82184920	.31850160	
11.77788360	.34549200	
11.73148320	.36805440	
11.68322640	.38631840	
11.63358720	.40039440	
11.58290040	.41005440	
11.53153920	.41491440	Coanda Surface
11.47994640	.41483160	inside of slot
11.42858880	.40989600	
11.37790320	.40024200	
11.32836000	.38599800	
11.28028920	.36725640	
11.23414200	.34418040	
11.19030720	.31696800	
11.14915440	.28584600	
11.11103400	.25107960	
11.069000	.22004	fairing of Coanda surface
11.004100	.18233700	into support plate
10.934250	.15478000	
10.861070	.13799710	
10.786200	.13236400	Coanda support plate
6.0000000	.13236400	upper surface

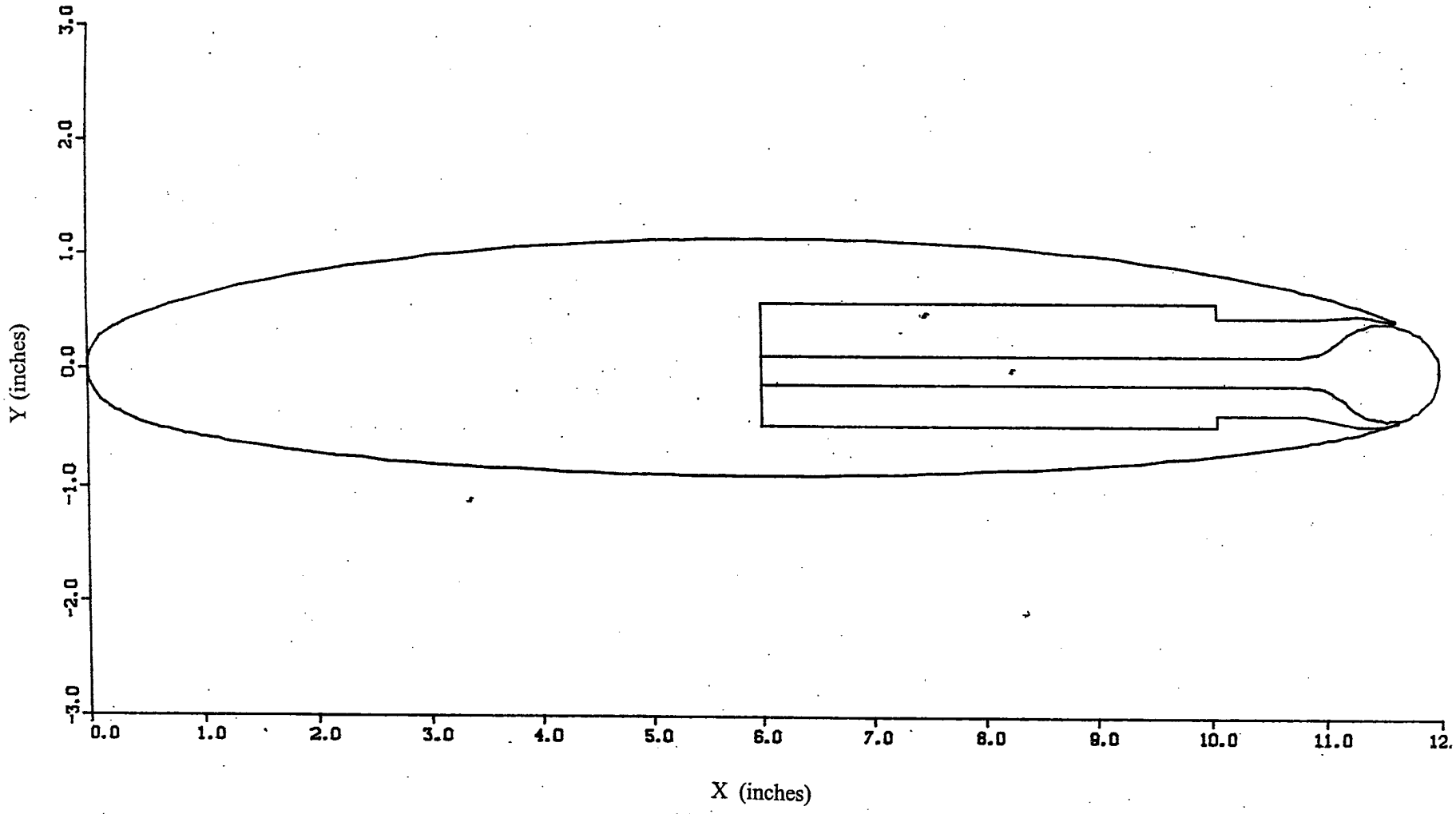

Figure B1. Line drawing of the LSB17 made from the coordinates of construction.

INITIAL DISTRIBUTION

Copies	Organization	Code	Name
1	ONR	333	R. Joslin
1	NAVSEA	SEA 05H	M. King
1	DTIC		
1	NSWCCD	3442	TIC(C)
1	NSWCCD	5010	Administrative Off.
1	NSWCCD	506	D. Walden
1	NSWCCD	5600	E. Ammeen
1	NSWCCD	5600	D. Hess
1	NSWCCD	5600	J. Feldman